JOURNAL OF GEOPHYSICAL RESEARCH, VOL. 105, NO. D12, PAGES 15,277–15,312, JUNE 27, 2000

Chemical composition of aerosols collected over the tropical North Atlantic Ocean

Anne M. Johansen, Ronald L. Siefert,[1] and Michael R. Hoffmann

Environmental Engineering Science, W. M. Keck Laboratories, California Institute of Technology, Pasadena

Abstract. Ambient aerosol samples were collected over the tropical northern Atlantic Ocean during the month of April 1996 onboard the R/V *Seward Johnson*. Dichotomous high-volume collector samples were analyzed for ferrous iron immediately after collection, while trace metals, anions, and cations were determined upon return to the laboratory. Data are analyzed with the aid of enrichment factor, principal component, and weighted multiple linear regression analyses. Average mineral aerosol concentrations amounted to 19.3 ± 16.4 $\mu g\ m^{-3}$ whereby the chemical characteristics and air mass back trajectories indicated the dust to be of a typical shale composition and Saharan origin. Calcite accounted for 3.0 and 7.9% of the mineral aerosol during the first and second halves of the cruise, respectively. Total iron concentrations (averaging 0.84 ± 0.61 $\mu g\ m^{-3}$) are crustally derived, of which $0.51 \pm 0.56\%$ is readily released as Fe(II). Eighty-six percent of this Fe(II) is present in the fine (<3 μm diameter) aerosol fraction and correlates with NSS-SO_4^{2-} and oxalate. Approximately 23% of the measured NSS-SO_4^{2-} in both size fractions appears to be biogenically derived, and the rest is of anthropogenic nature. Biogenic SO_4^{2-}/methanesulfonic acid (MSA) ratios could not be easily extracted by employing a multiple linear regression analysis analogous to that of *Johansen et al*. [1999], possibly due to the varying characteristics of the aerosol chemistry and air temperature during the cruise. Because of the presence of anthropogenic SO_4^{2-}, the non-sea-salt (NSS)-SO_4^{2-}/MSA ratio, 37.4 ± 16.4, is elevated over what would be expected if the NSS-SO_4^{2-} were purely biogenic. Cl^- depletion is seen in all samples and averages $18.3 \pm 9.1\%$. The release of Cl from the aerosol phase appears to occur through acid displacement reactions with primarily HNO_3 in the coarse and H_2SO_4 in the fine fraction.

1. Introduction

The present study focuses on the chemical characterization of the ambient aerosol over the Atlantic during the month of April 1996. It is part of a multidisciplinary effort to observe a possible link between trace metal abundance, its speciation in the atmosphere, and phytoplankton productivity. Specific focus was directed to the N_2 fixing cyanobacterium *Trichodesmium erythraeum*, which was studied by several groups aboard the ship.

The long-range atmospheric transport of weathered crustal material from the continents supplies a major portion of the nonbiogenic sediments that accumulate on the seafloor. Mineralogical similarities between the composition of African dust and sediments of the North Atlantic [*Delaney et al*., 1967] have confirmed that the arid regions of northern Africa, especially the Sahara and Sahel, are the source regions for atmospheric dust that reaches the North Atlantic Ocean. Information of the flux of mineral aerosol in marine sediments has also been used in the field of paleoclimate.

Considerable evidence, mainly provided by J. M. Prospero and colleagues, demonstrates that Saharan dust reaches the Caribbean [*Ellis and Merrill*, 1995; *Prospero et al*., 1970; *Prospero and Carlson*, 1972; *Talbot et al*., 1990], western North Atlantic [*Duce et al*., 1975], southern North America [*Savoie and Prospero*, 1977], and northeastern South America [*Prospero et al*., 1981; *Swap et al*., 1992; *Talbot et al*., 1990]. The deposition of mineral aerosol is also evident in the chemistry of island soils of the Atlantic and Caribbean regions [*Chester et al*., 1972; *Muhs et al*., 1990, 1987; *Paquet et al*., 1984; *Schütz and Sebert*, 1987]. Dust collection over the Atlantic Ocean and in the Caribbean was initiated in the late 1960s [*Chester et al*., 1972; *Delaney et al*., 1967; *Prospero*, 1968] and continues to be the focus of many research groups. The transport mechanism by which African dust is carried to the west seems well understood [*Chiapello et al*., 1997; *Prospero and Nees*, 1977; *Schütz*, 1980]. Models [*D'Almeida*, 1986; *Ellis and Merrill*, 1995] and aerosol optical thickness data of the dust and its transport [*Swap et al*., 1996] have further elucidated the seasonal and spatial variability of the mineral dust over the Atlantic Ocean.

Many atmospheric and oceanic processes are affected by the transport and deposition of mineral dust. The annual production of aeolian material from North Africa was estimated at ~400–700 Tg/yr [*D'Almeida*, 1987; *Schütz et al*., 1981]. Although the mass scattering efficiency of mineral aerosol is estimated at $\sim\frac{1}{4}$ of that for non-sea-salt sulfate [*Li et al*., 1996], the large mass concentrations of mineral aerosol indicate that their contribution and importance to the total burden of tropospheric aerosols has been underestimated so far, especially in regions such as the tropical and subtropical North Atlantic [*Andreae*, 1996; *D'Almeida*, 1987, 1986; *Li et al*., 1996; *Schollaert and Merrill*, 1998; *Tegen and Fung*, 1995; *Tegen et al*., 1996]. In the context of biogeochemical cycles the dissolution of mineral aerosol during atmospheric transport and after air-to-sea transfer releases important trace metals into surface

[1]Now at Chesapeake Biological Laboratory, University of Maryland Center for Environmental Science, Solomons.

Paper number 2000JD900024.
0148-0227/00/2000JD900024$09.00

waters that play an important role in phytoplankton metabolism. Recent studies have found Fe to be a rate-limiting nutrient to primary phytoplankton growth in certain regions of the open ocean [*Cooper et al*., 1996; *DiTullio et al*., 1993; *Kolber et al*., 1994; *Martin et al*., 1994; *Martin and Fitzwater*, 1988; *Martin et al*., 1991; *Paerl et al*., 1994; *Price et al*., 1994]; thus it has become the most studied trace metal.

On the basis of laboratory studies and field measurements the photoredox chemistry of ferric oxides and (oxy)hydroxides, which are believed to be the predominant forms of iron in the atmosphere, results in the production of ferrous iron (Fe(II)) in the presence of electron donors such as organic acids [*Erel et al*., 1993; *Faust and Hoigné*, 1990; *Faust and Zepp*, 1993; *Pehkonen et al*., 1993; *Siefert et al*., 1994; *Zuo*, 1995; *Zuo and Hoigné*, 1992, 1994]. Iron is also known to catalyze the oxidation of S(IV) by oxygen [*Berglund and Elding*, 1995; *Berglund et al*., 1993; *Conklin and Hoffmann*, 1988; *Faust and Allen*, 1994; *Kraft and van Eldik*, 1989; *Martin and Hill*, 1987] and to undergo fast redox cycling with Cu in surface waters [*Sedlak and Hoigné*, 1993, 1994]. Thus, despite the thermodynamic instability of the reduced from of iron, Fe(II) may be present in considerable amounts in atmospheric and surface waters. Fe(II) is far more soluble than Fe(III) and may therefore be more bioavailable in the surface water of the ocean. Although inorganic Fe(II) in seawater is rapidly oxidized by photo-induced H_2O_2, with a reaction halftime of a few minutes [*Millero et al*., 1991; *Moffett and Zika*, 1987], the newly precipitated Fe(III) will be finely dispersed and may therefore still be more bioavailable than the Fe(III) trapped in large particles of rapidly sinking crustal material. Numerous studies exist on the solubility of iron and its photochemical reactions in seawater [*Duce and Tindale*, 1991; *Kuma et al*., 1996; *Miller and Bruland*, 1994; *Millero et al*., 1995; *Moffett and Zika*, 1987; *O'Sullivan et al*., 1995; *Spokes and Liss*, 1995; *Voelker and Sedlak*, 1995; *Waite and Morel*, 1984; *Zhang and Terada*, 1994; *Zhuang et al*., 1990]. However, *Wells et al*. [1995] reaffirm the existing gap in the knowledge about the different physico-chemical forms of iron in the ocean.

Most studies of trace metals in the atmosphere have largely focused on the determination of their adundance, particle-size distribution and sources while neglecting oxidation states of the transition metal. Few studies exist on the speciation of iron in fog [*Behra and Sigg*, 1990; *Erel et al*., 1993; *Kotronarou and Sigg*, 1993; *Siefert et al*., 1998; *Zuo*, 1995] and in aerosols [*Kopcewicz and Kopcewicz*, 1991, 1992, 1998; *Siefert et al*., 1999, 1994, 1996; *Zhu et al*., 1993, 1997; *Zhuang et al*., 1992b]. Several of the listed aerosol iron speciation studies were performed in remote oceanic regions [*Siefert et al*., 1999; *Zhu et al*., 1993, 1997; *Zhuang et al*., 1992b]. Ferrous iron extraction experiments in the Zhu studies were carried out at pH 1, which *Zhu et al*. [1992] in a different study believe to be representative of marine aerosol. Furthermore, the samples analyzed by *Zhu et al*. [1993] and *Zhuang et al*. [1992a] had been collected over a period of a day to a week and subsequently analyzed after storage for a considerable length of time (weeks to months) during which sample bias may have been introduced from the oxidation of Fe(II). *Zhuang et al*. [1992a] observed a mean of 15% (this is the corrected value; see *Zhu et al*. [1993]) of the total iron in the form of soluble Fe(II) in Barbados, while *Zhu et al*. [1993] during sampling in the same location found Fe(II) to represent $<1\%$ of the total iron. In a later study in Barbados by *Zhu et al*. [1997], samples were analyzed immediately after collection, and the mean value for Fe(II) was 1.7%. *Siefert et al*. [1999] measured Fe(II) concentrations during the intermonsoon and SW monsoon seasons of 1995 over the Indian Ocean. A sequential extraction procedure, identical to the one carried out in the present study, was performed immediately after sample collection and revealed the following Fe(II) concentration percentages: on average, only 0.3% of Fe was present as Fe(II) after the first 30 min of extraction and, even after 22 hours, never more than 4% of the total Fe was released as Fe(II). These values are in close agreement with both studies by *Zhu et al*. [1993, 1997], but they differ from the larger values found by *Zhuang et al*. [1992b] both in Barbados and over the central North Pacific. In the present study we will present Fe(II) results obtained from the sequential extraction procedure [*Siefert et al*., 1999] carried out on samples collected during a month-long cruise between Barbados and Cape Verde.

Zhuang et al. [1992b] suggest that the iron and sulfur chemical cycles in remote marine aerosols are closely coupled. By incorporating this link between iron and sulfur into the climate feedback loop proposed by *Charlson et al*. [1987], *Zhuang et al*. [1992b] identify two potential positive feedback loops that would result in enhanced production of atmospheric Fe(II). The parent sulfur compound in this debate is the biogenically derived dimethyl sulfide (DMS), which is emitted from phytoplankton and outgassed into the atmosphere above the sea surface. In the atmosphere, DMS is oxidized in a series of steps which lead to the formation of non-sea-salt sulfate (NSS-SO_4^{2-}) and other sulfur-containing reaction products, such as methanesulfonic acid (CH_3SO_3H, MSA) [*Hynes et al*., 1986; *Yin et al*., 1986].

NSS-SO_4^{2-} can nucleate particles in the submicrometer size range which serve as cloud condensation nuclei (CCN) and influence the radiation balance of the atmosphere [*Charlson et al*., 1987]; thus extensive efforts have focused on elucidating the chemical and physical processes that lead to NSS-SO_4^{2-} particle formation from anthropogenic and biogenic sulfur sources. Biogenic sources are particularly important in the marine boundary layer of remote oceanic regions [*Andreae et al*., 1995; *Berresheim et al*., 1993; *Charlson et al*., 1987].

Sea-salt particles may act as seeds for the uptake and oxidation of sulfur gases and deposition of condensable sulfate vapors [*Keene et al*., 1998; *McInnes et al*., 1994; *O'Dowd et al*., 1997]. Sea salt may also strongly influence the oxidative properties of aerosol particles in the marine boundary layer through the production of halogen radicals [*Fan and Jacob*, 1992; *Finlayson-Pitts et al*., 1989; *Graedel and Keene*, 1995; *Keene et al*., 1996; *Pszenny et al*., 1993; *Sander and Crutzen*, 1996; *Vogt et al*., 1996]. These transient radical oxidants may have an effect on the biogenically emitted DMS and the speciation of trace metals.

Owing to the intricate chemistry of marine aerosols it appears essential to present all available chemical and physical information of the sampled aerosol particles when trying to interpret observed Fe(II) concentrations. In the present study we will present trace metal data along with anion and cation abundances since some of them may be directly or indirectly coupled with the iron speciation. Furthermore, these additional species elucidate the sources and source strengths of the sampled aerosol.

2. Sample Collection and Analysis

2.1. Sampling Location and Period

Samples were collected aboard the R/V *Seward Johnson* during a month-long cruise from Barbados (13.2°N, 59.5°W) to

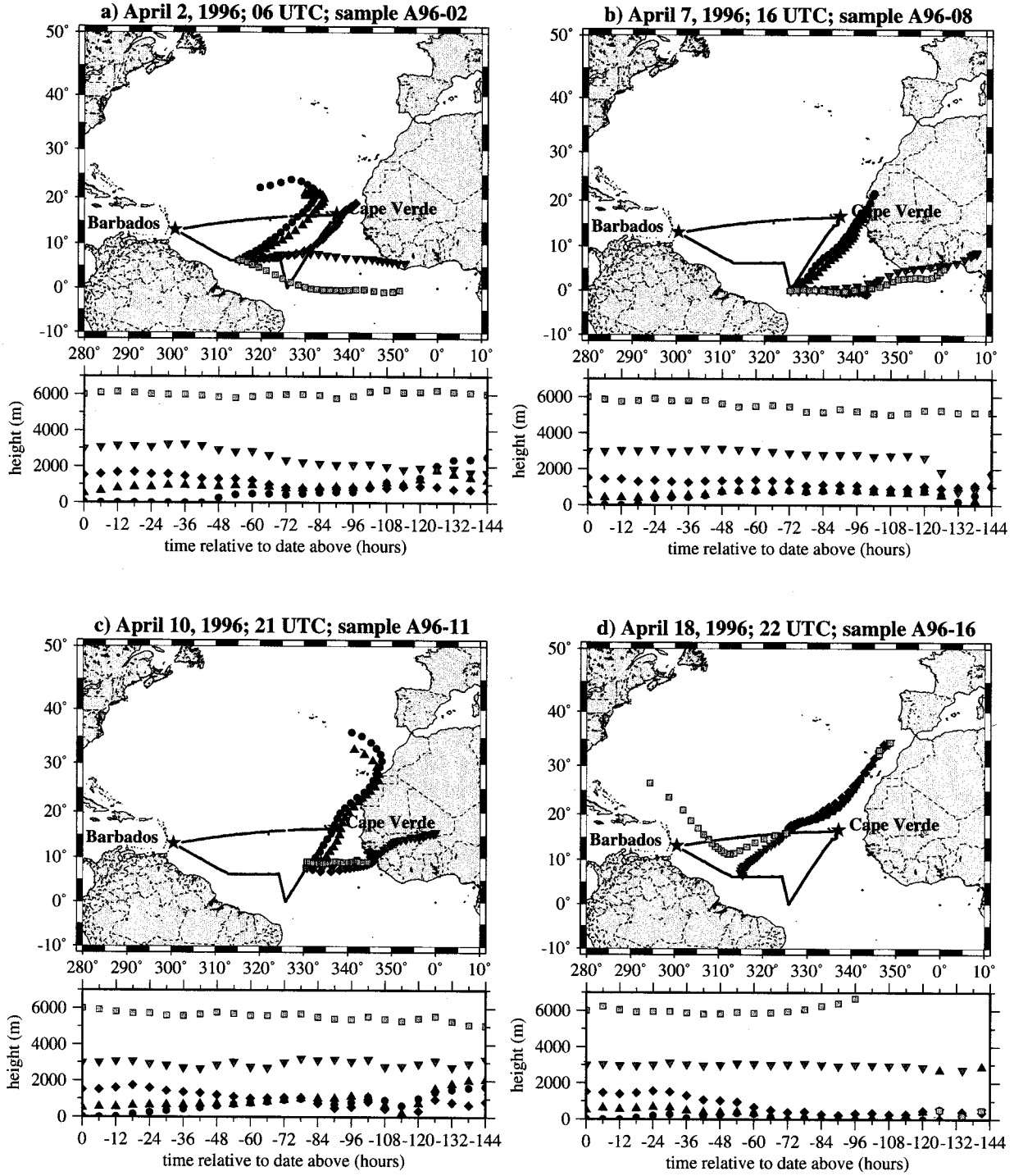

Figure 1. Six-day air mass back trajectory calculations at five different final elevations (circles, 20 m; triangles, 500 m; diamonds, 1500 m; inverted triangles, 3000 m; and squares, 6000 m) above sea level for (a) April 2, 1996; (b) April 7, 1996; (c) April 10, 1996; and (d) April 18, 1996.

Cape Verde (16.8°N, 23°W) and back to Barbados. The cruise track is outlined in Figure 1, where the southern track was initiated in Barbados on March 28, 1996; it intercepted the equator and ended in Cape Verde on April 13, 1996. The return to Barbados did not backtrack the same trace; instead, it followed a direct trajectory from Cape Verde to Barbados where it ended on April 26, 1996.

Six-day isentropic air mass back trajectories were calculated with the HYSPLIT trajectory model [*National Oceanic and Atmospheric Administration* (*NOAA*), 1997]. Although errors associated with these calculations are not reported with the HYSPLIT model, it can be assumed that they are considerable, especially the longer the back calculation is. On the basis of literature reports on the transport mechanism of African dust across the Atlantic Ocean [*Bergametti et al*., 1989; *D'Almeida*, 1986; *Prospero and Carlson*, 1972; *Prospero and Nees*, 1977;

Schütz, 1980; *Ellis and Merrill*, 1995], five different elevations were chosen for the trajectory calculations: 20, 500, 1500, 3000, and 6000 m. It is known that long-range transport of dust from the African deserts occurs at a high altitude, in the Saharan air layer (SAL), between 1.5 and 5–7 km.

The highest dust loadings at high altitudes are expected to occur during summer due to the temperature-dependent upward motion of dust-laden air [*Chiapello et al*., 1997]. However, on the basis of high-resolution radiometer aerosol optical thickness data collected over 4 years, *Swap et al*. [1996] found that dust outbreaks are most frequent and extensive during the first 6 months of the year, with an annual peak in outbreak activity observed during February through April.

Dust transport from Africa occurs throughout the year, but the source regions and main transport pathways change in concert with movements of the Inter-Tropical Convergence Zone (ITCZ) [*D'Almeida*, 1986; *Prospero et al*., 1981]. This seasonal north to south shift in dust storm activity in Africa from summer to winter has further been deduced from mineralogical signatures of the collected dust samples [*Arimoto et al*., 1995; *Bergametti et al*., 1989; *Chiapello et al*., 1997; *Delaney et al*., 1967; *Glaccum and Prospero*, 1980; *Schütz and Sebert*, 1987].

Thus, during the month of April, when our sampling took place, the seasonal shift to the north had initiated, and we expect the transport to take place from the northwestern part of the Sahara. The air mass back trajectories in Figure 1, however, present a more complex picture of the air mass origins during the month of April. Initially (Figure 1a), lower-altitude trajectories seem to sweep around from the western Atlantic, while they change their origin toward northwest Africa and even southern Europe for the remainder of the cruise (see Figures 1b–1d). The higher-elevation trajectories also vary significantly throughout the cruise. A similar trajectory pattern has been observed by *Talbot et al*. [1990] and *Swap et al*. [1992] during the month of April 1987. The 4 days depicted in Figure 1 are representative for the different weather patterns encountered in the present study and are further discussed in section 4.

2.2. Aerosol Collection

Ambient aerosol samples were collected with two collector types. A high-volume dichotomous virtual impactor (HVDVI) served for the collection of trace metals in two size fractions ($D_{p,50}$ = 3.0 μm), analogous to sampling performed in other studies from our laboratory [*Johansen et al*., 1999; *Siefert et al*., 1999]. This collector was built of polycarbonate with nylon screws in order to minimize trace metal contamination. Its total flow rate amounted to 335 ± 15 L min^{-1}, whereby the fine and coarse sample fractions were collected on two 90 mm diameter Teflon filters (Gelman Zefluor, 1 μm pore size). Total elemental composition, Fe(II) concentrations, and anion and cation abundances were determined from those fine and coarse filter samples.

Two low-volume collectors, running at flow rates of 27 L min^{-1}, were used for gravimetric analyses and for collection of total aerosol mass to be used in future experiments. For the low-volume collectors, inverted high-density polyethylene 2 L bottles served as rain shields for the Nucleopore polycarbonate filter holders which were loaded with acid-cleaned 47 mm diameter Gelman Zefluor filters (1 μm pore size). Anion and cation concentrations of *Johansen et al*. [1999] were determined from aqueous extractions of the corresponding low-volume filters, while in the present study, anions and cations were leached from the high-volume filters. This modification seemed appropriate since sampling efficiencies of the two collector types appeared to vary substantially, especially for large particles and at high wind speeds [*Johansen et al*., 1999].

The aerosol collectors and laboratory equipment were acid-cleaned before use by following similar procedures as outlined by *Patterson and Settle* [1976] employing ultrapure acids from Seastar Chemicals (Sidney, British Columbia, Canada) and 18.2 MΩ cm Milli-Q UV water. After Fe(II) analysis the remaining filter portions were stored in acid-cleaned polystyrene petri dishes sealed with Teflon tape, placed inside two plastic bags and a Tupperware container and stored in a refrigerator during the cruise. After the cruise the filters were sent back to the laboratory (via air freight, on dry ice) and stored in a freezer until analysis.

A sector sampling system controlled the operation of all the pumps, thereby stopping all aerosol collectors simultaneously when wind speed or wind direction were out of sector. The data logger was programmed to shut the pumps off when the wind speed was $\leq$0.2 m s^{-1} and when the relative wind direction was ±60° off of the bow of the ship. In general, samples represent daily averages, but owing to the ship's cruise track, actual sampling duration may vary.

The sampling characteristics of the HVDVI are such that ~10% of the fine particles end up on the coarse filter. This correction has been accounted for in all coarse concentrations reported in this study. As a result, errors associated with the coarse fraction, especially for species that are present in low concentrations in the coarse fraction (e.g., NSS-SO_4^{2-}, MSA, NH_4^+), may be considerably large. This needs to be kept in mind when computing ratios such as the bio-SO_4^{2-}/MSA ratio for the coarse fraction.

2.3. Chemical Analysis

2.3.1. Fe(II) analysis performed on board the ship. Several fractions of labile Fe(II) in both the fine and coarse particle fractions were determined by a sequential extraction procedure. These measurements were initiated immediately (within 1 hour) after sample collection to minimize possible oxidation of Fe(II) otherwise conceivable to occur during sample storage. Extraction and analytical procedures are described in detail by *Siefert et al*. [1999]. Three labile fractions of Fe(II) were determined in both the fine and coarse particle size fractions. The first portion of Fe(II) was released into a 4.2 pH formate buffer after 30 min of leaching; this portion is denoted as aqueous Fe(II) ($Fe(II)_{aq}$). Ferrozine was then added to the leaching solution containing the filter, and an absorption reading was made after 5 min. The additional Fe(II) released during this step is the 5-min ferrozine-Fe(II) ($Fe(II)_{FZ,5min}$). One last absorption reading was made after the ferrozine had 22 hours to act upon the filter containing the aerosol, producing a third Fe(II) fraction: 22-hour ferrozine-Fe(II) ($Fe(II)_{FZ,22hr}$). The sum of all three Fe(II) fractions determined in such manner is defined as total 22-hour Fe(II) ($Fe(II)_{total,22hourFZ}$). However, owing to the possibility of a bias introduced through the reduction of Fe(III) by ferrozine after 22 hours, it appears more accurate to define a labile Fe(II) fraction that is composed of the first two extractable portions only, thus excluding the 22-hour reading. It is this amount of Fe(II), defined as total 5-min FZ-Fe(II) ($Fe(II)_{total,5minFZ}$), which will be used preferentially when discussing the amount of Fe(II) leached out of the aerosol material.

2.3.2. Elemental analysis. Elemental analysis of 32 elements (Na, Mg, Al, K, Ca, Sc, Ti, V, Cr, Mn, Fe, Ni, Cu, Zn,

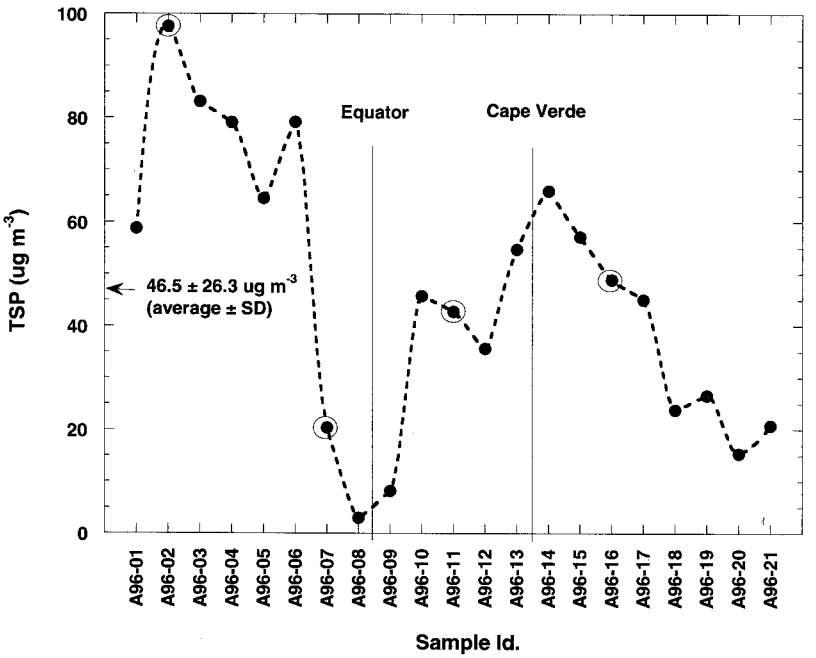

Figure 2. Total suspended particulates (TSP) versus sample identification (ID). Circled symbols represent samples for which air mass back trajectories are shown in Figure 1.

Ga, Ge, As, Se, Mo, Ru, Cd, Sn, Sb, Cs, Ba, La, Ce, Sm, Eu, Hf, Pb, and Th) was performed on the high-volume filters with an HP 4500 inductively coupled plasma–mass spectrometer (ICP-MS). The filter digestion technique is described by *Siefert et al*. [1999].

2.3.3. Ion analysis and gravimetric determination. For the ion analysis a small section of the high-volume filter was cut out, wetted with ~0.1 mL ethanol and then extracted overnight in 10 mL Milli-Q UV water. Anions were separated and quantified with a Dionex Bio LC ion chromatograph (IC) using an IonPac AS11 separator column and the corresponding AG11 guard column. Organic and inorganic anions were eluted with a gradient pump and a combination of four eluents (5 m*M* NaOH, 100 m*M* NaOH, 100% MeOH, MQ H_2O) whereby the NaOH concentration was ramped from an initial 0.45 m*M* to a final 34.25 m*M*. Inorganic anions that were quantified included fluoride, chloride, nitrite, bromide, nitrate, and sulfate and the organic anions acetate, glycolate, formate, methanesulfonate, and oxalate. Propionate, pyruvate, succinate, fumarate, phthalate, phosphate, and citrate were not detected.

Cations were separated and quantified isocratically with a DX 500 ion chromatograph (IC) with IonPac CS12/CG12 analytical and guard columns and a 20 m*M* MSA eluent. Sodium, ammonium, potassium, magnesium, and calcium concentrations were determined.

Daily average total suspended particulate (TSP) mass was determined by the difference in filter weights (equilibrated to 21°C and 50% relative humidity (RH)) before and after collection on the low-volume filters.

2.4. Statistical Analysis

Plotted error bars represent the standard deviation calculated through propagation of error in every parameter used. Estimated errors in the volume of air sampled, the filter section cut, the volume of the extraction solution, etc., were assumed to be 10%. Average concentrations reported throughout this study are accompanied by the standard deviation of the sample population.

In addition to interpreting the data based on an element's enrichment compared to a crustal tracer [*Taylor and McLennan*, 1985] (i.e., enrichment factor analysis), a multivariate statistical analysis was performed using SPSS software [*SPSS, Inc*., 1997] (i.e., principal component analysis). The principal component analysis was performed on the whole data set to learn about the source characteristics that make up the sampled aerosol material and to learn about possible correlations between certain chemical species. In a principal component analysis the correlation matrix of the observed variables is examined to reduce the number of descriptive variables into a smaller set of independent variables, the principal components. The principal components are orthogonal to each other and can be rotated in space to simplify interpretation of the data set. A common type of rotation is the Varimax rotation, during which orthogonality is retained. All principal components in the present study are Varimax rotated.

A principal component in this study can represent a source, such as crustal material, sea salt, and anthropogenic pollutants. An observed variable will display a number close to 1 if it correlates with the principal component; thus two variables with numbers close to 1 in one component correlate with each other. For example, the crustal component will exhibit values close to 1 for Al and other crustal elements, while the sea-salt component will exhibit values close to 1 for variables that are characteristic for sea salt, such as Na^+, Cl^-, and wind speed.

3. Results

3.1. Total Suspended Particulates (TSP)

Total suspended particulates (TSP) were determined for each of the low-volume filters. Figure 2 represents TSP as a function of sample. The abscissa in this and all analogous

Table 1. Average, Minimum, and Maximum Atmospheric Trace Metal and Ion Concentrations in Coarse, Fine, and Total Aerosol Fractions

	Coarse			Fine			Total		
Element	Average ± SD	Min	Max	Average ± SD	Min	Max	Average ± SD	Min	Max
Na, $\mu g\ m^{-3}$	1.99 ± 1.22	<0.0025	5.72	1.19 ± 0.58	0.15	2.21	3.18 ± 1.63	<0.15	7.63
Mg, $\mu g\ m^{-3}$	0.35 ± 0.22	<0.0002	0.92	0.25 ± 0.14	0.024	0.54	0.60 ± 0.33	<0.025	1.25
Al, $\mu g\ m^{-3}$	0.75 ± 0.66	<0.0004	2.19	0.79 ± 0.71	0.006	2.55	1.55 ± 1.32	<0.006	4.45
K, $\mu g\ m^{-3}$	0.22 ± 0.15	0.0021	0.52	0.19 ± 0.12	0.003	0.46	0.41 ± 0.25	0.0047	0.81
Ca, $\mu g\ m^{-3}$	0.42 ± 0.31	0.0015	1.25	0.26 ± 0.18	0.0024	0.64	0.68 ± 0.46	0.0039	1.67
Sc	0.13 ± 0.11	<0.002	0.35	0.14 ± 0.11	0.013	0.41	0.27 ± 0.21	<0.015	0.72
Ti	49.4 ± 38.8	<0.12	139	54.9 ± 42.5	7.52	152	104 ± 78.8	<7.64	291
V	1.02 ± 0.80	0.098	2.58	1.54 ± 1.03	0.18	3.42	2.57 ± 1.78	0.29	5.63
Mn	8.07 ± 6.91	<0.009	23.8	8.62 ± 7.49	0.88	26.8	16.7 ± 13.8	<0.89	45.6
Fe, $\mu g\ m^{-3}$	0.42 ± 0.36	<0.0008	1.04	0.43 ± 0.37	0.035	1.4	0.84 ± 0.61	<0.053	2.38
Zn	2.11 ± 1.18	0.62	4.64	5.59 ± 3.50	1.58	12.7	7.69 ± 4.53	2.2	16.4
Ga	0.33 ± 0.27	<0.0016	0.83	0.37 ± 0.30	0.025	1.15	0.67 ± 0.54	<0.027	1.85
Cs	0.041 ± 0.032	<0.0005	0.096	0.040 ± 0.031	0.004	0.116	0.081 ± 0.06	<0.004	0.197
Ba	5.18 ± 4.06	<0.018	11.5	5.19 ± 4.49	0.39	17.9	10.4 ± 8.0	<0.40	28
La	0.40 ± 0.35	<0.001	1.19	0.43 ± 0.41	0.029	1.4	0.84 ± 0.74	<0.042	2.53
Ce	0.82 ± 0.76	<0.0006	2.52	0.93 ± 0.91	0.055	3.15	1.75 ± 1.62	<0.089	5.37
Sm	0.07 ± 0.06	<0.001	0.2	0.07 ± 0.07	0.007	0.27	0.14 ± 0.13	<0.008	0.42
Eu	0.015 ± 0.013	<0.001	0.044	0.015 ± 0.014	<0.001	0.049	0.030 ± 0.026	<0.003	0.09
Hf	0.039 ± 0.027	<0.002	0.11	0.041 ± 0.028	0.006	0.11	0.080 ± 0.051	<0.053	0.2
Pb	0.29 ± 0.19	<0.003	0.6	0.72 ± 0.46	0.12	1.69	1.01 ± 0.59	<0.12	2.25
Th	0.11 ± 0.09	0.005	0.3	0.11 ± 0.09	0.01	0.32	0.21 ± 0.18	0.015	0.61
F^-	9.45 ± 15.27	0.97	71	7.07 ± 5.52	1.39	22.1	16.6 ± 18.1	3.64	83.8
NSS-F^-	9.25 ± 15.27	0.82	70.8	6.92 ± 5.51	1.2	22	16.2 ± 18.1	3.22	83.4
Br^-	4.78 ± 5.56	1.04	23.2	3.05 ± 1.43	1.32	5.39	7.83 ± 6.34	2.36	26.6
NSS-Br^-	−7.69 ± 6.32	−20	4.08	−4.66 ± 3.83	−11.3	2.88	−12.4 ± 9.17	−27.6	5.03
Cl^-, $\mu g\ m^{-3}$	3.14 ± 2.16	0.24	10.5	1.66 ± 0.89	0.16	3.3	4.80 ± 2.69	0.42	13.7
NSS-Cl^-, $\mu g\ m^{-3}$	−0.45 ± 0.40	−1.61	−0.11	−0.56 ± 0.42	−1.08	0.79	−1.01 ± 0.49	−2.35	−0.28
SO_4^{2-}, $\mu g\ m^{-3}$	0.65 ± 0.38	0.07	1.63	1.20 ± 0.60	0.19	2.35	1.82 ± 0.90	0.26	3.67
NSS-SO_4^{2-}, $\mu g\ m^{-3}$	0.15 ± 0.16	0.003	0.47	0.88 ± 0.51	0.14	1.99	1.03 ± 0.60	0.15	2.46
NO_3^-, $\mu g\ m^{-3}$	0.32 ± 0.16	<0.11	0.74	0.36 ± 0.12	<0.21	0.57	0.67 ± 0.27	<0.24	1.32
Glycolate	8.59 ± 9.04	<3.18	41.3	7.46 ± 3.09	<2.50	13.2	16.3 ± 11.3	<5.7	51.4
MSA	4.82 ± 3.58	0.98	16.4	22.0 ± 10.1	4.55	43.1	26.8 ± 9.5	8.15	46.9
Oxalate	18.6 ± 10.4	<5.03	38.7	31.5 ± 19.9	<7.0	68.9	52.2 ± 29.9	<12.4	100.8
NH_4^+	34.4 ± 13.9	8.47	61.5	141 ± 53	49	260	175 ± 62	68.5	299
Na^+, $\mu g\ m^{-3}$	2.00 ± 1.23	0.22	6.16	1.24 ± 0.57	0.18	2.36	3.24 ± 1.67	0.44	8.52
K^+	90.6 ± 45.5	24.5	247	91.2 ± 38.1	26.2	161	182 ± 75	65.7	408
Mg^{2+}	247 ± 140	43.8	725	156 ± 65	33.7	265	402 ± 189	79.3	990
Ca^{2+}	381 ± 302	10	1170	224 ± 168	8	554	605 ± 442	20	1580
NSS-Ca^{2+}	304 ± 273	0	1040	177 ± 153	−15.5	480	481 ± 402	0	1390

Sample number is same for all 21 samples. Concentrations in $ng\ m^{-3}$ unless otherwise noted.

concentration plots is chosen to represent the discrete samples instead of a time or location variable. This is done for simplification of the plot since sampling intervals and locations varied significantly.

TSP appears to vary considerably over this part of the tropical North Atlantic Ocean during April 1996, the mean being 46.5 $\mu g\ m^{-3}$ with a standard deviation of 26.3 $\mu g\ m^{-3}$. The maximum of 97.6 $\mu g\ m^{-3}$ is observed on April 2 for sample A96-02 and the minimum of 3.0 $\mu g\ m^{-3}$ is observed on April 7 for sample A96-08, both on the southern leg of the cruise. A large number of studies exist on the mineral dust loadings in the same geographical area as investigated here, but since our gravimetrically determined masses are inclusive (a mixture of mineral, sea salt, and anthropogenic and biogenic aerosol), absolute values cannot be compared until each contribution is separated. Owing to the relatively constant wind speeds throughout the cruise (5.6 ± 2.3 $m\ s^{-1}$), the sea-salt contribution is expected to be fairly constant; thus the variability observed in TSP can be attributed to the mineral dust loadings. Sea-salt and mineral dust contributions will be determined in section 4.

3.2. Trace Metals

Elemental concentrations for 32 elements were determined by ICP-MS. Since four of the elements, As, Se, Ru, and Cd, were below detection limit for most of the samples, they are omitted from further discussion. Large background concentrations for a series of elements (Cr, Ni, Cu, Ge, Mo, Sn, and Sb) are attributed to contamination from the filter material and/or from the acids used during filter digestion. Thus these elements also had to be excluded from further analysis. Average concentrations with standard deviations, and minimum and maximum concentrations of the remaining 21 elements, are listed in Table 1.

Principal component analysis of these 21 elements reveals that the crustal tracer Al is very closely correlated with Mg, K, Ca, Sc, Ti, V, Mn, Fe, Ga, Cs, Ba, La, Ce, Sm, Eu, Hf, and Th in both the fine and the coarse fractions. The varimax rotated principal component matrix is presented in Table 2. Component 1 describes 77% of total variance in the data set and is characterized by high correlations between typical crustal tracers in the fine fraction; note the large (i.e., close to 1) values (in

parentheses). Of these elements, Mg, K, and Ca, seem to have an additional source since their component scores are not as close to 1 as for the other mentioned elements. Another potential source of Mg, K, and Ca is sea salt. Additional Ca sources include those of anthropogenic origin [*Hopke*, 1985] and additional crustal origin in the form of $CaCO_3$ (calcite) and $CaSO_4$ (gypsum). Although, as pointed out, component 1 is most notably characterized by a fine crustal source, it appears to include some of the coarse crustal portion, since the corresponding component scores are not insignificant.

Component 2 of this analysis describes 11% of the variance and is denoted as the coarse crustal source, although, as mentioned above, some of the coarse crustal portion already appears in component 1. Furthermore, indicative from the large value for coarse Na and coarse Mg, a strong coarse sea-salt portion is included in this component. The component scores for TSP indicate that components 1 and 2 are the major contributors to the total mass loadings observed. Concentration plots for the mentioned crustal elements follow the same trend, as expected. Figure 3a shows Al versus sample identification (ID), which is representative of the other crustal elements extracted in components 1 and 2 in the principal component analysis.

Component 3 exhibits large scores for coarse and fine Zn as well as fine Pb. These are typical anthropogenic tracers [*Duce et al*., 1975; *Huang et al*., 1996] emitted from smelters and during the combustion of leaded fuel. Coarse Ca, which can have an anthropogenic source in association with the combustion of coal, oil, and fuel [*Hopke*, 1985], appears to correlate slightly with this component. To visualize the contribution of this anthropogenic source, fine and coarse Zn are plotted in stacked bars in Figure 3b. There seems to be a relatively constant background concentration of total Zn of around 4 ng m^{-3}, overlain by a sudden increase in both the fine and coarse fractions during the latter part of the cruise. The Pb concentration plot, not shown, is clearly a combination of both the Al and the Zn plots: the first half of the cruise is identical in signature to Al and the latter half of the cruise, with exception of the last sample, displays the features of Zn. This indicates that Pb is not enriched over the crustal portion during the first part of the cruise but that later another source containing Pb and Zn becomes predominant. This is in accordance with decreasing Pb concentrations since 1970 observed by *Huang et al*. [1996], who compared Pb concentrations at Bermuda to other elements typically associated with pollutants, Zn and Sb. Air mass back trajectories suggest that the anthropogenic sources are located either in northwestern Africa or southern Europe; see Figures 1c and 1d.

The fourth component, and the last component in this analysis with a significant component score, may be representative of a fine sea-salt component. Note the large fine Na and wind speed scores. As the wind speed increases, the surface of the ocean is roughened, which leads to increased sea spray in the atmosphere. This is detected as larger sea-salt concentrations on the filters. Other sea-salt components such as Mg, K, and Ca display scores that are significant. The Na concentration plot is shown in Figure 3c. It needs to be pointed out that Na as presented here is the total Na concentration; therefore it includes sea-salt and crustal fractions. The water-soluble fractions of Na, Mg, K, and Ca are also determined and presented in section 4.

Table 2. Varimax Rotated Principal Component Matrix for Trace Metals for 21 Samples

	Component				
	1 Crustal, Fine	2 Crustal, Coarse	3 Anthropogenic Zn and Pb	4 Sea Salt, Fine (?)	5
Percent of variance	77.0	11.1	4.7	3.4	0.9
Na, coarse	−0.112	(0.795)	0.192	0.450	−0.258
Na, fine	0.400	0.388	−0.089	(0.796)	−0.065
Mg, coarse	0.128	(0.844)	0.343	0.272	−0.198
Mg, fine	(0.763)	0.444	0.098	0.446	0.048
Al, coarse	0.592	(0.788)	0.088	0.056	0.019
Al, fine	(0.927)	0.360	0.004	0.098	0.031
K, coarse	0.307	(0.865)	0.258	0.263	0.089
K, fine	(0.838)	0.416	0.088	0.323	0.075
Ca, coarse	0.192	(0.730)	0.533	0.265	0.216
Ca, fine	(0.775)	0.355	0.259	0.353	0.189
Sc, coarse	0.563	(0.795)	0.145	0.065	0.048
Sc, fine	(0.923)	0.358	0.054	0.117	0.032
Ti, coarse	0.614	(0.740)	−0.078	0.001	−0.106
Ti, fine	(0.857)	0.478	−0.074	0.055	−0.051
V, coarse	0.520	(0.804)	0.167	0.126	0.175
V, fine	(0.728)	0.475	0.293	0.276	0.254
Mn, coarse	0.614	(0.764)	0.057	0.077	−0.040
Mn, fine	(0.906)	0.361	−0.064	0.150	0.032
Fe, coarse	0.601	(0.768)	0.133	0.095	0.050
Fe, fine	0.924	0.344	0.077	0.128	0.024
Zn, coarse	−0.015	0.324	(0.862)	−0.232	−0.118
Zn, fine	−0.185	0.028	(0.944)	−0.065	−0.006
Ga, coarse	0.546	(0.791)	0.206	0.078	0.001
Ga, fine	(0.919)	0.344	0.066	0.139	0.050
Cs, coarse	0.481	(0.809)	0.214	0.175	0.172
Cs, fine	(0.890)	0.394	0.133	0.169	0.063
Ba, coarse	0.486	(0.783)	0.295	0.104	−0.010
Ba, fine	(0.902)	0.343	0.112	0.164	0.078
La, coarse	0.612	(0.771)	0.026	0.114	0.069
La, fine	(0.919)	0.378	−0.034	0.088	0.041
Ce, coarse	0.614	(0.775)	0.054	0.069	0.000
Ce, fine	(0.926)	0.362	−0.025	0.087	0.038
Sm, coarse	0.601	(0.777)	0.012	0.138	0.063
Sm, fine	(0.920)	0.374	−0.048	0.090	0.033
Eu, coarse	0.589	(0.782)	−0.014	0.136	0.083
Eu, fine	(0.912)	0.377	−0.041	0.114	0.045
Hf, coarse	0.554	(0.704)	−0.156	−0.129	−0.111
Hf, fine	(0.937)	0.232	−0.066	0.082	−0.148
Pb, coarse	0.388	(0.841)	0.124	0.103	0.120
Pb, fine	0.330	0.411	(0.732)	0.293	0.242
Th, coarse	0.579	(0.795)	0.025	0.116	0.065
Th, fine	(0.913)	0.383	−0.002	0.115	0.040
TSP	(0.621)	(0.668)	0.001	0.357	0.003
Wind speed	0.567	0.143	−0.353	(0.634)	0.198

Parentheses indicate large values (i.e., close to 1).

3.3. Fe and Fe(II)

Principal component analysis reveals that Fe closely tracks the crustal tracers in both fine and coarse fractions. When looking at the sequentially extracted Fe(II) contributions superimposed by the total coarse and fine Fe in Figures 4a and 4b, respectively, a weak correlation may be observed between the $Fe(II)_{total,22hourFZ}$ and the total Fe for both size fractions. The $Fe(II)_{aq}$ and $Fe(II)_{FZ,5min}$ contributions, which are the Fe(II) fractions of most interest for reasons explained above, do not appear to display obvious correlations with the total Fe concentrations. Samples A96-01, A96-02, and A96-21 were not analyzed for Fe(II) owing to time constraints aboard the ship during set up and dismantling of the laboratory equipment.

Absolute values for coarse-$Fe(II)_{total,5minFZ}$ range from 0 to

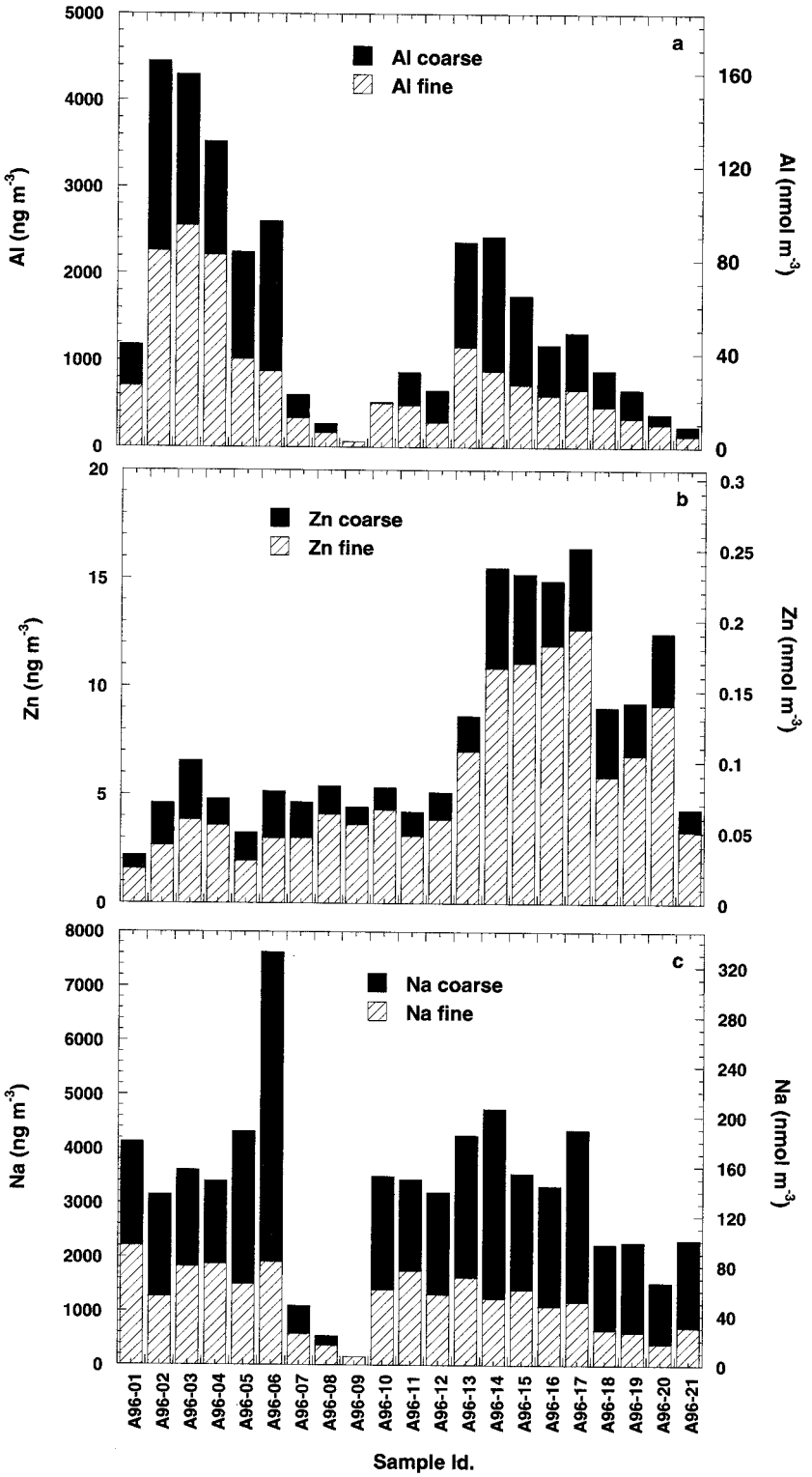

Figure 3. Coarse and fine fraction trace metal concentrations versus sample ID. for (a) Al, (b) Zn, and (c) Na.

1.14 ng m^{-3}, averaging 0.44 ± 0.31 ng m^{-3}. This represents relative contributions to total coarse Fe of 0 to 4.2%, with a geometric mean of 0.15 ± 0.96% (the geometric mean is preferred for this number since it is a ratio). Percentages are plotted in Figure 5, which shows that the maximum percentage of 4.2% is observed for sample A96-09, near the equator, when the coarse Fe concentration is at the detection limit encountered with the ICP-MS; see Figure 4a. Thus this percentage is associated with large errors and may be an outlier. A more reasonable value would be somewhere close to what samples A96-08 and A96-10 display in Figure 5. When recalculating the average percentage coarse-$Fe(II)_{total,5minFZ}$ in coarse Fe without sample A96-09, the geometric mean drops to 0.12 ± 0.19% and the maximum becomes 0.72%.

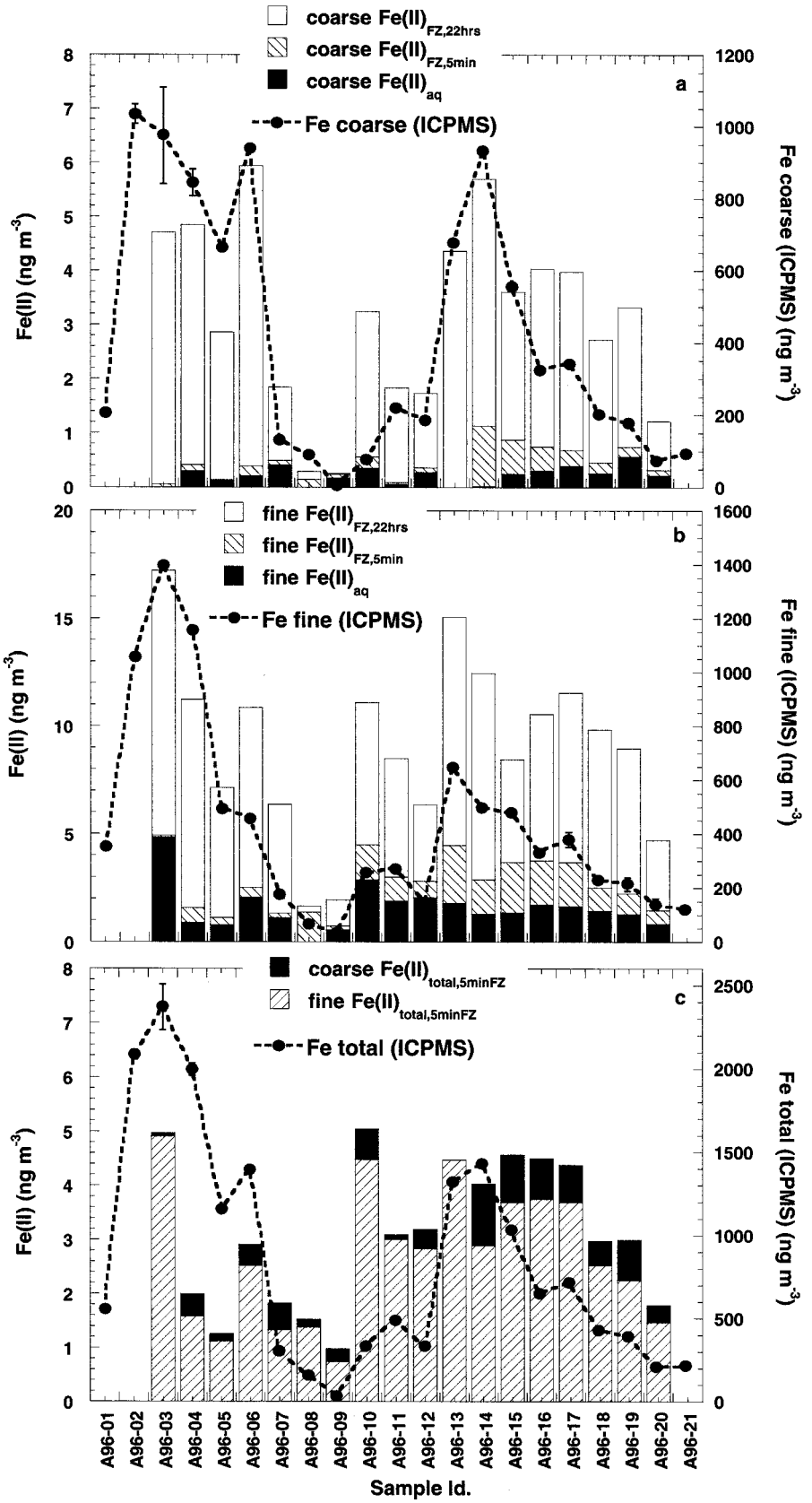

Figure 4. Fe(II) concentrations versus sample ID. (a) Fe(II) in the coarse fraction, (b) Fe(II) in the fine fraction, and (c) total Fe(II) released after 5 min in ferrozine (see text for details).

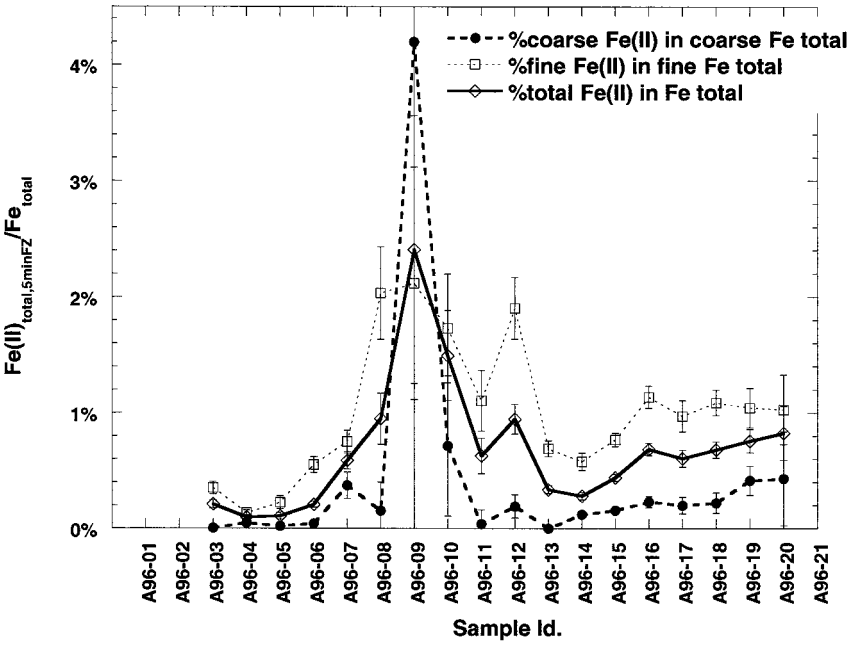

Figure 5. Relative Fe(II) concentrations (in percent of total Fe) versus sample ID for coarse, fine, and total Fe(II).

Fine $Fe(II)_{total,5minFZ}$ varies between 0.74 and 4.91 ng m^{-3} and averages 2.70 ± 1.27 ng m^{-3}. On average, this corresponds to an increase by a factor of 6 compared to the coarse $Fe(II)_{total,5minFZ}$. In other words, ~86% of the readily released Fe(II) is present in the fine Fe fraction. This is visualized in Figure 4c where the fine and coarse $Fe(II)_{total,5minFZ}$ fractions are plotted in stacked bars. Percentage-wise, the fine $Fe(II)_{total,5minFZ}$ varies between 0.14 and 2.12% of total fine Fe and displays a geometric mean of 0.82 ± 0.6%.

The effect of the larger amount of Fe(II) released from the fine fraction is not obliterated when relating the fine $Fe(II)_{total,5minFZ}$ to the combined coarse and fine Fe. Since Fe is almost evenly distributed between coarse and fine fractions, the average values being 419 ± 355 and 425 ± 366 ng m^{-3}, respectively, the effective fine and coarse percentages in total Fe are halved. This is also illustrated in Figure 5, where the percentage of total $Fe(II)_{total,5minFZ}$ in total Fe (the solid line) is roughly evenly spaced between the coarse and fine percentages, except for sample A96-09. When considering coarse and fine fractions together, the $Fe(II)_{total,5minFZ}$ amounts to 0.51 ± 0.56% (geometric mean) of the combined total Fe. If sample A96-09 is left out, the geometric mean becomes 0.46 ± 0.36%. The average total value for $Fe(II)_{total,5minFZ}$ is 3.14 ± 1.35 ng m^{-3}, with a minimum of 0.98 ng m^{-3} and a maximum of 5.05 ng m^{-3}.

Average fractions extracted during the sequential extraction procedure for the coarse and fine filters vary. It appears that the fine Fe(II) is more readily released than the coarse Fe(II). In the coarse fraction, 12 ± 15% are released in the first extraction, as opposed to 18 ± 8% in the fine fraction. In the second extraction an additional 7 ± 12% and 12 ± 18% are released in the coarse and fine fractions, respectively. This may be a function of the surface area of the particles, which would be larger for the fine fraction, but it may also be a result of differential weathering processes of the size fractions leading to the different compositions of Fe phases in the two size fractions. Because of differential deposition rates of coarse and fine fractions and their diverse transport histories, their chemical transformation pathways may also be significantly different, giving rise to varying levels of available Fe(II).

Ferrous iron levels observed in this study are in the same range as those found in an analogous study by our group [*Siefert et al*., 1999], which was carried out over the Indian Ocean. The total Fe(II) used by *Siefert et al*. [1999] included the third, 22 hour ferrozine fraction, while in this study we decided to concentrate on the first two Fe(II) fractions only; thus values need to be adjusted in order to be compared with each other. When considering the absolute values of Fe(II) extracted, they are very similar during the two cruises, but because the total Fe during the Indian Ocean cruise was larger than during the present cruise, the percentages are somewhat smaller. Thus, on average, 0.3% of Fe was present as $Fe(II)_{total,5minFZ}$ during the Indian Ocean cruise compared to 0.46% (A96-06 excluded) in the present study.

Compared to other studies performed over remote oceanic regions, results from this and our previous cruise [*Siefert et al*., 1999] are in the same range as found by *Zhu et al*. [1993, 1997] in Barbados. However, *Zhuang et al*. [1992a] reported considerable larger values (15%, corrected value, see *Zhu et al*. [1993]) of Fe(II) in Barbados. The absolute Fe(II) concentration is also larger by a factor of ~30. Because their samples had been stored over a considerable amount of time before analysis, chances exist that artifacts were introduced.

A new principal component analysis that includes Fe(II) and ions, while omitting some of the redundant trace metals from the principal component analysis in Table 2, is shown in Table 3. The main characteristics of each principal component remain the same as for the previous analysis. The fine Fe correlates with component 1, which represents predominantly the fine crustal source, while the coarse Fe correlates with component 2 and with component 1. The coarse and fine $Fe(II)_{total,22hrsFZ}$ which include the 22 hour ferrozine fractions

Table 3. Varimax Rotated Principal Component Matrix for Trace Metals and Ions for 21 Samples

	Component				
	1 Crustal, Fine Plus Some Coarse	2 Sea Salt Plus Some Crustal Coarse	3 Anthropogenic Zn and Pb and NSS-SO_4^{2-}	4 MSA/Sea Salt Fine	5 MSA Coarse
Percent of variance	59.0	17.2	8.2	4.9	2.7
Na, coarse	0.188	(0.927)	0.188	0.168	0.003
Na, fine	(0.675)	0.478	−0.062	(0.494)	−0.101
Mg, coarse	0.362	(0.787)	0.380	0.066	−0.057
Mg, fine	(0.913)	0.282	0.066	0.263	−0.067
Al, coarse	(0.753)	(0.547)	0.200	−0.035	−0.052
Al, fine	(0.988)	0.073	−0.021	0.022	0.009
K, coarse	0.539	(0.716)	0.348	0.145	−0.023
K, fine	(0.957)	0.206	0.060	0.170	−0.009
Ca, coarse	0.465	(0.545)	(0.620)	0.195	−0.097
Ca, fine	(0.919)	0.110	0.190	0.277	−0.108
Fe, coarse	(0.780)	(0.518)	0.206	−0.021	−0.093
Fe, fine	(0.988)	0.068	0.038	0.033	0.026
Zn, coarse	0.058	0.214	(0.844)	−0.274	0.179
Zn, fine	−0.140	0.019	0.897	0.003	0.128
La, coarse	(0.786)	(0.568)	0.140	0.019	−0.041
La, fine	(0.986)	0.092	−0.047	0.017	−0.002
Pb, coarse	0.590	(0.637)	0.221	−0.001	0.150
Pb, fine	0.503	0.229	(0.743)	0.307	0.016
Th, coarse	(0.751)	(0.611)	0.141	0.034	−0.040
Th, fine	(0.981)	0.109	−0.015	0.049	0.004
Fe(II), $coarse_{total,22hrsFZ}$	0.603	(0.641)	0.384	0.126	0.036
Fe(II), $fine_{total,22hrsFZ}$	(0.704)	0.313	0.301	0.349	0.291
Fe(II), $coarse_{total,5minFZ}$	−0.176	0.251	(0.743)	−0.149	−0.092
Fe(II), $fine_{total,5minFZ}$	0.375	0.143	0.348	(0.530)	0.452
Na^+, coarse	0.129	(0.945)	0.191	0.122	0.022
Na^+, fine	0.556	(0.634)	−0.095	(0.459)	−0.118
Mg^{2+}, coarse	0.126	(0.948)	0.184	0.114	0.037
Mg^{2+}, fine	(0.663)	(0.574)	−0.015	(0.408)	−0.070
K^+, coarse	0.286	(0.925)	0.082	0.097	0.087
K^+, fine	(0.765)	0.508	−0.153	0.062	−0.020
Ca^{2+}, coarse	0.481	0.543	(0.625)	0.188	−0.110
Ca^{2+}, fine	(0.864)	0.152	0.241	0.342	−0.129
NSS-Ca^{2+}, coarse	0.515	0.434	(0.664)	0.188	−0.128
NSS-Ca^{2+}, fine	(0.869)	0.073	0.280	0.308	−0.124
NH_4^+, coarse	0.068	(0.575)	0.290	(0.473)	0.404
NH_4^+, fine	0.093	0.371	(0.701)	0.255	−0.037
NO_3^-, coarse	0.109	(0.676)	(0.546)	0.373	0.051
NO_3^-, fine	0.400	(0.569)	0.383	0.391	−0.130
SO_4^{2-}, coarse	0.180	(0.864)	0.428	0.133	0.004
SO_4^{2-}, fine	0.387	0.427	0.523	(0.614)	−0.052
NSS-SO_4^{2-}, coarse	0.229	0.235	(0.872)	0.102	−0.046
NSS-SO_4^{2-}, fine	0.301	0.324	(0.648)	(0.596)	−0.030
MSA, coarse	−0.291	0.030	−0.133	−0.109	(0.825)
MSA, fine	0.237	0.303	0.143	(0.882)	−0.062
Cl^-, coarse	0.126	(0.945)	0.181	0.119	0.029
Cl^-, fine	(0.613)	(0.595)	−0.202	0.343	−0.147
Oxalate, coarse	−0.170	0.013	(0.936)	0.013	−0.002
Oxalate, fine	−0.147	0.204	(0.861)	0.166	−0.144
(Cation-anion), coarse	0.537	(0.554)	(0.552)	0.173	−0.162
(Cation-anion), fine	(0.877)	0.248	−0.170	0.170	−0.026
TSP	(0.792)	(0.530)	0.116	0.193	−0.108
Wind speed	(0.611)	0.091	−0.366	(0.602)	−0.142

Parentheses indicate large values.

correlate with the total Fe in the corresponding fractions; the coarse $Fe(II)_{total,22hrsFZ}$ correlates with component 2 and the fine $Fe(II)_{total,22hrsFZ}$ with component 1. This substantiates the observation previously made when visually comparing the ICP-MS Fe fractions with the $Fe(II)_{total,22hrsFZ}$ fractions in Figure 4. It is of interest to note that the $Fe(II)_{total,5min}$ fractions are not correlated with the first two crustal components, but rather with the anthropogenic component (component 3)

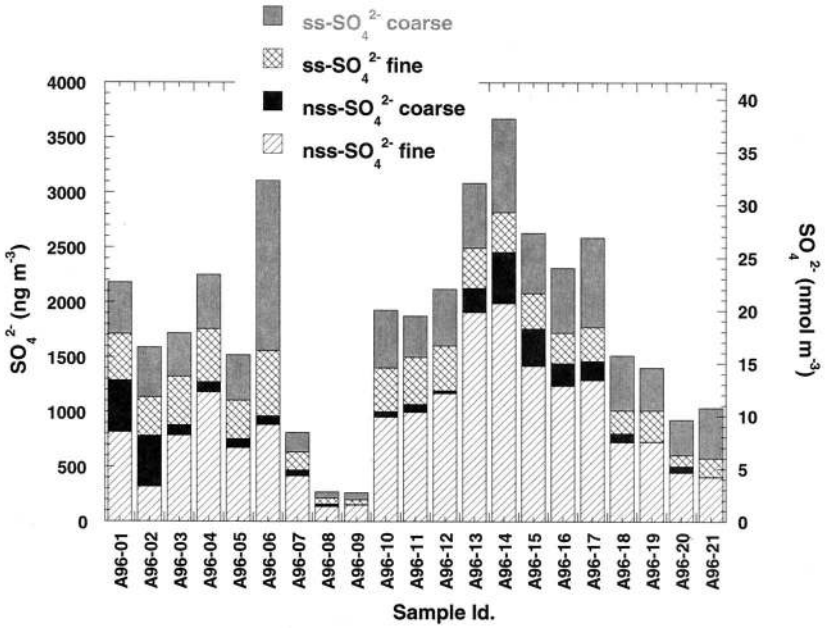

Figure 6. Sea-salt and non-sea-salt SO_4^{2-} contributions in coarse and fine fractions versus sample ID.

and component 4. The coarse $Fe(II)_{total,5min}$ correlates with component 3, which is high in coarse NO_3^-, NSS-SO_4^{2-} and oxalate, all typical anthropogenic tracers, which may have a direct effect on the speciation of Fe in the particle. The fine $Fe(II)_{total,5min}$ correlates with component 4, which may carry an anthropogenic and/or biogenic signature since the fine NSS-SO_4^{2-} scores are slightly elevated and the fine MSA scores are high. Thus it appears that the Fe(II) that is immediately released (after 5 min with FZ) is a function of constituents in the aerosol matrix with which it may have undergone chemical and photochemical reactions and/or it shares the same source as the anthropogenic component, while the combined Fe(II) (released after 22 hours in FZ) is more a function of the total Fe available in the aerosol phase.

3.4. Anions

Table 1 lists the average ± one standard deviation (SD), minima and maxima of each ionic species determined in the coarse and fine filter fractions. Inorganic anions measured include F^-, Cl^-, Br^-, NO_3^-, and SO_4^{2-}. Although NO_2^- was detected in a few of the samples, values are very close to the detection limit and are therefore excluded from further analysis. Sea-salt (SS) and non-sea-salt (NSS) contributions to F^-, Cl^-, Br^-, and SO_4^{2-} are determined from measured Na^+ concentrations and the constant ratio of these species expected in seawater [*Millero and Sohn*, 1992].

Of the organic anions analyzed, acetate and formate appear to be impacted by occasional contamination that is also detected for the standards of these species and occasionally in the blanks; thus acetate and formate are not considered further. Glycolate, methanesulfonic acid (MSA), and oxalate are quantified and listed in Table 1.

3.4.1. NSS-SO_4^{2-} and MSA. NSS-SO_4^{2-} is believed to be derived from anthropogenic sources as a result of the oxidation of anthropogenic SO_2, and from biogenic sources, from the oxidation of the biogenically emitted dimethylsulfide (DMS). Average NSS-SO_4^{2-} concentrations observed in the present study, 1.03 ± 0.60 $\mu g\ m^{-3}$, are on the same order of magnitude as reported in numerous other investigations performed in the same area [*Davison et al*., 1996; *Harrison et al*., 1996; *Li-Jones and Prospero*, 1998; *Savoie et al*., 1989b]. This value is a factor of 2 above what is observed in typical remote oceanic regions [*Saltzman et al*., 1983], while the concentrations encountered near the equator, for samples A96-08 and A96-09, are much lower, around 0.15 $\mu g\ m^{-3}$. On average, 23% of the total SO_4^{2-} detected in the coarse fraction is non-sea-salt-derived while the corresponding number for the fine fraction is almost 3 times larger, 73%. Of the total NSS-SO_4^{2-}, 87% is present in the fine fraction. Figure 6 illustrates the various portions of SO_4^{2-} in coarse and fine fractions and the sea-salt and non-sea-salt contributions.

Since the operationally defined fine fraction in the present study has an aerodynamic upper particle diameter cutoff of 3 μm, the observed larger contribution of NSS-SO_4^{2-} to the fine fraction may arise from a combination of effects. NSS-SO_4^{2-} particles in the submicrometer size range, which serve as cloud condensation nuclei (CCN), are formed from gas-to-particle conversion, and sea-salt aerosol in the 2–10 μm range, with a peak production in droplets of 4 μm diameter [*Sievering et al*., 1992], may act as seeds for the uptake and oxidation of sulfur gases and deposition of condensable sulfate vapors [*Keene et al*., 1998; *McInnes et al*., 1994]. Both of these mechanisms add NSS-SO_4^{2-} to the fine particle fraction, but only the production of new CCN has an influence on the radiation balance of the atmosphere [*Charlson et al*., 1987], while the deposition of low vapor pressure S-containing gases onto preexisting hygroscopic sea-salt particles removes S gases that could potentially have been transformed into CCN [*O'Dowd et al*., 1997].

In addition to the presence of anthropogenic NSS-SO_4^{2-}, biogenic sources of sulfur that contribute to NSS-SO_4^{2-} are particularly important in the marine boundary layer of remote oceanic regions [*Andreae et al*., 1995; *Berresheim et al*., 1993; *Charlson et al*., 1987]. MSA is one of the oxidation products of DMS that is used as a surrogate for the biogenically derived NSS-SO_4^{2-} (bio-SO_4^{2-}). Since MSA has a low vapor pressure, it

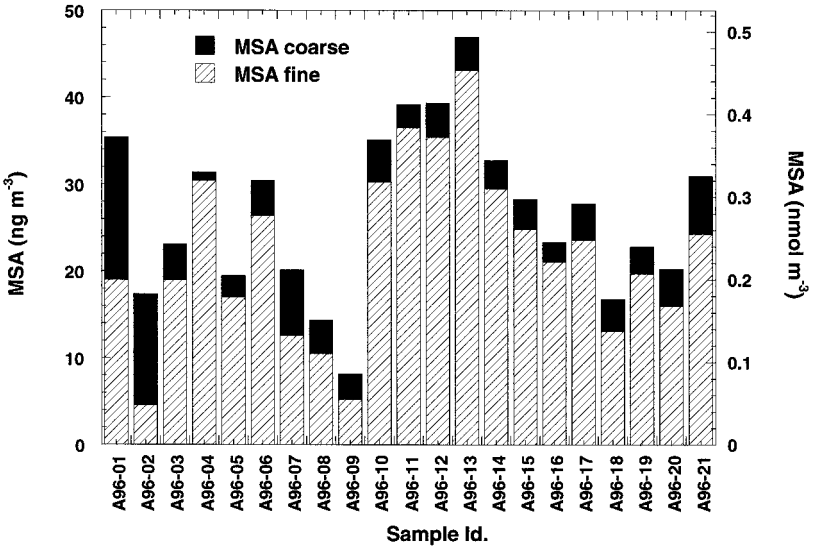

Figure 7. MSA concentrations in coarse and fine fractions versus sample ID.

partitions readily into the particle phase and is therefore easily sampled. Furthermore, it is believed that the only determining factor of the bio-SO_4^{2-}/MSA ratio is temperature [*Hynes et al*., 1986] (see introductory section of *Johansen et al*. [1999] for a more detailed discussion on this issue). Owing to MSA's low vapor pressure and the presence of sea-salt particles in the marine environment, MSA has been found to be distributed on larger particles, in the micrometer size range, presumably as a function of sea-salt aerosol surface area [*Kerminen et al*., 1997; *O'Dowd et al*., 1997; *Pszenny*, 1992; *Qian and Ishizaka*, 1993; *Quinn et al*., 1993].

MSA concentrations in both fine and coarse fractions are shown in Figure 7. On average, 79% of the MSA is present in the fine (<3 μm diameter) size fraction. This is in agreement with what has been seen by the investigators mentioned above. Total MSA concentrations vary from 8.15 to 46.9 ng m^{-3} and average 26.8 $\pm$ 9.5 ng m^{-3}. In a recent study performed in Barbados, *Li-Jones and Prospero* [1998] observed concentrations of MSA which ranged from 7 to 33 ng m^{-3} with a mean of 22 ng m^{-3}. Other reported values for MSA over the Atlantic Ocean are also in close agreement with ours [*Bürgermeister and Georgii*, 1991; *Davison et al*., 1996; *Ellis et al*., 1993; *Huebert et al*., 1996; *Putaud et al*., 1993].

In Table 3, fine MSA correlates somewhat with fine NSS-SO_4^{2-} in component 4, while coarse MSA, which makes up only 1/5 of the total MSA, appears in component 5 without another significant correlation. Fine NSS-SO_4^{2-} is almost equally split between components 3 and 4, whereby component 3 is anthropogenic and component 4 is possibly biogenic since MSA is used as a tracer for bio-SO_4^{2-}.

It is important to identify and quantify each contributing source of SO_4^{2-} in order to accurately determine its biogenic portion. Sea salt is one source that can be subtracted from the total SO_4^{2-} with precision owing to the known SO_4^{2-}/Na^+ ratio in seawater and the measured Na^+ concentration. Other sources, such as anthropogenic, biogenic, and crustal (in the form of $CaSO_4$ and/or $CaCO_3$), demand an analogous such tracer for which the corresponding ratio can be determined in a multivariate linear regression analysis. This procedure was carried out by *Johansen et al*. [1999] and proved to be very effective in determining the relative contributions of SO_4^{2-}. In our previous study [*Johansen et al*., 1999], Pb was used as the surrogate for anthropogenic SO_4^{2-}, MSA for biogenic SO_4^{2-}, Na^+ for SS-SO_4^{2-}, and NSS-Ca^{2+} for gypsum SO_4^{2-}. Analogous linear regression analyses are carried out in the present study and presented in section 4.

3.4.2. NO_3^- and organic acids. Total nitrate, as indicated in Table 1, varies from <0.24 to 1.32 μg m^{-3} with an average of 0.67 $\pm$ 0.27 μg m^{-3}. These values are in close agreement with observations by other investigators [*Berresheim et al*., 1991; *Davison et al*., 1996; *Ellis et al*., 1993; *Galloway et al*., 1993; *Harrison et al*., 1996; *Huebert et al*., 1996; *Li-Jones and Prospero*, 1998; *Savoie et al*., 1989b] carried out in the same region, where the low concentration corresponds to a clean marine atmospheric situation and the high concentration is typical for a somewhat polluted air mass.

Slightly more than half of the total NO_3^- (53%) is typically associated with the coarse particle fraction. This is in agreement with observations made by a series of investigators [*Bassett and Seinfeld*, 1984; *Berresheim et al*., 1991; *Huebert et al*., 1996; *Savoie and Prospero*, 1982; *Sievering et al*., 1990; *Sisterson*, 1989] that demonstrated that most NO_3^- is found in the supermicron mode associated with Na^+ and Cl^-, while most of the NSS-SO_4^{2-} is contained in the submicron mode. This is in strong contrast with the behavior of other anthropogenic tracers; their content is considerably higher in the fine than in the coarse fraction: almost 3 times as much NSS-SO_4^{2-} is present in the fine fraction, while the corresponding value of Zn is 2.6 and for Pb 2.5.

Figure 8 presents NO_3^- concentrations in stacked bars in both coarse and fine fractions. The coarse NO_3^- appears to vary more strongly than the fine NO_3^- throughout the cruise. In the principal component analysis in Table 3, both size fractions correlate somewhat with component 2, which is representative of the coarse crustal component and some sea salt. In addition, coarse NO_3^- correlates with component 3, which represents the anthropogenic source.

The mass ratio of NO_3^-/NSS-SO_4^{2-} has been used by some investigators [*Berresheim et al*., 1991; *Ellis et al*., 1993; *Li-Jones and Prospero*, 1998; *Prospero and Savoie*, 1989; *Savoie et al*.,

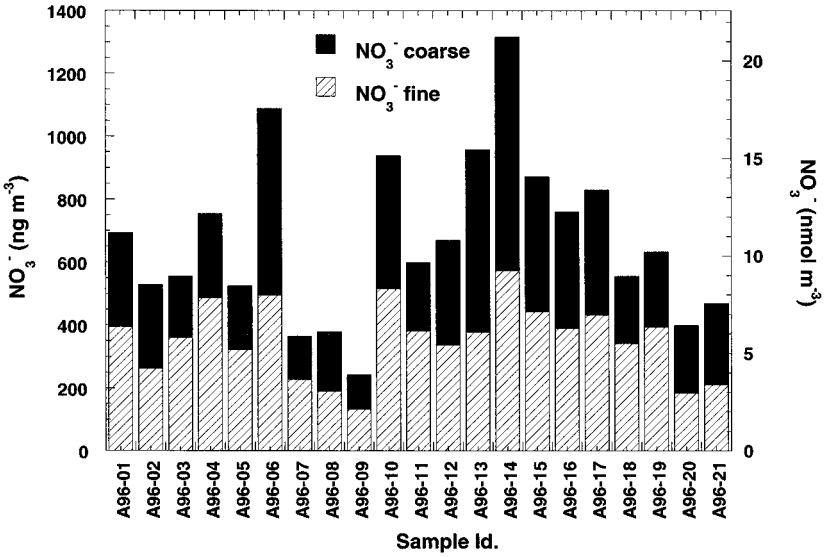

Figure 8. NO_3^- concentrations in coarse and fine fractions versus sample ID.

1989b] to identify the origin of the pollutant air masses. A ratio of 0.4 is typically found in European air masses, and ratios close to 1.1 have been observed in air masses that emerge from the southwest sub-Sahara. These reported values are not corrected for possible biogenic sources of NSS-SO_4^{2-}. When comparing with the analogous ratio in the present samples, we get a value of 0.5 for the combined coarse and fine concentrations, indicating a European origin. However, when treating coarse and fine fractions separately, we obtain 2.1 and 0.3, respectively. These values are associated with considerable scatter and do not seem reliable for the use of source identification.

Glycolate varies from <5.7 to 51.4 ng m^{-3} and averages 16.3 ± 11.3 ng m^{-3}. With exception of the sample with the maximum concentration, A96-18, and three samples with minimum concentrations near the equator (samples A96-08, A96-09, and A96-10), the rest of the samples display small variability.

Oxalate, plotted in Figure 9, on the other hand, displays a pattern comparable to that of Zn in Figure 3b. It also correlates both in the fine and coarse fractions with the anthropogenic component in the principal component analysis in Table 3. Total oxalate concentrations vary from <12.4 to 100.8 ng m^{-3} and average 52.2 ± 29.9 ng m^{-3}. About 60% of the total oxalate is present in the fine fraction. Oxalate is secondarily produced in the atmosphere by photochemically induced reactions involving organic precursors, and it is found to be the final dicarboxylic acid to accumulate during oxidation of larger diacids [*Kawamura and Ikushima*, 1993]. It is therefore expected to correlate with the anthropogenic component.

3.4.3. Halogens. Concentrations for F^-, Cl^-, and Br^- are summarized in Table 1 and plotted in Figures 10a, 10b, and 10c, respectively. Note the negative values for the NSS contributions of Cl^- and Br^- in Table 1. This indicates that Cl^- and Br^- are depleted relative to concentrations that are expected from observed Na^+ abundances. Fluoride, on the other hand, is highly enriched over the expected sea-salt contribution: 95.8 ± 3.4% (geometric mean) of total F^- is NSS. When

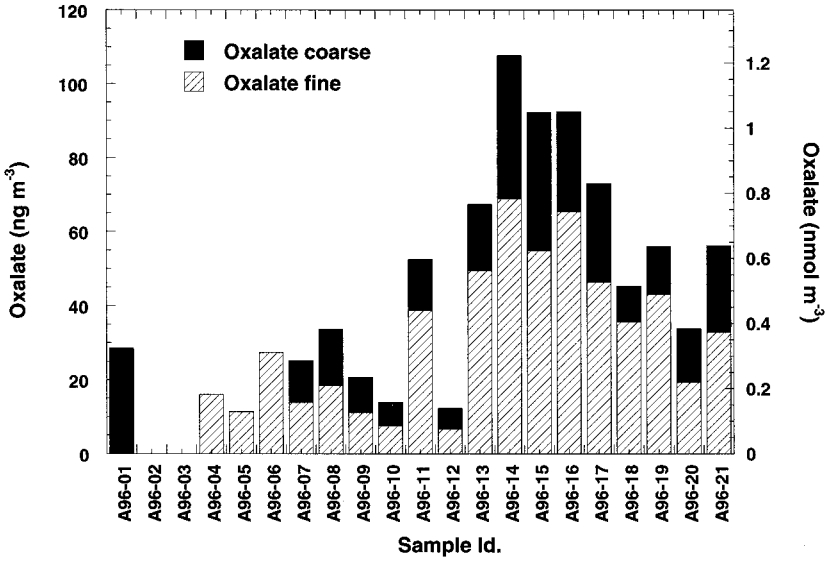

Figure 9. Oxalate concentrations in coarse and fine fractions versus sample ID.

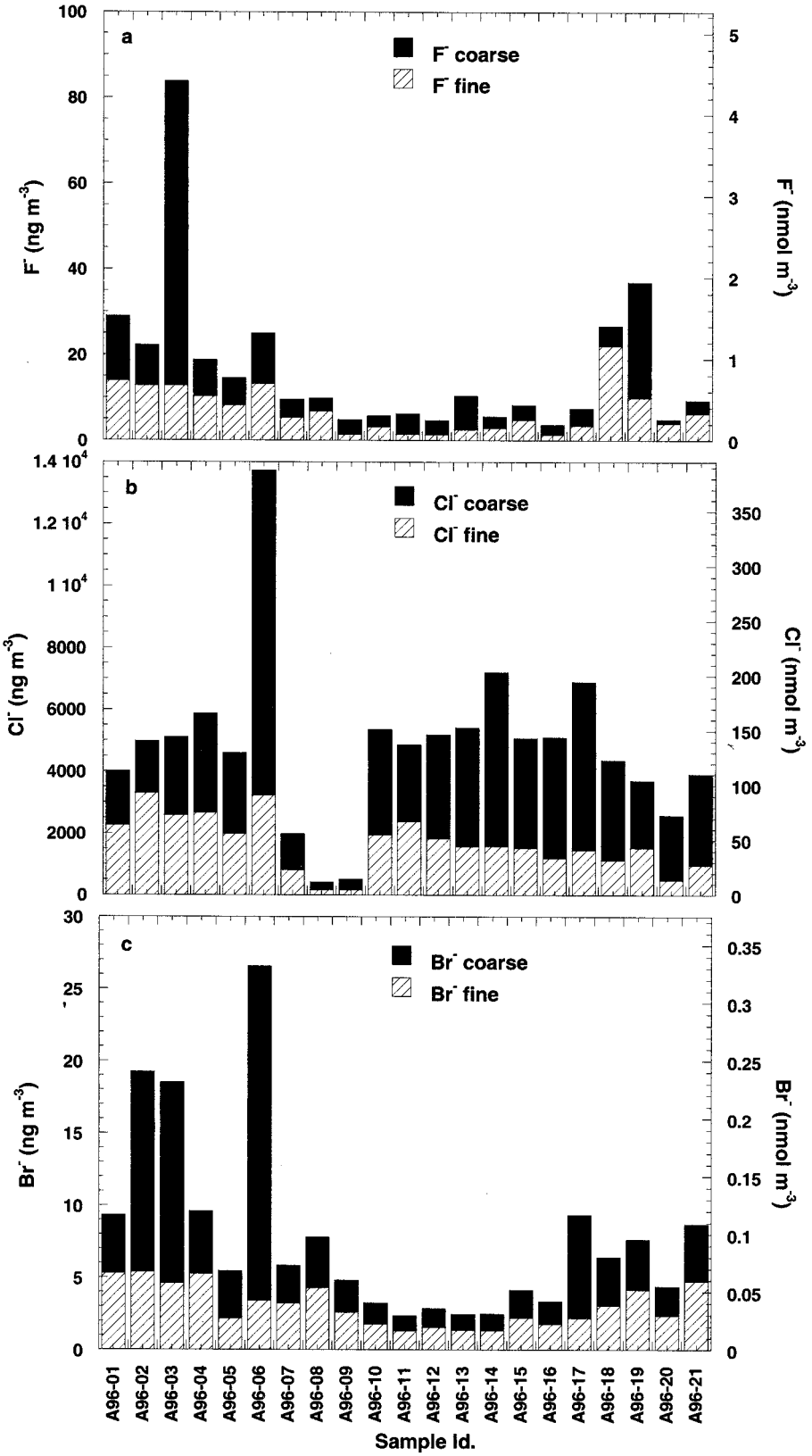

Figure 10. Halogen concentrations in coarse and fine fractions versus sample ID: (a) F^-, (b) Cl^-, and (c) Br^-.

included in the principal component analysis (not shown), coarse F^- correlates with the crustal component, while fine F^- anticorrelates with the fine MSA/sea-salt component. No obvious explanation is found for these observations.

Coarse Br^- correlates with the coarse sea-salt and crustal component (component 2) in the principal component analysis, showing its sea-salt origin. However, fine Br^- anticorrelates with the same component that fine F^- anticorrelates with,

the fine MSA/sea-salt component (component 4). With the exception of two samples (A96-08 and A96-09), bromide is depleted when calculating the SS contribution. The degree of depletion of Br^-, defined as the absolute value of (observed Br^--SS-Br^-)/SS-Br^-, is expressed in percentages, and it averages 51.6 ± 24.9% (geometric mean). The deficit varies between 3.8 and 91.8%. Large Br^- deficits have commonly been seen in marine aerosols, and this is the topic of great interest in conjunction with the ozone loss observed shortly after sunrise in the Arctic [*Barrie et al*., 1988; *Bottenheim et al*., 1990]. Bromine has been proposed to be active as the principal free radical chain carrier in an autocatalytic cycle that leads to ozone destruction and the transfer of Br species from aerosol to gas phase [*Fan and Jacob*, 1992; *McConnell et al*., 1992; *Vogt et al*., 1996]. In a model by *Vogt et al*. [1996] involving the production of reactive bromine and chlorine species, the particle phase depletion of Br^- amounted to 90% and that of Cl^- to 1%.

Depletion of Cl^- in the present study is observed for all samples, and in accordance with the model by *Vogt et al*. [1996] the Cl^- deficit is considerably smaller than that for Br^- but still larger than the deficit predicted by the model. Absolute values for Cl^- deficits are plotted in Figure 11. Samples A96-01 and A96-02 display a very different behavior from the rest of the samples. Since they carry the characteristics of being outliers, they are excluded from the following Cl^- deficit analysis. Chloride deficits average 18.3 ± 9.1% and vary from 10.6 to 47.1%, whereby a higher percentage deficit is found in the fine fraction (29.7 ± 9.9%) compared to the coarse fraction (11.9 ± 13.3%). This may be a consequence of the relative larger surface area of smaller particles compared to larger particles, and/or it may be a function of the presence of other chemical species which may react with Cl^- and subsequently lead to its volatilization. Further mechanisms for the depletion of Cl from the aerosol phase are discussed in section 4.

3.5. Cations

3.5.1. Na^+, K^+, Mg^{2+}, and Ca^{2+}. Water-soluble portions of Na^+, K^+, Mg^{2+}, and Ca^{2+} as determined by IC are presented in stacked bar plots in Figures 12a, 12b, 12c, and 12d, respectively. Their average concentrations and maxima and minima are listed in Table 1.

Typically, Na^+ is used to determine the sea-salt component in the aerosol particles since the water-soluble Na^+ is assumed to originate solely from seawater. Thus all Na^+ in Figure 12a is sea-salt derived and is used to compute the sea-salt component of the other three cations in Figure 12 based on the constant concentrations encountered in seawater [*Millero and Sohn*, 1992]. A comparison between the water-soluble fraction of these alkali and alkaline earth metals and their total concentrations as determined by ICP-MS is presented in section 4.

Total Na^+ concentrations vary from 0.44 to 8.52 $\mu g\ m^{-3}$ and average 3.24 ± 1.67 $\mu g\ m^{-3}$, of which 62% is present in the coarse particle fraction. The resulting sea-salt concentration varies from 1.4 to 27.8 $\mu g\ m^{-3}$ and averages 10.6 ± 5.5 $\mu g\ m^{-3}$. This falls within the range of sea-salt concentrations observed in Barbados, Cape Verde, and the Atlantic [*Arimoto et al*., 1995; *Davison et al*., 1996; *Li-Jones and Prospero*, 1998; *Savoie and Prospero*, 1977]; however, the mean value is larger by up to a factor of 2 compared to our samples. *Putaud et al*. [1993] reported a mean value very close to the present observation from samples collected in calm tropical North Atlantic waters under conditions comparable to the ones encountered during the present cruise. Compared to the TSP, which was determined from the low-volume filters, the sea-salt accounts for, on average (geometric mean), 24.3 ± 9.8%.

Magnesium, as can be seen in Figure 12c, closely traces the Na^+ concentrations. The NSS-Mg^{2+} varies from small negative to small positive values, which fall within the error of the analysis techniques. Thus water-soluble Mg^{2+} appears to be exclusively sea-salt derived, implying that the Saharan dust collected on the present samples is not a significant source of water-soluble Mg. This is in agreement with observations made by *Savoie and Prospero* [1980] in the same sampling area, the tropical North Atlantic. Over the northern Indian Ocean [*Johansen et al*., 1999], however, Mg^{2+} was slightly enriched over the sea-salt component and seemed to be of crustal origin.

Potassium, on the other hand, does exhibit a NSS water-soluble portion (see Figure 12b). The NSS contribution varies from 15.5 to 82.2% of the total water-soluble K^+, with a geometric mean of 32.5 ± 18.2%. The fine aerosol particles contain 73% of this portion of K^+.

In the case of calcium the NSS contribution accounts for 64.9 ± 20.3% (geometric mean) of the total water-soluble Ca^{2+}; see Figure 12d. This is in perfect agreement with observations by *Savoie and Prospero* [1980]. In contrast to potassium, the majority (63%) of the water-soluble NSS-Ca^{2+} is present in the coarse fraction. This indicates that the sources of NSS water-soluble potassium and calcium may not be identical. Even if the geographic source is the same, the particles releasing the potassium and the calcium are of different size ranges. The coarse size fraction is typical of crustal material. However, clay particles may be fine enough to preferentially end up in the fine filter mode (<3 μm). Thus it is conceivable that the mineral aerosol contained a potassium-rich dust of smaller particle size mixed in with larger calcite particles. In addition, potassium is a tracer for biomass burning [*Andreae*, 1983; *Echalar et al*., 1995], which would end up in the fine particle mode, as observed here.

3.5.2. NH_4^+ and acid neutralization. Ammonium has typically been observed in association with particles in the accumulation mode, together with NSS-SO_4^{2-} and MSA [*Huebert et al*., 1996]. Our observations are in agreement with those findings: 73% of the NH_4^+ is contained in the fine particle mode; see Figure 13a. Total ammonium concentrations vary from 68.5 to 299 ng m^{-3} and average 175 ± 62 ng m^{-3}. These concentrations are close to observations made [*Harrison et al*., 1996; *Huebert et al*., 1996] over the Azores in marine air masses.

Ammonia, mostly of continental origin [*Quinn et al*., 1992], is the primary basic gas in the atmosphere and is readily absorbed by atmospheric particles whereby it neutralizes acid aerosol. First, it neutralizes H_2SO_4 since the vapor pressure of H_2SO_4 is considerably smaller than that for HNO_3, and then, if sufficient ammonia is available, it will react with HNO_3 [*Seinfeld and Pandis*, 1997]. Thus the NH_4^+/NSS-SO_4^{2-} ratio gives an estimate of the neutralization and the speciation of the acid in the aerosol. We find that the molar ratio of NH_4^+/NSS-SO_4^{2-} in the fine fraction, where 73% of the total NH_4^+ and 87% of the total NSS-SO_4^{2-} are present, is, on average (geometric mean), 0.96 ± 0.46. This indicates that the particles consist mainly of bisulfate. However, as can be seen in Figure 13b, the ratio in the fine fraction (dashed curve) ranges from 0.4 (near Cape Verde) to 2.1 (at the equator). A molar ratio of <0.5 represents a very acidic atmosphere, where the sulfate species in the aerosol particles are mainly H_2SO_4 and HSO_4^-. In the case of a molar ratio above 2, there is sufficient ammo-

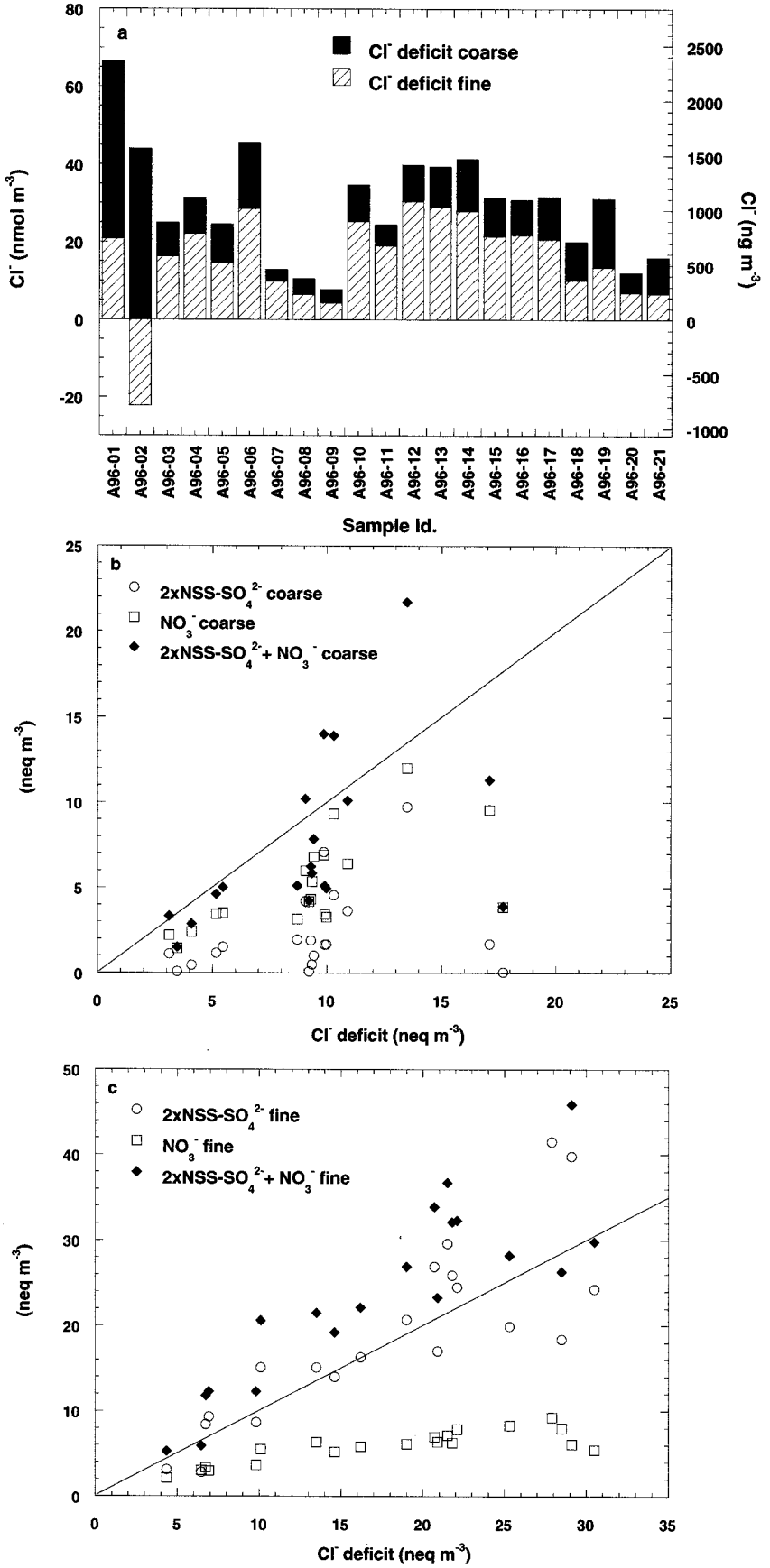

Figure 11. (a) Cl^- deficit versus sample ID. (b) Nanoequivalent (neq) mineral acid concentrations versus Cl^- deficit in coarse fraction and (c) neq mineral acid concentrations versus Cl^- deficit in fine fraction.

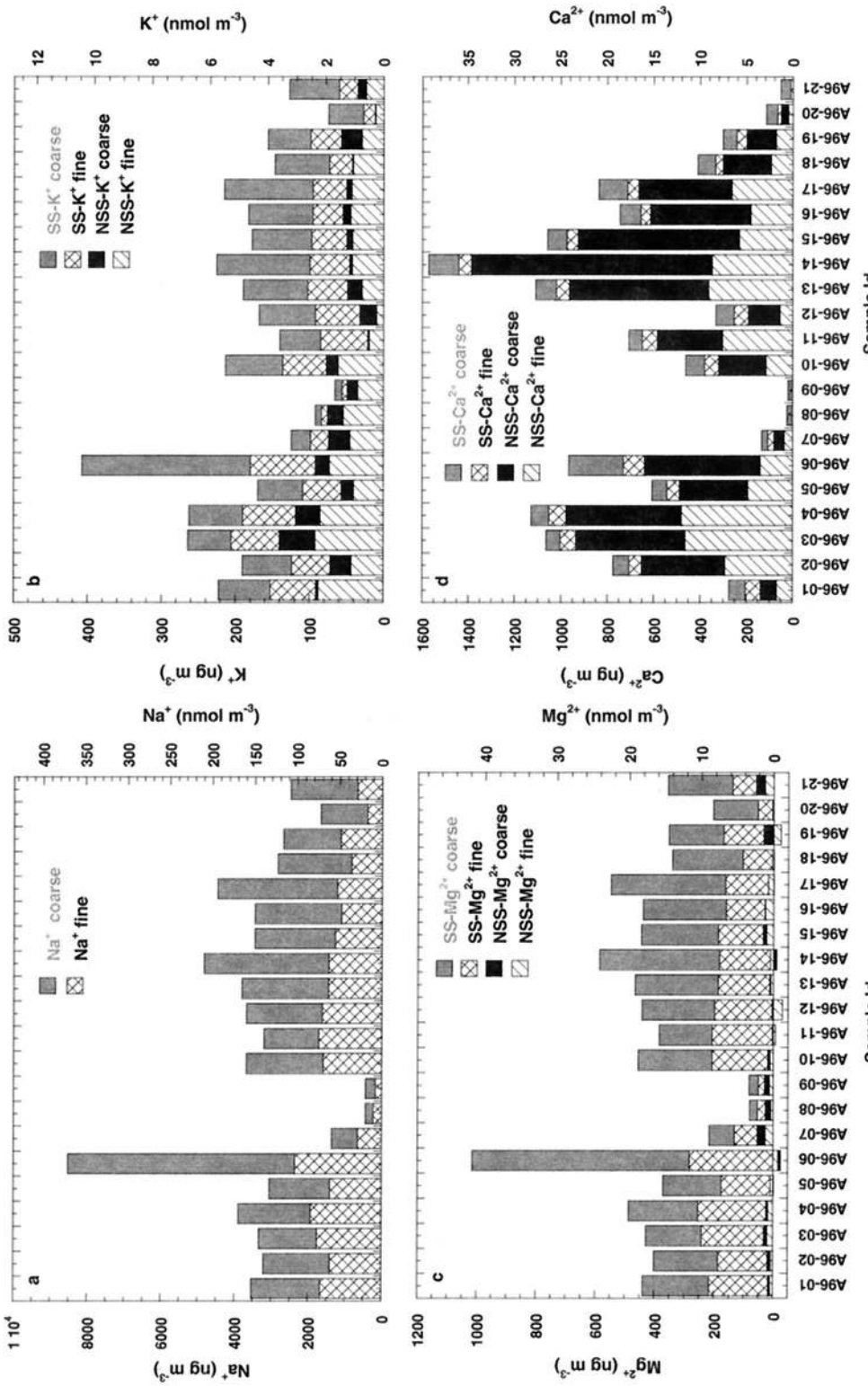

Figure 12. Water-soluble sea-salt and non-sea-salt fractions of (a) Na^+, (b) K^+, (c) Mg^{2+}, and (d) Ca^{2+}, in coarse and fine fractions versus sample ID.

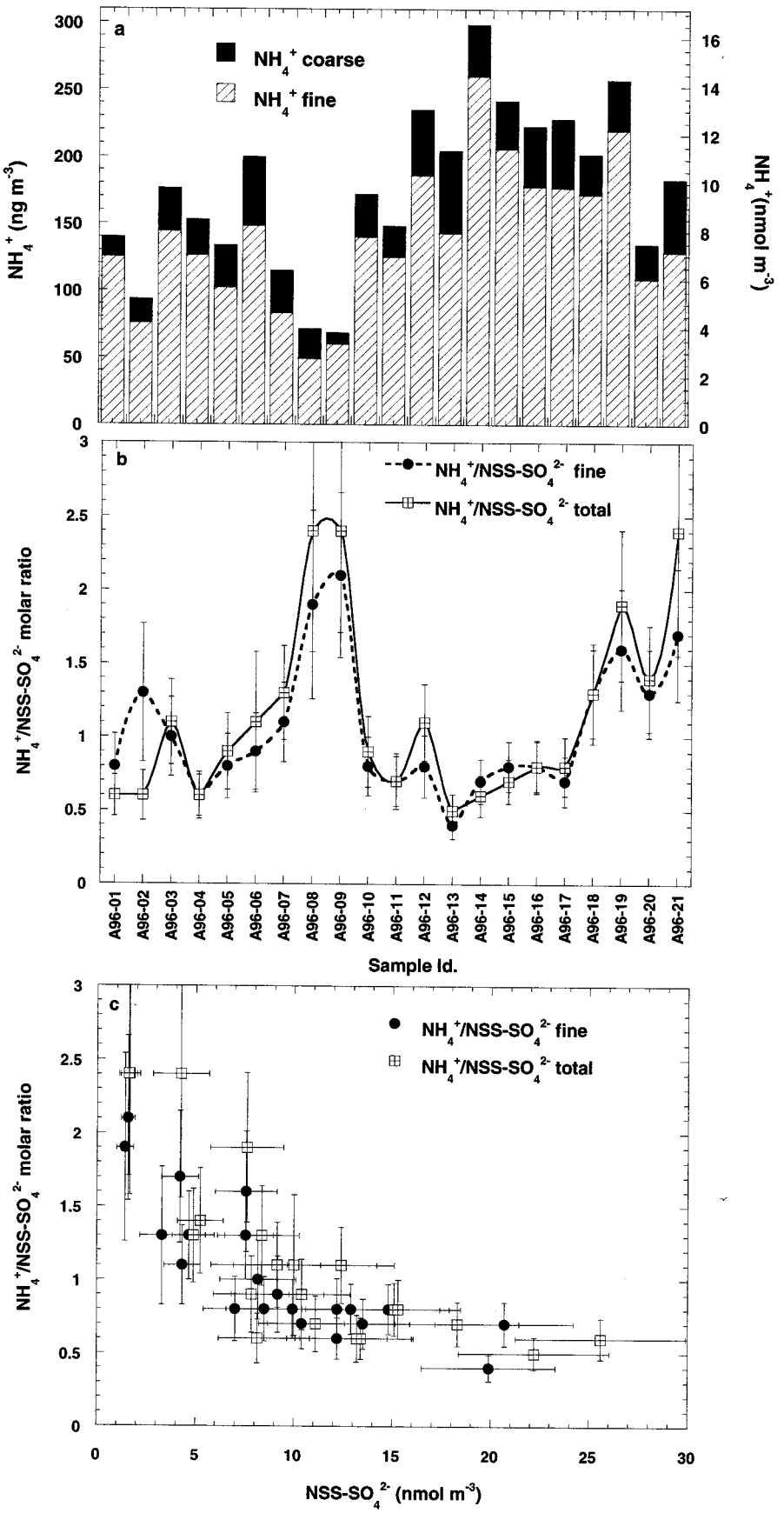

Figure 13. (a) NH_4^+ and (b) $NH_4^+/NSS\text{-}SO_4^{2-}$ versus sample ID. (c) $NH_4^+/NSS\text{-}SO_4^{2-}$ versus $NSS\text{-}SO_4^{2-}$ in fine fraction and fine and coarse combined (total).

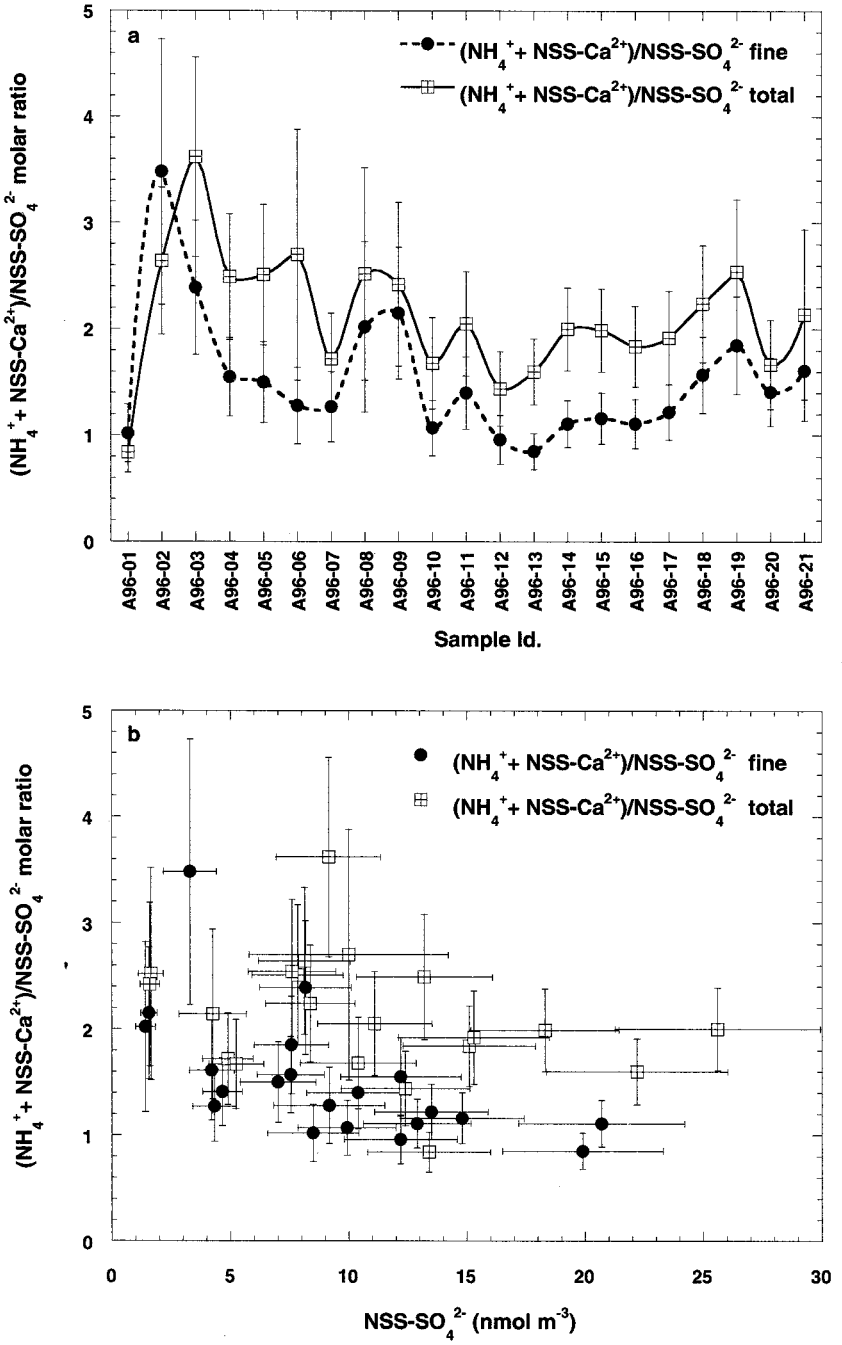

Figure 14. (a) $(NH_4^+ + NSS\text{-}Ca^{2+})/NSS\text{-}SO_4^{2-}$ versus sample ID. (b) $(NH_4^+ + NSS\text{-}Ca^{2+})/NSS\text{-}SO_4^{2-}$ versus $NSS\text{-}SO_4^{2-}$ in fine fraction and fine and coarse combined (total).

nium in the particle phase to neutralize the available sulfuric acid and some nitric acid. The coarse molar $NH_4^+/NSS\text{-}SO_4^{2-}$ ratio is not shown, since its variability is very large due to the large associated error with the small coarse $NSS\text{-}SO_4^{2-}$ concentrations in the denominator. However, the total ratio is plotted in Figure 13b as the solid curve. It traces closely the fine $NH_4^+/NSS\text{-}SO_4^{2-}$ curve but in general displays slightly larger values, averaging 1.03 ± 0.61.

The lowest ratios are observed near Cape Verde, when dust concentrations and especially $NSS\text{-}Ca^{2+}$ abundances are large. Since it appears (see section 4) that most of the $NSS\text{-}Ca^{2+}$ is associated with primary $CaCO_3$ rather than with primary $CaSO_4$, the CO_3^{2-} may act as an additional neutralizing species.

Owing to the size cutoff of our collector (3 μm particle diameter), an appreciable amount of particulate crustal material ends up on the fine filter; 37% of total $NSS\text{-}Ca^{2+}$ is present in the fine fraction, averaging 177 ± 153 ng m^{-3}. Carbonate is available for reaction with acidic $NSS\text{-}SO_4^{2-}$, especially in the fine fraction where most of the $NSS\text{-}SO_4^{2-}$ is present. $NSS\text{-}Ca^{2+}$ peaks near Cape Verde, when the low $NH_4^+/NSS\text{-}SO_4^{2-}$ ratios indicate very acidic conditions. Inclusion of the neutralizing ability of CO_3^{2-} of one proton (as $NSS\text{-}Ca^{2+}$) in the

Table 4. Previously Reported Mineral Dust Concentrations in the Tropical Atlantic Ocean Region

Sampling Location	Mineral Dust, $\mu g\ m^{-3}$	Sampling Interval	Reference
Barbados	2.5	annual average, 25 months, <1968	*Prospero* [1968]
Barbados	11.0	annual average, 1970–1992	*Prospero et al.* [1996]
Barbados	104	annual maximum event, March 1978	*Prospero et al.* [1981]
Barbados	15–18	annual maximum monthly mean, 1978	*Prospero et al.* [1981]
Barbados	20.5 ± 17.9	July–September 1974	*Savoie and Prospero* [1977]
Barbados	15.0	annual average, 1990–1991	*Arimoto et al.* [1995]
Barbados	8.8, 3.8	median values, April, 1990 and 1991	*Arimoto et al.* [1995]
Barbados	~24, ~20	median values, April, 1989 and 1990	*Ellis and Merrill* [1995]
French Guiana	100.0	annual maximum event, March 1978	*Prospero et al.* [1981]
French Guiana	29, 23	annual maximum monthly means, 1978 and 1979	*Prospero et al.* [1981]
Off the coast of northern Brazil	1–25	maximum and minimum, February–March 1971	*Talbot et al.* [1990]
Tropical North Atlantic Ocean	25.0	September–October 1988	*Losno et al.* [1992]
Tropical North Atlantic Ocean	22.0	May–July 1969	*Prospero and Carlson* [1972]
Tropical North Atlantic Ocean	7.7	July–November 1971	*Aston et al.* [1973]
Near the African Coast	57.0	average in northeastern trades, March 1971	*Chester et al.* [1972]
Southeast of Cape Verde	133	maximum event, March 1971	*Chester et al.* [1972]
Cape Verde	29.8 ± 37.9	July–September 1974	*Savoie and Prospero* [1977]
Near the ITCZ	0.25	average, March 1971	*Chester et al.* [1972]

numerator (i.e., $(NH_4^+ + NSS\text{-}Ca^{2+})/NSS\text{-}SO_4^{2-}$) of the ratio gives a new measure of the neutralization and speciation in the particle phase. As seen in Figure 14, this new ratio is generally higher than the one that does not include CO_3^{2-}, as expected. When before the lowest ratio was 0.4 in the fine fraction, it now is 0.85. For such a value the most abundant species is HSO_4^-. The $(NH_4^+ + NSS\text{-}Ca^{2+})/NSS\text{-}SO_4^{2-}$ for the fine fraction averages (geometric mean) 1.44 ± 0.60 (also indicative of bisulfate) and shows a maximum of 3.48 in sample A96-02. Mineral aerosol characteristics at the beginning of the cruise are considerably different from those encountered near Cape Verde; this is discussed in further detail in section 4. Thus the large ratios observed at the start and end of the cruise for the fine and for the coarse and fine fractions combined may be inaccurately elevated since the $NSS\text{-}Ca^{2+}$ may not necessarily be present in the form of primary $CaCO_3$ in those samples. The same ratio $(NH_4^+ + NSS\text{-}Ca^{2+})/NSS\text{-}SO_4^{2-}$ for the total aerosol averages 2.0 ± 0.6.

Acid-base neutralization can also be discussed in terms of charge imbalances observed between total anionic and cationic charges. However, since both H^+ and CO_3^{2-} are not detectable with the IC, an observed charge imbalance cannot be directly attributed to the either one of the two species. In the present case, the carbonate derived from the excess $NSS\text{-}Ca^{2+}$ correlates well with the anionic charge deficit that is observed in all but one sample. The charge deficit amounts to 12% in the fine and 16% in the coarse fraction. Thus it appears as if no additional protons are present that would acidify the aerosol over what was obtained from the ratios that include the carbonate neutralization capacity.

4. Discussion

4.1. Mineral Aerosol

Aluminum is typically used as the tracer to quantify the mineral aerosol abundance in the atmosphere, where the concentrations are computed from measured Al concentrations and Al average concentration in bulk continental crust: 8.41 wt % Al [*Taylor and McLennan*, 1985]. Although, as will be shown below, the average crustal composition is usually a good estimate, it is not always representative of all crustal sources. For the sake of comparison of the present findings with those observed in other studies in the same area, we first report mineral dust loadings based on the 8.41% average crustal Al content. The average total dust loading thus computed amounts to 18.4 ± 15.6 $\mu g\ m^{-3}$, ranging from 0.8 to 52.9 $\mu g\ m^{-3}$. The mineral dust is almost evenly distributed between the two size fractions (51% in the fine fraction). Figure 3a presents Al concentrations as a function of sample ID. It can be deduced that minimum mineral dust concentrations occur near the equator, in samples A96-08 and A96-09, while maximum concentrations are observed near the beginning of the cruise. These mineral dust concentrations fall within the range of values reported by a several investigators. See Table 4 for comparison with previously reported dust concentrations from Barbados to Africa. Our observed concentrations are in good agreement with those found by other investigators in the same region during the same time of the year.

Air mass back trajectories for the maximum and minimum dust events in the present study display very similar upper elevation air mass back trajectories; compare Figures 1a and 1b. However, the lower elevation air mass back trajectories differ considerably for the two samples. During sample A96-02 the lower trajectories appear to sweep around from the middle of the Atlantic Ocean, without touching the African continent, while the corresponding trajectories for the minimum mineral dust loading event, A96-08, emanate from northwest Africa. This observation seems counterintuitive, since dust concentrations are larger when the lower level trajectories do not come in direct contact with the African continent. A possible explanation for the observed mineral dust concentration pattern may be that the high-elevation trajectories carry all the dust particles, in the SAL, as previously reported [*Prospero and Carlson*, 1972; *Schütz*, 1980; *Ellis and Merrill*, 1995], and that these particles settle out later during the trajectory of an air mass.

From sample A96-13 and until the end of the cruise, trajectories display very different characteristics. Sample A96-16, in Figure 1d, illustrates trajectories that are representative for this latter part of the cruise. Air masses that have traveled along upper level trajectories do not seem to be the source of mineral dust to these samples since they originate from the Caribbean, eastern North America, and/or northern South

Table 5. Enrichment Factors

	Na	Mg	K	Ca	Sc	Ti	V	Mn	Fe	Zn	Cs	Ba	La	Ce	Sm	Eu	Hf	Pb	Th
Enrichment Factors Assuming Continental Bulk Composition According to Taylor and McLennan [1985]																			
Average	11.13	1.32	3.19	0.81	0.52	1.36	0.73	0.66	0.68	12.40	4.46	2.37	2.62	2.67	2.07	1.32	1.89	8.76	3.19
SD	7.49	0.64	1.46	0.34	0.08	0.76	0.34	0.12	0.11	16.13	1.48	0.53	0.96	0.58	0.77	0.72	2.97	4.25	1.17
Enrichment Factors Assuming Shale Composition According to Taylor and McLennan [1985]																			
Average	25.40	2.68	1.03	1.86	1.14	1.49	1.23	1.04	0.96	9.94	0.85	0.97	0.43	1.42	1.08	1.38	1.93	3.34	0.89
SD	17.09	1.30	0.47	0.78	0.17	0.84	0.57	0.19	0.15	12.94	0.28	0.22	0.16	0.31	0.40	0.76	3.03	1.62	0.32

America. Samples A96-13 and A96-14 are collected in close proximity to Cape Verde and may therefore contain material from local sources, also indicated by relatively larger Pb and Zn concentrations (see Figure 3b).

The trajectories presented in Figure 1 seem very representative for the month of April over this region of the tropical North Atlantic Ocean. *Swap et al*. [1992] and *Talbot et al*. [1990] display air mass trajectories and streamline fields over the tropical Atlantic Ocean during the month of April 1987 which are very similar to the present trajectories. This indicates that the trajectories depend on the location of the West African Subtropical High which may vary significantly during the month of April.

It appears from the trajectories that the samples are divided into two groups with different air mass origins: one group is collected during the southern leg of the cruise and the other one during the northern leg. It is of interest to determine whether this difference is also reflected in mineralogical characteristics. Enrichment (over the crustal component) factor analyses of trace metals and the comparison of the water-soluble versus total concentrations of alkali and alkaline earth elements serve to elucidate the mineralogical composition of the sampled mineral dust.

Averaged ratios for the enrichment factor analysis using the crustal bulk composition according to *Taylor and McLennan* [1985] are presented in Table 5. Concentrations used in this analysis are derived from the fully digested filters; thus concentration are inclusive, regardless of the initial chemical composition of the phases present on the filter. A value above 1 signifies that the element is enriched over what would be expected if the aerosol were of average crustal composition only.

As found by the principal component analysis, Zn and Pb are of anthropogenic origin; therefore their elevated enrichment factors are, on average, 12.4 and 8.8, respectively. The rest of the trace metals, with exception of V, which may originate from the combustion of heavy fuel, are typically crustal derived; thus values close to 1 are expected. This is, however, not the case in the present analysis. Some elements are present at levels that are too low (Sc, V, Mn, and Fe) and others are present at levels that are too high (Ti, Cs, Ba, La, Ce, Sm, Eu, Hf, and Th). It is also interesting to note that Ca, which has a sea-salt component and therefore should be enriched, displays a factor that is typically lower than 1. On the basis of the compilation of *Faure* [1998] of the chemical composition of igneous and sedimentary rocks, several enrichment factor analyses are carried out in order to find the rock type that best matches the trace metal concentrations in the samples. Sandstone, low-Ca granite, basalt, deep-sea clay and carbonate rocks (not shown) display enrichment factors that do not match the samples well either. However, shale and high-Ca granites appear to be relatively good proxies for the trace metal composition of the samples, whereby shale is the best surrogate. The average enrichment factors for shale are also presented in Table 5. With the exception of Na, Mg, Ca, Zn, La, Hf, and Pb, the enrichment factors are very close to 1, indicating no enrichment. As mentioned above, Zn and Pb are of anthropogenic origin and therefore are enriched over crustal concentrations. Sodium and Mg are mainly sea-salt derived, while most of the Ca has an additional, water-soluble source. Lanthanum and Hf are the only elements for which the discrepancy cannot be explained.

The typical composition of shale from *Turekian and Wedephol* [1961], used here, not only describes the heavier trace metals in the mineral aerosol sampled, but it also accounts for the right amount of crustal-derived Na. This becomes apparent when comparing the water-soluble Na^+ concentrations as determined by the IC, with the sea-salt Na computed from the total ICP-MS Na, after subtracting the crustal (shale) contribution; see Plate 1a. Stacked bars are ICP-MS derived concentrations: the crustal component (in red and orange) is determined from the observed Al concentrations and the composition for shale, while the remaining Na is assumed to be sea-salt (dark and light blue) derived. Overlain, by a dashed line, is the total water-soluble Na^+ concentration as determined by IC. Although not shown, the corresponding plots for Na in all the other igneous and sedimentary rocks experimented with above, exhibit crustal Na concentrations which are significantly larger than those for shale, thus increasing the discrepancy between ICP-MS and IC determined sea-salt Na concentrations. Plates 1b–1d are plotted in a manner analogous to Plate 1a. However, since both the crustal and the sea-salt (from the sea-salt ICP-MS Na) components in the ICP-MS-determined concentrations can be computed, some samples display an excess or a deficit (plotted in green) compared to what would be expected if shale were the perfect crustal proxy. If the added up computed sea-salt and crustal concentration is larger than what is actually detected in the sample, the deficit is plotted as a negative bar. In that case, the shale composition must be overpredicting the concentration of the element in that sample since the sea-salt composition is assumed to be very accurate. This is especially seen for K, throughout the cruise and in both size fractions. In Figure 12, water-soluble K^+ appears to have an additional source other than sea salt, which is mostly present in the fine fraction. This is also detected when comparing the sea-salt K determined from the ICP-MS concentrations (blue bars) with the IC determined total K^+ (dashed line). Even though shale does not satisfactorily describe the observed crustal K concentrations, it should be noted that none of the other igneous and sedimentary rocks do so to a better degree. The enrichment of K in both the water-soluble as well as the non-water-soluble fractions may possibly be a product of biomass burning [*Andreae*, 1983; *Echalar et al*., 1995]. It is conceivable that some of the K contained in the ash particles was released in the water extrac-

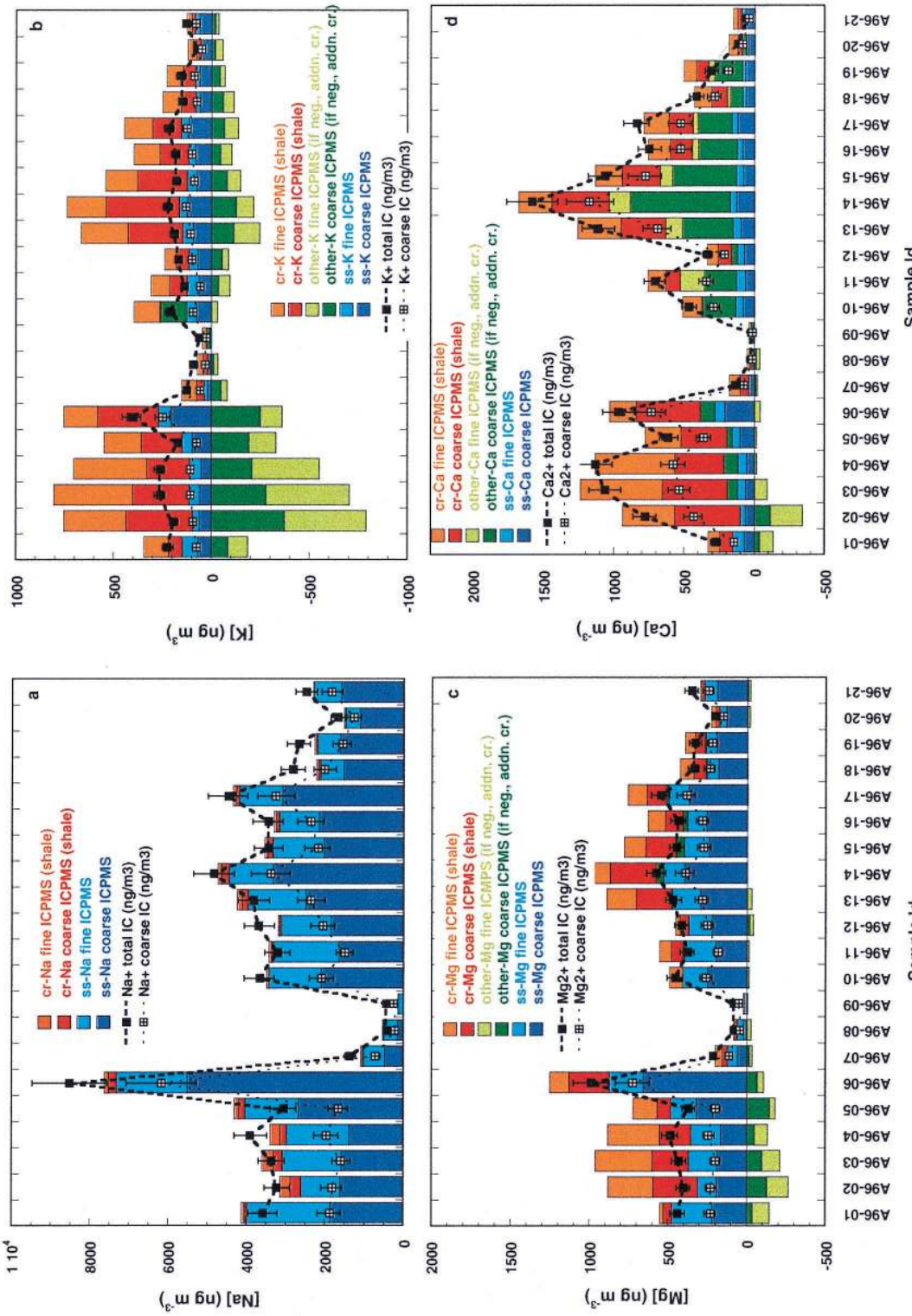

Plate 1. ICP-MS and IC determined concentrations of (a) Na, (b) K, (c) Mg, and (d) Ca versus sample ID in coarse and fine fractions. Crustal concentrations are determined from average shale composition (see text for details).

tion, detected by the IC, while the rest was trapped inside the particle, only to be detected by the acid digestion for the ICP-MS samples.

Either the presence of a third component or the underprediction of the shale composition is implied when the green bars are positive. This is the case in Plate 1d for Ca, especially during the latter part of the cruise. Sandstone and even more so carbonate rocks significantly overpredict the Ca that should be present in the samples. High-Ca granites (not shown) and shale display very similar plots. Although shale is a good proxy for the mineral composition encountered, no one single composition would satisfactorily describe all the samples simultaneously as seen from the Ca, Mg, and K plots. This is based on the observation that at the beginning of the cruise, K, Mg, and Ca are overpredicted with regard to shale, while in the latter part of the cruise the overprediction becomes smaller for K and disappears for Mg, while for Ca, shale underpredicts the crustal component. Thus it is apparent that the mineral dust composition varies between the first and the second half of the cruise.

If shale were a good representation of the mineral composition in the present samples, then Plate 1d indicates that most of the Ca in the shale has to be present in a water-soluble form since concentrations of the IC-determined Ca^{2+} closely follow the total Ca concentrations as determined by the ICP-MS. This water-soluble Ca is believed to be calcite ($CaCO_3$). Calcite has previously been observed in aerosol samples over the Atlantic Ocean [*Glaccum and Prospero*, 1980; *Savoie and Prospero*, 1980; *Schütz and Sebert*, 1987; *Zhu et al*., 1992]. Furthermore, the water-soluble NSS-Ca^{2+} component in the coarse fraction, where most (63%) of the NSS-Ca^{2+} is present, correlates with the deficit in anionic charges in the principal component analysis in Table 3. The observed charge deficit is believed to arise from the CO_3^{2-} which is not detected by IC. Additional calcite appears on the samples in the second half of the cruise, not only in close proximity to Cape Verde but along the entire northern leg back to Barbados. This is another indication that two somewhat distinct mineral aerosol sources prevail during the first and the second part of the cruise.

Glaccum and Prospero [1980] determined that the mineralogical composition of aerosols carried from Cape Verde to Barbados and Miami were very similar to that of an average shale, in agreement with our observations. Shale is made up of a number of different minerals, and it carries the implication of very small particle size. The mineral composition of the aerosols over the Atlantic Ocean has been found to be made up of mica, quartz, kaolinite, chlorite, montmorillonite, plagioclase, microcline, and calcite [*Anderson et al*., 1996; *Chester et al*., 1972; *Delaney et al*., 1967; *Glaccum and Prospero*, 1980], which is the composition of a typical shale. Shale is a weathering product whose composition depends not only on the mineral form from which it was formed but also on the chemical environment of weathering, which in turn is largely the result of climate. The weathering may have occurred at the location of the parent material and/or during transport by water and wind, having been sorted and possibly concentrated in the process. Resistant materials, such as quartz; incompletely weathered minerals, such as feldspar; and minerals formed by precipitation from aqueous solution, notably calcite, may be present. A consequence of the differential density and shape of the distinct mineral phases in the shale aerosol would be that the composition changes as the dust is transported across the Atlantic. Greater sedimentation velocities of the larger and heavier mineral particles, such as quartz, are preferentially removed from the air mass relative to the small and flaky clay particles. Such a selective separation was observed in samples collected along the trajectory of an air mass by *Glaccum and Prospero* [1980]. In the present case, however, this does not explain the apparent different mineralogical composition encountered during the first and second halves of the present cruise.

According to a number of investigators [*Chiapello et al*., 1997; *Paquet et al*., 1984; *Schütz and Sebert*, 1987] a high amount of calcite in the mineral aerosol can be considered an indicator for aerosol matter originating from the northern Sahara, where calcite is the major compound of marine sedimentary deposits and outcrops [*Schütz and Sebert*, 1987]. This would imply that during the latter half of the cruise, when calcite is more abundant, the air mass trajectories should have emanated from over the northern Sahara. The present trajectories are not a clear indicator for that since some of them appear to originate from southern Europe (see Figures 1c and 1d). However, as stated above, the trajectories are associated with considerable errors, which increase rapidly with their length. Thus the trajectories that seem to originate from Europe may very well have come from northern Africa.

Chiapello et al. [1997] investigated the relationship between Fe, Ca, K, Si, and Al to identify aerosol originating from three different source regions in Africa. In comparing their air mass trajectories with ours, it seems that throughout the cruise, air masses in the present study originate from the north and west Saharan sector, which includes Spanish Sahara, Morocco, and west Algeria. During the months of March and April all the dust events at Sal Island (Cape Verde) originated from this north and west Saharan sector [*Chiapello et al*., 1997]; thus, owing to the apparent seasonality of the wind patterns, we expect to see the same sector as the origin for our mineral aerosol. *Chiapello et al*. [1997] found that the ratios of Fe/Ca, Ca/Al, and K/Ca were good indicators to classify the mineral aerosol into one of the three sectors. Owing to the elevated Ca concentrations in the latter part of the present cruise compared to the first half, all three of these ratios varied to an extent that would indicate two different mineralogical characteristics. The Fe/Ca geometric mean decreased from 1.71 to 0.93, the Ca/Al ratio increased from 0.31 to 0.64, and the K/Ca ratio decreased from 0.86 to 0.57, from the first half of the cruise to the latter part. Compared with Chiapello et al.'s ratios, this would classify the mineral aerosol collected during the first half of the cruise to originate from the central Sahara, while the mineral aerosol from the latter half would have emanated from the northern Sahara.

Other investigators [*Arimoto et al*., 1995; *Bergametti et al*., 1989; *Chiapello et al*., 1997; *Delaney et al*., 1967] have used the Fe/Al ratio to determine source regions of Africa. Fe/Al is found to be higher in dust originating from a Sahelian source compared with dust from the vicinity of Morocco. This increase in Fe/Al ratios may result from changes in clay minerals [*Bergametti et al*., 1989]: The Sahelian regions are known to present abundant ferrallitic soils; thus iron is the dominant element in clay minerals from this region, while in clay minerals that originate from Morocco, iron only appears as a minor component. Fe/Al ratios from the Sahelian regions range from 1.5–1.8, while those from the northern Sahara range from 0.3 to 1.1. In the present samples we observe Fe/Al ratios on the fine and coarse fractions combined that average 0.56 ± 0.09 (geometric mean) and vary only in a very small range, from

0.47 to 0.9. The geometric mean of the first nine samples is 0.53, while that for the rest of the samples, representing the latter part of the cruise, is insignificantly larger, 0.59. Very similar values are found when treating fine and coarse fractions separately. Thus it appears from these observations that the Fe/Al ratio does not indicate a Sahelian source region throughout the cruise. On the basis all the ratios investigated above, the mineral aerosol sampled during the entire cruise seems to originate from the Sahara, whereby it may be that the second half of the cruise is more typical of the northern Sahara, rich in calcite, and the first part of the cruise of central Sahara.

In summary, shale appears to be the best proxy for the mineral aerosol composition sampled during the present cruise. On the basis of the heavier trace metals, there seems be no variability in mineralogical composition between samples, thus indicating a common source region, the Saharan desert. Mineralogical differences are only indicated in the concentrations of alkali and alkaline earth elements. Excess water-soluble Ca^{2+} (over that expected from shale and sea salt), presumably present in the form of $CaCO_3$, is abundant in the latter part of the cruise, which suggests that the air masses emanated from the northern Sahara, while the mineral aerosol during the first half of the cruise may have originated from central Saharan sources. With an average Al concentration of 8% in shale [*Turekian and Wedepohl*, 1961], the computed dust loading concentrations will increase by 5% from the values determined on the basis of the average crustal composition presented above. Thus the average dust loadings amount to 19.3 ± 16.4 $\mu g\ m^{-3}$ and range from 0.8 to 55.6 $\mu g\ m^{-3}$. On average, the mineral aerosol accounts for ~42% of the TSP. This value is most probably skewed since the TSP is determined from the low-volume filters, while the mineral dust loadings are derived from the Al concentrations on the high-volume filters. Previously, *Johansen et al*. [1999] showed that the sampling efficiency for the two samplers utilized in this study differ appreciably, especially during high winds and for the larger particles. The low-volume sampler appears to be more efficient at collecting large particles, which leads to presently determined TSP values that are larger than TSP values that would have been determined from the high-volume filters.

Calcite ranges from 0.01 to 3.47 $\mu g\ m^{-3}$ and averages 1.27 ± 0.98 $\mu g\ m^{-3}$ (~3% of TSP; note the comment made above about the different samplers used). The calcite content amounts to 3.0 and 7.9% of the mineral aerosol during the first and second half of the cruise, respectively. The calcite content peaks in sample A96-14, showing 11.5% of calcite, and it reaches a minimum near the equator, in sample A96-08, when it represents 0.6% of the mineral aerosol. *Zhu et al*. [1992] found calcite to comprise 5.0–5.3% of the dust in Barbados, while *Glaccum and Prospero* [1980] observed 3.9% calcite in the same location. These values are in the same range as those determined in the present study. *Savoie and Prospero* [1980] measured soluble Ca concentrations in Barbados and Miami which were about a factor of 2 lower than in Sal Island (Cape Verde), accounting for 6.4, 6.6, and 11.3% of the mineral aerosol, respectively. These values are in agreement with our observations during the second part of the cruise. While the calcite content in the fine fraction does not change significantly between the two halves of the cruise, the calcite in the coarse fraction is considerably larger during the second half, 10.4 as opposed to 5.4% during the first part.

4.2. Sea-Salt Aerosol

Although most sea-salt-derived ions can be considered conservative and inert to chemical reactions occurring in the aerosol phase, the few anions that may play a role need to be studied in greater detail owing to their oxidative character. Furthermore, the sole presence of the sea salt in the atmosphere may have an effect on the uptake and oxidation of sulfur gases, which in turn play an important role in the radiation balance of the atmosphere.

Of the water-soluble cations in the collected aerosol, Na^+ is typically used as the tracer for the sea-salt component. In the present samples, sea-salt concentrations computed from Na^+ vary from 1.4 to 27.8 $\mu g\ m^{-3}$ and average 10.6 ± 5.5 $\mu g\ m^{-3}$. See Figure 12a for concentrations in coarse and fine fractions as a function of sample. Compared with the mineral aerosol, the sea-salt component varies to a much smaller extent and amounts to ~55% of the mass of the mineral dust component in the aerosol. The sea salt represents ~23% of the TSP (again, note the different samplers used). Combining the sea-salt and crustal masses accounts for ~68% of the TSP, while ~32% of the TSP has another source. Since anthropogenic and biogenic sources are unlikely to add the missing aerosol mass, the low-volume collectors appear to be more efficient in collecting aerosol particles, particularly in the larger size range [see also *Johansen et al*., 1999].

Sea-salt particles in the fine fraction appear to correlate with MSA and NSS-SO_4^{2-} in the principal component analysis presented in Table 3. This is in agreement with observations by a series of investigators [*Kerminen et al*., 1997; *O'Dowd et al*., 1997; *Pszenny*, 1992; *Qian and Ishizaka*, 1993; *Quinn et al*., 1993; *Saltzman et al*., 1983]. The low vapor pressure of the gaseous species H_2SO_4 and MSA leads to their immediate condensation onto available preexisting aerosol surface area. The major contributor to aerosol surface area over the oceans may under most circumstances be the sea-salt particles in the size range 1–5 μm [*Sievering et al*., 1992]. Thus these droplets may provide the primary sink for low vapor pressure aerosol precursor species which could otherwise form and grow new particles on CCN. Furthermore, sea spray is buffered at a high pH, at which SO_2 oxidation by ozone proceeds at a substantial rate [*O'Dowd et al*., 1997]. This may significantly modify the marine sulfur cycle by providing a rapid removal for SO_2 from the atmosphere.

Sea-salt aerosol has also been found to be the source of halogen radicals [*Fan and Jacob*, 1992; *Finlayson-Pitts*, 1983; *Finlayson-Pitts et al*., 1989; *Graedel and Keene*, 1995; *Keene et al*., 1996; *Pszenny et al*., 1993; *Sander and Crutzen*, 1996; *Vogt et al*., 1996]. These transient radical oxidants strongly influence the oxidative properties of aerosol particles in the marine boundary layer. Reactive Cl can initiate photochemical reactions in an analogous manner to $OH^{\cdot}$ and have major consequences for the oxidation of hydrocarbons and DMS [*Keene et al*., 1996, 1990; *Langer et al*., 1996; *Pszenny et al*., 1993; *Sander and Crutzen*, 1996; *Stickel et al*., 1992; *Vogt et al*., 1996]. The release of reactive Cl species from the aerosol phase can be traced by examining the depletion of Cl^- compared to expected sea-salt concentrations. However, there exist additional mechanisms by which Cl^- is depleted from the aerosol phase.

Chloride deficits have typically been found to correlate with the proximity to continental landmasses and thus assumed to depend on the concentrations of anthropogenic pollutants such as NSS-SO_4^{2-} and NO_3^- [*Sturges and Shaw*, 1993]. Ther-

modynamically favorable acid displacement reactions between mineral acids (H_2SO_4, HNO_3) and Cl^-, with subsequent HCl volatilization [*Duce and Hoffmann*, 1976; *Duce et al*., 1973; *Sturges and Barrie*, 1988], have been assumed responsible for these observations. *Johansen et al*. [1999] found that the Cl^- deficit observed during two different seasons over the northern Indian Ocean depended strongly on the matrix of the aerosol particles. The largest deficits were measured during the SW monsoon, when NO_3^- and NSS-SO_4^{2-} concentrations were very small and therefore acid displacement reactions were less important. Instead, the Cl^- deficit appeared to correlate well with the discrepancy between total anion and cation charges, which would be a consequence of the Cl being released in the form of reactive species, such as Cl_2, HOCl, $ClNO_2$, NOCl, and BrCl. Evidence of the existence of several highly reactive Cl gases has been shown experimentally [*Finlayson-Pitts*, 1983; *Finlayson-Pitts et al*., 1989; *Graedel and Keene*, 1995; *Keene et al*., 1990; *Pszenny et al*., 1993; *Vogt et al*., 1996].

To find a possible correlation in the present samples between the Cl^- deficit on one hand and anthropogenic pollutants and charge deficits on the other, the Cl^- deficit for both size fractions is included in the principal component analysis (not shown). The chloride deficit in the coarse fraction, and less so in the fine, correlates with component 2, which is analogous to component 2 in the principal component analysis in Table 3. This component represents the sea salt and to a lesser degree a coarse crustal source, including coarse NO_3^-, the latter of which may be partly responsible for the volatilization of HCl in the coarse fraction. Component 2 also correlates with the charge deficit observed between the anions and cations in the coarse fraction. When plotting neq concentrations of NO_3^-, NSS-SO_4^{2-} as a function of Cl^- deficit for the coarse fraction (in Figure 11b), the correlation is slight and concentrations of NO_3^- are typically 30–40% below Cl^- deficit concentrations. The line in the plot represents the 1:1 ratio of nmols of Cl^- deficit and neq of mineral acid. For the data points that fall to the lower right of the line the Cl^- deficit is larger than the mineral acid available for the acid displacement reaction. Even the addition of the available NSS-SO_4^{2-} to the NO_3^- concentrations in the coarse fraction does not bring the mineral acid abundance up to match the Cl^- deficit concentration for 76% of the samples. This is indicative of the presence of another potential mechanism that leads to the Cl^- deficit. As mentioned, the Cl^- deficit also correlates with the charge discrepancy between cations and anions. Since the release of Cl in the form of reactive species, such as Cl_2, HOCl, $ClNO_2$, NOCl, and BrCl may not be replaced by a detectable ion (such as, e.g., CO_3^{2-}), it is conceivable that the charge difference may become a measure of the extent of Cl^- released in this form. However, the charge difference amounts to concentrations that are on average ~115% larger than the Cl^- deficit. Thus, in the coarse aerosol fraction it seems that a combination of mechanisms is responsible for the depletion of Cl^-: both the acid displacement reaction with HNO_3 and H_2SO_4 and the Cl release in the form of reactive species. The depletion of Cl in the form of volatile reactive Cl species may include reactions with Br [*Fan and Jacob*, 1992; *McConnell et al*., 1992; *Vogt et al*., 1996] and with gas-phase species such as NO_2, $ClONO_2$, N_2O_5, and O_3 [*Finlayson-Pitts*, 1983; *Finlayson-Pitts et al*., 1989; *Graedel and Keene*, 1995; *Keene et al*., 1990; *Pszenny et al*., 1993; *Vogt et al*., 1996].

The fine fraction Cl^- deficit correlates with the fine MSA/sea-salt component (component 4), which also carries a significant signature of fine NSS-SO_4^{2-}. This NSS-SO_4^{2-} appears to be the main actor for the deficit of Cl^- in the fine fraction, clearly visible in Figure 11c, where the data points representing the NSS-SO_4^{2-} neq concentrations versus Cl^- deficit (open circles) fall around the 1:1 line. These observations are in agreement with *Sievering et al*.'s [1990] findings from samples collected in Bermuda, where they observed that the fine fraction (<1 μm) aerosol Cl^- displacement appears to be more likely by SO_4^{2-} than by NO_3^-.

Kerminen et al. [1998] also found that MSA and oxalate replace Cl^- from supermicron sea-salt particles. However, concentrations of MSA and oxalate are so small compared to NSS-SO_4^{2-} and NO_3^- that their effect would be minute and undetectable in the present case.

4.3. SO_4^{2-} Contributions

Sulfate in the atmosphere is composed from a series of different sources. It is of special interest to determine the various contributions to NSS-SO_4^{2-} since particles in the submicrometer size range may serve as CCN and influence the radiation balance of the atmosphere [*Charlson et al*., 1987].

Weighted linear regression analysis has been shown [*Johansen et al*., 1999] to be a useful tool for identifying the sources and determining the source strengths of SO_4^{2-}. Tracers are used to represent the various sources: typically, Na^+ serves as the sea salt, MSA as the biogenic, and Pb or NO_3^- as the anthropogenic tracer. The principal component analysis in Table 3 gives an indication of which species can be used as surrogates for the different SO_4^{2-} sources. Component 3 carries high scores for fine and coarse NSS-SO_4^{2-}, which appears to correlate strongly with fine and coarse Zn and fine Pb and less with coarse NO_3^- and coarse NSS-Ca^{2+}. Thus Zn, Pb, and NO_3^- may be potential anthropogenic tracers, while NSS-Ca^{2+} may describe a gypsum component that was, e.g., observed over the Indian Ocean by *Johansen et al*. [1999].

Exploration of the various tracer combinations in the regression analysis did not uncover a regression that satisfactorily describes the present system. Table 6 lists the best model runs for each of the size fractions, fine, coarse, and total. In each case, the corresponding SO_4^{2-} is the dependent variable, and the tracers used for the various sources represent the set of independent variables. The model can be tested by inspecting the statistical information that accompanies it (refer to *Johansen et al*. [1999] and *Zar* [1996] for a detailed description). In addition, there is a convenient way of testing the models in the present case: The ratio of SS-SO_4^{2-}/Na^+ is constant and known, 0.252 [*Millero and Sohn*, 1992]; thus the corresponding coefficient extracted in the model should be close to 0.252. However, this is not the case in any of our models. Furthermore, in an optimal situation the intercept with the ordinate (denoted, "constant," in the models) should be close to zero, and the significance of the null hypothesis for this constant should be large if the regression can be forced through the origin. In that case the dependent variable is satisfactorily described by the selected independent variables. This is also not observed in the presented models.

The value of real interest is the coefficient for the biogenic SO_4^{2-} contribution (bio-SO_4^{2-}), bio-SO_4^{2-}/MSA, which is thought to depend only on atmospheric temperature [*Bates et al*., 1992; *Berresheim et al*., 1989, 1991; *Bürgermeister and Georgii*, 1991; *Hynes et al*., 1986; *Prospero et al*., 1991; *Pszenny et al*., 1989; *Saltzman et al*., 1985, 1983; *Savoie and Prospero*, 1989, 1994; *Savoie et al*., 1992; *Savoie et al*., 1989a]. A priori knowl-

Table 6. Model Outputs From Weighted Linear Regressions With Coarse, Fine, and Total SO_4^{2-} Fractions as Dependent Variables

Dependent Variable	Model Summary			Independent Variables	Unstandardized Coefficients		Standardized Coefficients			95% Confidence Interval for *B*	
	R^2	*F*	Significance		*B*	SE	*b*	*t*	Significance	Lower Bound	Upper Bound
SO_4^{2-} coarse	0.990	402.981	0.000	(constant)	−169.761	33.858		−5.014	0.000	−241.537	−97.984
				Na^+ coarse	0.222	0.008	0.799	28.854	0.000	0.205	0.238
				MSA coarse	37.442	2.764	0.369	13.544	0.000	31.581	43.302
				NSS-Ca^{2+} coarse	0.485	0.053	0.348	9.232	0.000	0.373	0.596
				Zn coarse	23.361	11.224	0.073	2.081	0.054	−0.432	47.154
SO_4^{2-} fine	0.940	88.564	0.000	(constant)	−98.610	121.202		−0.814	0.427	−354.324	157.103
				Na^+ fine	0.194	0.080	0.161	2.414	0.027	0.024	0.363
				MSA fine	23.863	4.175	0.414	5.715	0.000	15.054	32.673
				Pb fine	757.756	75.435	0.657	10.045	0.000	598.602	916.909
SO_4^{2-} total	0.961	98.888	0.000	(constant)	−344.949	188.144		−1.833	0.085	−743.797	53.899
				Na^+ total	0.198	0.030	0.393	6.717	0.000	0.136	0.261
				MSA total	33.901	5.047	0.361	6.717	0.000	23.202	44.600
				NSS-Ca^{2+} coarse	1.278	0.213	0.452	6.009	0.000	0.827	1.728
				Zn total	34.757	11.123	0.210	3.125	0.007	11.179	58.336

Table 7. Model Outputs From Weighted Linear Regressions With Coarse and Fine Nonbiogenic SO_4^{2-} Fractions as Dependent Variables

Dependent Variable	Model Summary			Independent Variables	Unstandardized Coefficients		Standardized Coefficients			95% Confidence Interval for *B*	
	R^2	*F*	Significance		*B*	SE	*b*	*t*	Significance	Lower Bound	Upper Bound
Nonbiogenic SO_4^{2-} coarse	0.990	572.168	0.000	Na^+ coarse	0.224	0.014	0.748	16.254	0.000	0.195	0.253
				NSS-Ca^{2+} coarse	0.393	0.110	0.220	3.567	0.002	0.162	0.624
				Zn coarse	20.372	19.393	0.062	1.022	0.320	−21.519	62.262
Nonbiogenic SO_4^{2-} coarse	0.991	627.703	0.000	Na^+ coarse	0.199	0.021	0.664	9.304	0.000	0.154	0.244
				NSS-Ca^{2+} coarse	0.308	0.122	0.173	2.515	0.022	0.051	0.565
				NO_3^- coarse	0.386	0.228	0.186	1.695	0.107	−0.092	0.864
Nonbiogenic SO_4^{2-} coarse	0.982	526.778	0.000	Na^+ coarse	0.242	0.016	0.806	14.740	0.000	0.207	0.276
				Zn coarse	70.431	18.014	0.214	3.910	0.001	32.727	108.134
Nonbiogenic SO_4^{2-} fine	0.975	375.377	0.000	Na^+ fine	0.270	0.067	0.295	4.040	0.001	0.130	0.410
				Pb fine	971.587	98.378	0.721	9.876	0.000	765.680	1177.495

edge of this ratio would serve to determine the SO_4^{2-} concentrations in the atmosphere which are purely biogenically derived from measured MSA concentrations. The bio-SO_4^{2-}/MSA ratios determined in the linear regression analyses appear in parentheses in Table 6; 37.4 ± 2.8 for the coarse SO_4^{2-}, 23.9 ± 4.2 for the fine SO_4^{2-}, and 33.9 ± 5.0 for the total SO_4^{2-}. These values are slightly lower than the calculated NSS-SO_4^{2-}/MSA ratio, which is the ratio typically reported in literature. The geometric mean for the NSS-SO_4^{2-}/MSA ratio in the combined fine and coarse fractions amounts to 37.4 ± 16.4 (compared to 33.9 ± 5.0 in Table 6), whereby it ranges from 11.1 to 75.1. The lowest ratio of 11.1 is observed in sample A96-09, when crustal, anthropogenic, and sea-salt abundances are very low. Thus this value may represent a true bio-SO_4^{2-}/MSA ratio valid at the measured temperature, 26°C. This one observation happens to be in accordance with Figure 5 of *Johansen et al*. [1999], which presents a bio-SO_4^{2-}/MSA temperature relationship found during two seasons over the Arabian Sea.

NSS-SO_4^{2-}/MSA ratios reported in literature are not typically corrected for anthropogenic contributions; thus, very often they are higher than the true biogenic ratio. *Savoie et al*. [1989b] found that ratios of 35.7 dropped to 15.2 when corrected for anthropogenic SO_4^{2-} contributions using NO_3^-. In the remote tropical Pacific Ocean [*Saltzman et al*., 1985, 1983], where continental inputs are believed to be minimal, low NSS-SO_4^{2-}/MSA values of ~15 were observed. These values are close to what the biogenic SO_4^{2-}/MSA ratio is expected to be in tropical regions. Values in the same range were found over the Arabian Sea [*Johansen et al*., 1999] during two seasons where samples were corrected for additional inputs, other than biogenic SO_4^{2-}. In the same study the SW monsoon season represented very clean marine conditions, during which biogenically derived MSA concentrations were appreciable and anthropogenic sources were negligible. The uncorrected NSS-SO_4^{2-}/MSA ratio in those samples averaged ~14, which is, as expected, very close to the real bio-SO_4^{2-}/MSA, corrected for the small anthropogenic SO_4^{2-} concentrations; 13.5. NSS-SO_4^{2-}/MSA values (uncorrected for anthropogenic contributions) in the range of 30–40, comparable to what we determined in the present case, have been observed over the Atlantic Ocean [*Davison et al*., 1996; *Galloway and Rodhe*, 1991; *Galloway et al*., 1993]. They were always attributed to continental contamination.

A couple of potential reasons exist for the difficulty in extracting biogenic SO_4^{2-}/MSA ratios in the expected range (around 15 or lower) from the application of the linear regression analysis, as done by *Johansen et al*. [1999]. In a linear regression analysis the ratio between the tracer and the corresponding SO_4^{2-} portion needs to remain constant for each sample for it to be successful. Circumstances in which this condition may not hold true include sampling of air masses of very different source regions and large temperature variations between and within samples. During the present cruise, both the air mass characteristics and the temperature varied considerably throughout the duration of the trip. Temperatures ranged from 21 to 28°C. In the regime of 24 to 28°C, according to Figure 5 of *Johansen et al*. [1999], one may expect an increase in the bio-SO_4^{2-}/MSA ratio of ~2 per degree increase in temperature. Thus the outcome of the model can therefore not be reliable. The same argument holds for the ratio between the anthropogenic tracer and the corresponding anthropogenic SO_4^{2-} fraction. Some investigators [*Li-Jones and Prospero*, 1998; *Savoie et al*., 1989b] have used the magnitude of the ratio NO_3^-/NSS-SO_4^{2-} to determine whether or not the observed pollutants were of European or African origin. By analogy, it is expected that the anthropogenic SO_4^{2-} in relation to Pb and Zn will vary according to their source regions.

The insufficient number of samples prevents us from classifying samples into air mass origin and temperature groups. Owing to the complex characteristics of this data set, it appears difficult to ascertain the biogenic and anthropogenic inputs of SO_4^{2-} into the atmosphere in an analogous manner as carried out by *Johansen et al*. [1999], where air mass origins were very consistent for each season of the year.

As an alternative, the magnitude of the various SO_4^{2-} contributions can be estimated by assuming that the bio-SO_4^{2-}/MSA ratio temperature dependence in Figure 5 of *Johansen et al*. [1999] is a reasonable approximation for the bio-SO_4^{2-} concentrations for each sample. The bio-SO_4^{2-}/MSA ratio follows an exponential dependence: bio-SO_4^{2-}/MSA = 0.06 exp(0.198 T(C°)). In an analogous manner as performed above, weighted linear regressions with the remaining nonbiogenic SO_4^{2-} and appropriate tracers could reveal the magnitude of the other sources and prove the justified use of Figure 5 of *Johansen et al*. [1999]. Table 7 lists the outcome of the best models for linear regressions on the coarse and fine nonbiogenic SO_4^{2-} fractions. Tracers for the nonbiogenic coarse and fine SO_4^{2-} fractions are chosen based in correlations observed in the principal component analysis, identical to the reasoning followed when the linear regressions from Table 6 were performed. Linear regressions with the total nonbiogenic SO_4^{2-} were unsuccessful, and as a consequence, they are not shown in Table 7.

The coarse NSS-SO_4^{2-} fraction includes an anthropogenic component, which appears to correlate with coarse NO_3^- and with Zn in both size fractions. Coarse NSS-Ca^{2+} also shows an indication of correlating with coarse NSS-SO_4^{2-}; thus it is conceivable to believe that gypsum, $CaSO_4$, is present in the samples. $CaSO_4$ has been observed in aerosol particles and may be a result of the reaction between acid sulfates and silicate minerals brought together by in-cloud processes [*Andreae et al*., 1986]. In addition, $CaSO_4$ may be associated with the combustion of fossil fuels [*Hopke*, 1985], and it may originate from crustal sources such as evaporite deposits and gyspiferous soils, as has been observed over the northern Indian Ocean [*Johansen et al*., 1999; *Savoie et al*., 1987]. However, $CaSO_4$ observed on samples collected over the Atlantic Ocean has been attributed to be a conversion product of calcite reacting with atmospheric sulfur species on the filter during sample collection [*Glaccum and Prospero*, 1980]. Thus the dust is not believed to contain any primary gypsum.

The first two models in Table 7 differ only in the choice of the anthropogenic tracer. Although the statistics show that the second model, which includes NO_3^-, is slightly better than the first one, in which Zn is the anthropogenic tracer, the coefficient for SS-SO_4^{2-}/Na^+ shows a value closer to the one expected in seawater (0.252) in the model with Zn. Since the ordinate intercept is negligible in both cases with a large significance for its null hypothesis, the linear regression is forced through the origin. Compared with the linear regression carried out on coarse SO_4^{2-} in Table 6, the ones carried out on the coarse nonbiogenic SO_4^{2-} in Table 7 result in better models. Nevertheless, the first model in Table 7 does not perfectly describe the observed coarse SO_4^{2-} concentrations, as is visualized in Figure 15a. The anthropogenic and gypsum contributions are calculated based on the coefficients found in the first

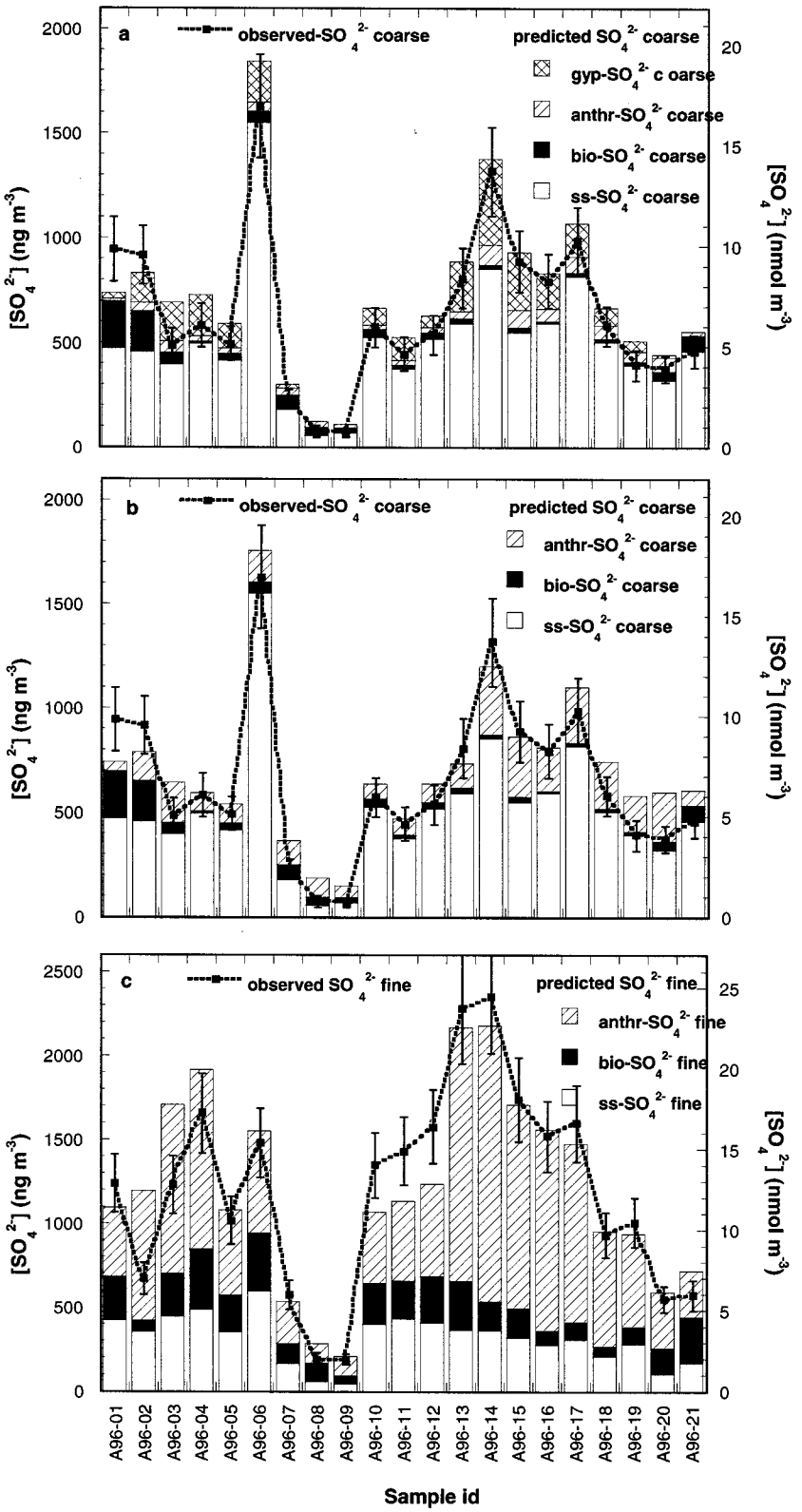

Figure 15. Model predictions (based on multiple linear regression analyses) for SO_4^{2-} contributions from different sources (in stacked bars) compared with observed SO_4^{2-} concentrations versus sample ID (a) in the coarse fraction, assuming the presence of gypsum, (b) in the coarse fraction, neglecting gypsum, and (c) in the fine fraction.

model in Table 7; the sea-salt component on the other hand is determined from the constant value 0.252 and not from the coefficient in the model. This corresponds to an overestimation of the sea-salt component by 11% compared to what the model output would predict. The biogenic fraction is determined from the observed MSA concentrations and the corresponding ratio found from the exponential temperature dependence in Figure 5 of *Johansen et al*. [1999]. Figure 15a shows that with exception of the first two samples, the model overpredicts total coarse SO_4^{2-} by on average 9.9%, some of which may be attributed to the larger sea-salt fraction used by assuming that the SS-SO_4^{2-}/Na^+ ratio is 0.252 instead of 0.224. Since other characteristics of the aerosol material (discussed above) have shown that the NSS-Ca^{2+} most probably is derived from calcite instead of gypsum, the use of NSS-Ca^{2+} in the model may also lead to an overprediction of SO_4^{2-}.

Figure 15b shows the contributions to coarse SO_4^{2-} when neglecting the existence of $CaSO_4$, corresponding to the third linear regression output in Table 7. As in the other two models, the intercept becomes negligible and the regression is forced through the origin. This time, the SS-SO_4^{2-}/Na^+ ratio that is returned by the linear regression is only 4% smaller than the expected value of 0.252. Nevertheless, the model overpredicts coarse SO_4^{2-} more than the previous model that included $CaSO_4$. The average overprediction, excluding samples A96-08 and A96-09 (due to their large discrepancy from the model because of low concentrations and attributed large errors), amounts to 13.6%.

In both the models for the coarse SO_4^{2-} contributions (first and third in Table 7), presented in Figures 15a and 15b, the coarse biogenic SO_4^{2-} component accounts for ~7% (50 ± 57 ng m^{-3}) of the total coarse SO_4^{2-}, which translates into ~24% of the coarse NSS-SO_4^{2-}. If neglecting the presence of $CaSO_4$, the rest (~76%) of the NSS-SO_4^{2-} would be of anthropogenic origin, which accounts for ~21% (148 ± 83 ng m^{-3}) of the total SO_4^{2-}.

It is not clear which of the two models for the coarse SO_4^{2-} better fits the observed concentrations. Because gypsum has generally not been seen over the Atlantic Ocean, it may be an artifact from the reaction of $CaCO_3$ with H_2SO_4 collected on the filter, as indicated by *Glaccum and Prospero* [1980]. The degree of $CaCO_3$ to $CaSO_4$ conversion will depend on the availability of NSS-SO_4^{2-} and thus on the characteristics of each air mass. Since we measure the combined concentration of $CaCO_3$ and $CaSO_4$ (as NSS-Ca^{2+}), no distinction can be made between the two. Thus, although an attempt is made here to separate the temperature effect from the linear regression, there appear to be additional parameters that influence the linear regression analyses such that no good fit of the observed coarse SO_4^{2-} concentrations is achieved. The most probable causes are in the large variability in aerosol origin, which would manifest itself in nonconstant ratios for the anthropogenic tracer and in the possibility of the presence of a small and varying quantity of $CaSO_4$ which cannot unambiguously be described by the tracer NSS-Ca^{2+}.

Fine SO_4^{2-}, as found in the linear regression analysis from Table 6 and in the principal component analysis in Table 3, does not seem to correlate with NSS-Ca^{2+}. Thus the presence of a potential source of gypsum SO_4^{2-} does not complicate the situation for the linear regression of the fine fraction. After subtracting the biogenic SO_4^{2-} from the total fine SO_4^{2-}, the nonbiogenic SO_4^{2-} remainder is used in the linear regression analysis presented at the end of Table 7. Since the intercept is close to zero, the model is forced through the origin. The SS-SO_4^{2-}/Na^+ ratio given by the linear regression, 0.270, is 8% above what is expected for sea salt. Figure 15c shows the predicted contributions in the stacked bars in comparison to the observed fine SO_4^{2-} concentration, represented by the dotted curve. It is clear that the model overestimates the beginning, underestimates the middle, and fits nicely for the latter part of the cruise. This observation strengthens the argument about the different characteristics of the air masses sampled. On average, the model overestimates fine SO_4^{2-} by 5.8%. The origins are approximately 16% (188 ± 97 ng m^{-3}) biogenic, 58% (704 ± 443 ng m^{-3}) anthropogenic, and 26% (311 ± 144 ng m^{-3}) sea salt. The biogenic contribution to NSS-SO_4^{2-} in the fine fraction amounts to 22%, while the rest is anthropogenically derived.

4.4. Fe(II)

Ferrous iron released after 22 hours of extraction time with added ferrozine is found to correlate with the corresponding total Fe, while Fe(II) after 5 min extraction with ferrozine ($Fe(II)_{total,5min}$) correlates with anthropogenic tracers such as NO_3^-, NSS-SO_4^{2-}, and oxalate. This seems to suggest that the Fe(II) after 22 hours depends on the total iron that is available in the sample, regardless of its initial form, while the $Fe(II)_{total,5min}$ abundance depends on additional factors. The dependence of Fe(II) concentrations on the mentioned anthropogenic tracers is in agreement with observations made in numerous field and laboratory studies, indicating that Fe(II) is photochemically produced in the presence of organic acids and ferric oxides and (oxy)hydroxides [*Erel et al*., 1993; *Faust and Hoigné*, 1990; *Faust and Zepp*, 1993; *Pehkonen et al*., 1993; *Siefert et al*., 1994; *Zuo*, 1995; *Zuo and Hoigné*, 1992, 1994]. Iron is also known to catalyze the oxidation of S(IV) by oxygen [*Berglund and Elding*, 1995; *Berglund et al*., 1993; *Conklin and Hoffmann*, 1988; *Faust and Allen*, 1994; *Kraft and van Eldik*, 1989; *Martin and Hill*, 1987]. Furthermore, the correlation with NO_3^- and NSS-SO_4^{2-} may also be indicative of a lower aerosol pH which increases Fe(II) stability relative to its oxidation.

The ratios NH_4^+/NSS-SO_4^{2-} and (NH_4^+ + NSS-Ca^{2+})/NSS-SO_4^{2-} are indicators of the acidity in the aerosol particle which may serve to study the observed Fe(II) concentrations. These ratios are presented in Figures 13 and 14. When neglecting the acid-neutralizing capacity of $CaCO_3$, the aerosol particles collected during several sampling periods are relatively acidic. This is reflected in the low values (close to 0.5) of the NH_4^+/NSS-SO_4^{2-} ratio seen near Cape Verde (Figure 13b). In Figure 16a this ratio is plotted as a function of $Fe(II)_{total,5min}$ in both fine and total fractions (coarse values are not presented for reasons given above). A relationship is apparent in Figure 16a between acidic conditions and the observed Fe(II) concentrations. After taking into account the acid neutralizing capacity of $CaCO_3$, which is especially abundant near Cape Verde, there appears to be a similar tendency in the data set (Figure 16b). This time, the increase in Fe(II) concentration as a function of a decreasing (NH_4^+ + NSS-Ca^{2+})/NSS-SO_4^{2-} ratio is more pronounced in the fine fraction; this may be due to the lower $CaCO_3$ abundances in the fine fraction compared to the coarse fraction.

It is interesting to note that when comparing $Fe(II)_{total,5min}$ with total Fe (in Figure 4c), the samples appear to be divided into three groups: the first part of the cruise, where total Fe is considerable but $Fe(II)_{total,5min}$ is small, the middle part of the cruise, near the equator, when total Fe is small and Fe(II) is

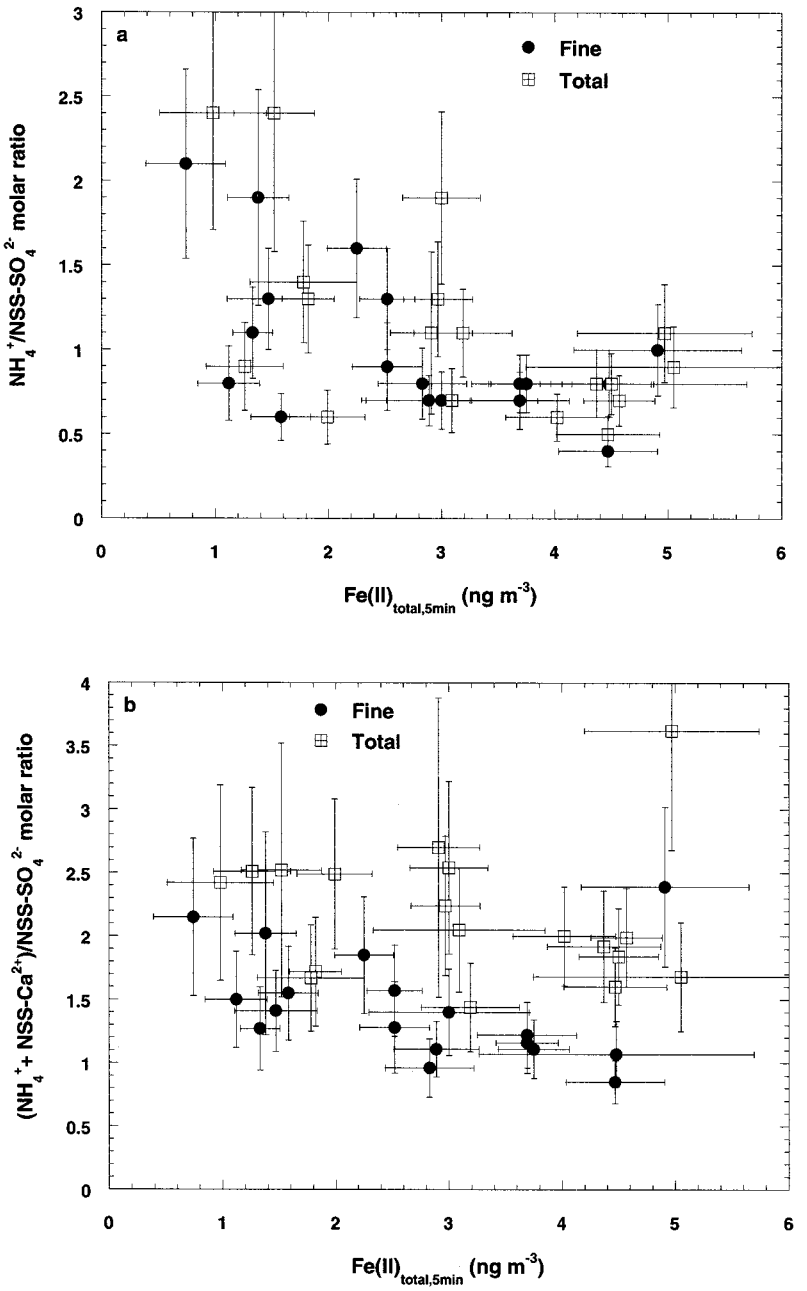

Figure 16. (a) $NH_4^+/NSS\text{-}SO_4^{2-}$ and (b) $(NH_4^+ + NSS\text{-}Ca^{2+})/NSS\text{-}SO_4^{2-}$ versus $Fe(II)_{total,5minFZ}$ concentrations in fine fraction and fine and coarse combined (total).

not negligible, and the last part of the cruise, when total Fe takes on a middle range, while $Fe(II)_{total,5min}$ is considerable. The same effect can be recognized in Figure 5, in terms of percent of $Fe(II)_{total,5min}$ in total Fe. This observation is in agreement with the general mineralogical characteristics found during the present cruise. The low mineral dust concentrations near the equator may indicate that the air mass may have traveled a considerable amount of time during which most particles may have settled out of the boundary layer, but the remaining ones had sufficient time to undergo chemical transformation producing more Fe(II). Similar reasoning may be used for interpreting the $Fe(II)_{total,5min}$ versus total Fe changes observed during the latter part of the cruise, when mineral aerosol material seems to be from one and the same source (i.e., the northern Sahara). As the aerosol is transported from Cape Verde (sample A96-14) to Barbados, both total Fe and $Fe(II)_{total,5min}$ drop off, see Figure 4c, due to sedimentation of the particles. However, during the same time the relative contribution of Fe(II) is increasing; see Figure 5. This may, again, be a function of the time available for the iron phases in the aerosol particle to undergo photochemical reduction that leads to increased Fe(II) concentrations. The increase in the combined percentage coarse and fine $Fe(II)_{total,5min}$ is a factor of 2.9 from sample A96-14 to sample A96-20. This effect is more pronounced in the coarse than in the fine fraction, where the relative $Fe(II)_{total,5min}$ increases by factors of 3.6 and 1.8, respectively.

Another interesting feature, which is revealed in the princi-

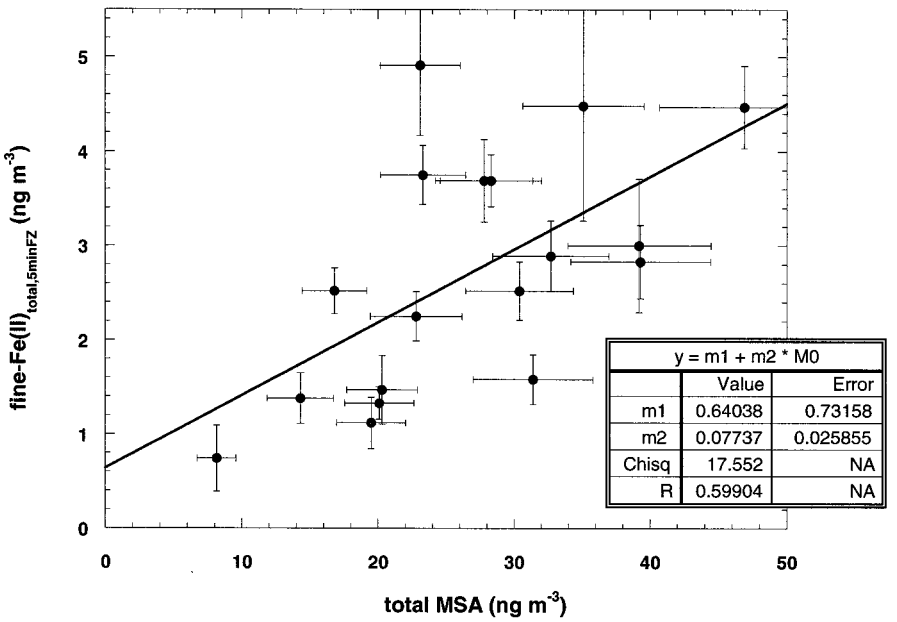

Figure 17. $Fe(II)_{total,5minFZ}$ in fine fraction versus MSA.

pal component analysis presented in Table 3, is that $Fe(II)_{total,5min}$ in the fine fraction, where 86% of the $Fe(II)_{total,5min}$ is present, correlates with MSA (in component 4). A weak relationship is affirmed by plotting fine $Fe(II)_{total,5minFZ}$ versus total MSA, as shown in Figure 17. In an iron enrichment experiment in underproductive surface ocean water, *Turner et al*. [1996] observed an increase in DMS production as predicted by a number of investigators [*Martin et al*., 1994; *Martin and Fitzwater*, 1988; *Martin et al*., 1991; *Zhuang et al*., 1992b]. Since DMS is oxidized to MSA and NSS-SO_4^{2-}, it may be plausible to detect a feedback in the MSA concentration from the increased Fe(II) input into the surface waters of the ocean.

5. Conclusions

Mineralogical characteristics of the mineral aerosol and back trajectories of the air masses sampled in the present cruise appear to indicate a Saharan desert origin; larger calcite concentrations observed during the second half of the cruise suggest a more northern Sahara source. On the basis the observed ratios between trace metals and the abundances of alkali and alkaline earth elements, the mineralogical composition of the collected mineral dust is best described as shale. This conclusion is in agreement with observations made by other investigators [*Glaccum and Prospero*, 1980].

Mineral dust aerosol concentrations based on the composition of shale amount to an average of 19.3 ± 16.4 $\mu g\ m^{-3}$ and range from 0.8 to 55.6 $\mu g\ m^{-3}$. This value is only 5% larger than that obtained if assuming an average crustal composition, which matches well with the numerous other studies performed in the same area. The variability of the mineral dust concentrations collected during the present study is considerably larger than that of the sea-salt aerosol observed. Sea-salt aerosol concentrations average 10.6 ± 5.5 $\mu g\ m^{-3}$ and range from 1.4 to 27.8 $\mu g\ m^{-3}$. Calcite and ammonium sulfate and nitrate concentrations add only small amounts to the total of the suspended particulate matter: 1.3 ± 1.0 $\mu g\ m^{-3}$ and 1.9 ± 0.9 $\mu g\ m^{-3}$, respectively.

The only source of iron in the aerosol is mineral dust. Total iron concentrations average 0.84 ± 0.61 $\mu g\ m^{-3}$ and range from <0.05 to 2.38 $\mu g\ m^{-3}$. The Fe is evenly distributed between the coarse, 0.42 $\mu g\ m^{-3}$, and fine aerosol fractions, 0.43 $\mu g\ m^{-3}$. Ferrous iron accounts for only 0.51 ± 0.56% of the total iron, with an average concentration of 3.14 ± 1.35 ng m^{-3}. Eighty-six percent of Fe(II) is present in the fine aerosol fraction, and it appears to be more rapidly released from the particulate phase compared to the coarse fraction. These low relative Fe(II) concentrations are in the same range as those found by *Zhu et al*. [1993, 1997] in Barbados and by *Siefert et al*. [1999] over the northern Indian Ocean.

Ferrous iron concentrations appear to be independent of the total available Fe and instead show a correlation with NSS-SO_4^{2-}, oxalate, and MSA. The excess NSS-SO_4^{2-} adds acidity to the aerosol particles and may be responsible for the increased stability of Fe(II) with respect to oxidation to the less soluble Fe(III). Oxalate is the final product of photochemically induced reactions involving many organic precursors, and it is known to be an efficient electron donor for the photochemical reduction of Fe(II) in atmospheric waters. Thus the observed correlation between the oxalate abundance and Fe(II) may be a direct consequence of this photo-induced reduction of solid iron phases in the aerosol particles. The extent of conversion of the Fe(III) to Fe(II) will depend on the time that the aerosol particle has spent in the atmosphere before it was sampled. Therefore we observe an increase in the relative Fe(II) concentrations between the African continent and Barbados by a factor of 2.9.

NSS-SO_4^{2-} concentrations average 1.03 ± 0.60 $\mu g\ m^{-3}$, most of which is present in the fine fraction (87%). From our analysis it appears that ~22% of the fine NSS-SO_4^{2-} is of biogenic origin and the remainder is anthropogenic. In the coarse fraction the biogenic NSS-SO_4^{2-} contribution accounts for 24%,

while the rest is of anthropogenic origin, assuming that no primary $CaSO_4$ is present in the samples.

The chloride deficits range from 10.6 to 47.1% and average 18.3 ± 9.1%. In these samples the deficit can be attributed to acid displacement reactions with HNO_3 and H_2SO_4. In the coarse fraction, which contains an appreciable amount of the NO_3^- (57% of the total), the acid displacement reaction between HNO_3 and Cl^- appears to be the main contributor to the deficit. In the fine fraction the reaction between H_2SO_4 and Cl^- seems to be responsible for the observed deficit.

Acknowledgments. The authors wish to thank Doug Capone from the Chesapeake Biological Laboratory, University of Maryland, Solomons, Maryland, for the invitation to join him and his team on the R/V *Seward Johnson* during the month of April 1996. Research support was provided by the National Science Foundation and by the Environment Now Foundation. Their support is greatly appreciated.

References

Anderson, J. R., P. R. Buseck, T. L. Patterson, and R. Arimoto, Characterization of the Bermuda tropospheric aerosol by combined individual-particle and bulk-aerosol analysis, *Atmos. Environ.*, *30*(2), 319–338, 1996.

Andreae, M. O., Soot carbon and excess fine potassium: Long-range transport of combustion-derived aerosols, *Science*, *220*, 1148–1151, 1983.

Andreae, M. O., Raising dust in the greenhouse, *Nature*, *380*, 389–390, 1996.

Andreae, M. O., R. J. Charlson, H. S. Bruynseels, R. Van Grieken, and W. Maenhaut, Internal mixture of sea salt, silicates, and excess sulfate in marine aerosols, *Science*, *232*, 1620–1623, 1986.

Andreae, M. O., W. Elbert, and S. J. de Mora, Biogenic sulfur emissions and aerosols over the tropical South Atlantic, 3, Atmospheric dimethylsulfide, aerosols and cloud condensation nuclei, *J. Geophys. Res.*, *100*, 11,335–11,356, 1995.

Arimoto, R., R. A. Duce, B. J. Ray, W. G. Ellis Jr., J. D. Cullen, and J. T. Merrill, Trace elements in the atmosphere over the North Atlantic, *J. Geophys. Res.*, *100*, 1199–1213, 1995.

Aston, S. R., R. Chester, L. R. Johnson, and R. C. Padgham, Eolian dust from the lower atmosphere of the eastern Atlantic and Indian Oceans, China Sea and Sea of Japan, *Mar. Geol.*, *14*, 15–28, 1973.

Barrie, L. A., J. W. Bottenheim, R. C. Schnell, P. J. Crutzen, and R. A. Rasmussen, Ozone destruction and photochemical reactions at polar sunrise in the lower Arctic atmosphere, *Nature*, *334*, 138–141, 1988.

Bassett, M. E., and J. H. Seinfeld, Atmospheric equilibrium model of sulfate and nitrate aerosols-II. Particle size analysis, *Atmos. Environ.*, *18*(6), 1163–1170, 1984.

Bates, T. S., J. A. Calhoun, and P. K. Quinn, Variations in the methanesulfonate to sulfate molar ratio in submicrometer marine aerosol particles over the South Pacific Ocean, *J. Geophys. Res.*, *97*, 9859–9865, 1992.

Behra, P., and L. Sigg, Evidence of redox cycling of iron in atmospheric water droplets, *Nature*, *344*, 419–421, 1990.

Bergametti, G., L. Gomes, G. Coude-Gaussen, P. Rognon, and M.-N. Le Coustumer, African dust observed over Canary Islands: Source-regions identification and transport pattern for some summer situations, *J. Geophys. Res.*, *94*, 14,855–14,864, 1989.

Berglund, J., and L. I. Elding, Manganese-catalyzed autoxidation of dissolved sulfur dioxide in the atmospheric aqueous phase, *Atmos. Environ.*, *29*(12), 1379–1391, 1995.

Berglund, J., S. Fronaeus, and L. I. Elding, Kinetics and mechanism for manganese-catalyzed oxidation of sulfur(IV) by oxygen in aqueous solution, *Inorg. Chem.*, *32*, 4527–4538, 1993.

Berresheim, H., M. O. Andreae, G. P. Ayers, and R. W. Gillett, Distribution of Biogenic Sulfur Compounds, *ACS Symp. Ser.*, *393*, 352–366, 1989.

Berresheim, H., M. O. Andreae, R. L. Iverson, and S. M. Li, Seasonal variations of dimethylsulfide emissions and atmospheric sulfur and nitrogen species over the western north Atlantic Ocean, *Tellus*, *Ser. B*, *43*, 353–372, 1991.

Berresheim, H., F. L. Eisele, D. J. Tanner, L. M. McInnes, D. C. Ramsey-Bell, and D. S. Covert, Atmospheric sulfur chemistry and cloud condensation nuclei (CCN) concentrations over the northeastern Pacific coast, *J. Geophys. Res.*, *98*, 12,701–12,711, 1993.

Bottenheim, J. W., L. A. Barrie, E. Atlas, L. E. Heidt, H. Niki, R. A. Rasmussen, and P. B. Shepson, Depletion of lower tropospheric ozone during Arctic spring: The polar sunrise experiment 1988, *J. Geophys. Res.*, *95*, 18,555–18,568, 1990.

Bürgermeister, S., and H.-W. Georgii, Distribution of methanesulfonate, nss-sulfate and dimethylsulfide over the Atlantic and the North Sea, *Atmos. Environ.*, *Part A*, *25*(3/4), 587–595, 1991.

Charlson, R. J., J. E. Lovelock, M. O. Andreae, and S. G. Warren, Oceanic phytoplankton, atmospheric sulphur, cloud albedo and climate, *Nature*, *326*, 655–661, 1987.

Chester, R., H. Elderfield, J. J. Griffin, L. R. Johnson, and R. C. Padgham, Eolian dust along the eastern margins of the Atlantic Ocean, *Mar. Geol.*, *13*, 91–105, 1972.

Chiapello, I., G. Bergametti, and B. Chatenet, Origins of African dust transport over the northeastern tropical Atlantic, *J. Geophys. Res.*, *102*, 13,701–13,709, 1997.

Conklin, M. H., and M. R. Hoffmann, Metal ion-sulfur(IV) chemistry, 3, Thermodynamics and kinetics of transient iron(III)-sulfur(IV) complexes, *Environ. Sci. Technol.*, *22*, 899–907, 1988.

Cooper, D. J., A. J. Watson, and P. D. Nightingale, Large decrease in ocean-surface CO_2 fugacity in response to in situ iron fertilization, *Nature*, *383*, 511–514, 1996.

D'Almeida, G. A., A model for Saharan dust transport, *J. Clim. Appl. Meteorol.*, *25*, 903–916, 1986.

D'Almeida, G., On the variability of desert aerosol radiative characteristics, *J. Geophys. Res.*, *92*, 3017–3026, 1987.

Davison, B., C. O'Dowd, C. N. Hewitt, M. H. Smith, R. M. Harrison, D. A. Peel, E. Wolf, R. Mulvaney, M. Schwikowski, and U. Baltensperger, Dimethyl sulfide and its oxidation products in the atmosphere of the Atlantic and Southern Oceans, *Atmos. Environ.*, *30*(10/11), 1895–1906, 1996.

Delaney, A. C., D. W. Parkin, J. J. Griffin, E. D. Goldberg, and B. E. F. Reiman, Airborne dust collected at Barbados, *Geochim. Cosmochim. Acta*, *31*, 885–909, 1967.

DiTullio, G. R., D. A. Hutchins, and K. W. Bruland, Interaction of iron and major nutrients controls phytoplankton growth and species composition in the tropical North Pacific Ocean, *Limnol. Oceanogr.*, *38*(3), 495–508, 1993.

Duce, R. A., and E. J. Hoffmann, Chemical fractionation at the air/sea interface, *Annu. Rev. Earth Planet. Sci.*, *4*, 187–228, 1976.

Duce, R. A., and N. W. Tindale, Atmospheric transport of iron and its deposition in the ocean, *Limnol. Oceanogr.*, *36*(8), 1715–1726, 1991.

Duce, R. B., W. H. Zoller, and J. L. Moyers, Particulate and gaseous halogens in the Antarctic atmosphere, *J. Geophys. Res.*, *78*, 7802–7811, 1973.

Duce, R. A., G. L. Hoffman, and W. H. Zoller, Atmospheric trace metals at remote Northern and Southern Hemisphere sites: Pollution of natural, *Science*, *187*, 59–61, 1975.

Echalar, F., A. Gaudichet, H. Cachier, and P. Artaxo, Aerosol emissions by tropical forest and savanna biomass burning: Characteristic trace elements and fluxes, *Geophys. Res. Lett.*, *22*, 3039–3042, 1995.

Ellis, W. G., Jr., and J. T. Merrill, Trajectories for Saharan dust transported to Barbados using Stokes's Law to describe gravitational settling, *J. Appl. Meteorol.*, *34*, 1716–1726, 1995.

Ellis, W. G., Jr., R. Arimoto, D. L. Savoie, J. T. Merrill, R. A. Duce, and J. M. Prospero, Aerosol selenium at Bermuda and Barbados, *J. Geophys. Res.*, *98*, 12,673–12,685, 1993.

Erel, Y., S. O. Pehkonen, and M. Hoffmann, Redox chemistry of iron in fog and stratus clouds, *J. Geophys. Res.*, *98*, 18,423–18,434, 1993.

Fan, S.-M., and D. J. Jacob, Surface ozone depletion in Arctic spring sustained by bromine reactions on aerosol, *Nature*, *359*, 522–524, 1992.

Faure, G., *Principles and Applications of Geochemistry*, Macmillan, Indianapolis, Indiana, 1998.

Faust, B. C., and J. M. Allen, Sunlight-initiated partial inhibition of the dissolved iron(III)-catalyzed oxidation of S(IV) species by molecular oxygen in aqueous solution, *Atmos. Environ.*, *28*(4), 745–748, 1994.

Faust, B. C., and J. Hoigné, Photolysis of Fe(III)-hydroxy complexes as sources of OH radicals in clouds, fog and rain, *Atmos. Environ.*, *Part A*, *24*(1), 79–89, 1990.

Faust, B. C., and R. G. Zepp, Photochemistry of aqueous iron(III)-polycarboxylate complexes: Roles in the chemistry of atmospheric and surface waters, *Environ. Sci. Technol.*, *27*, 2517–2522, 1993.

Finlayson-Pitts, B. J., Reaction of NO_2 with NaCl and atmospheric implications of NOCl formation, *Nature*, *306*, 676–677, 1983.

Finlayson-Pitts, B. J., M. J. Ezell, and J. N. Pitts Jr., Formation of chemically active chlorine compounds by reactions of atmospheric NaCl particles with gaseous N_2O_5 and $ClONO_2$, *Nature*, *337*, 241–244, 1989.

Galloway, J. N., and H. Rodhe, Regional atmospheric budgets of S and N fluxes: How well can they be quantified?, *Proc. R. Soc. Edinburgh*, *Sect. B*, *97*, 61–80, 1991.

Galloway, J. N., D. L. Savoie, W. C. Keene, and J. M. Prospero, The temporal and spatial variability of scavenging ratios for nss sulfate, nitrate, methanesulfonate and sodium in the atmosphere over the North Atlantic Ocean, *Atmos. Environ*., *Part A*, *27*(2), 235–250, 1993.

Glaccum, R. A., and J. M. Prospero, Saharan aerosols over the tropical North Atlantic—Mineralogy, *Mar. Geol*., *37*, 295–321, 1980.

Graedel, T. E., and W. C. Keene, Tropospheric budget of reactive chlorine, *Global Biogeochem. Cycles*, *9*(1), 47–77, 1995.

Harrison, R. M., J. D. Peak, and A. D. Kaye, Atmospheric aerosol major ion composition and cloud condensation nuclei over the northeast Atlantic, *J. Geophys. Res*., *101*, 4425–4434, 1996.

Hopke, P. K., Appendix: Selected source profiles, in *Receptor Modeling in Environmental Chemistry*, pp. 267–314, John Wiley, New York, 1985.

Huang, S., R. Arimoto, and K. Rahn, Changes in atmospheric lead and other pollution elements at Bermuda, *J. Geophys. Res*., *101*, 21,033–21,040, 1996.

Huebert, B. J., L. Zhuang, S. Howell, K. Noone, and B. Noone, Sulfate, nitrate, methanesulfonate, chloride, ammonium, and sodium measurements from ship, island, and aircraft during the Atlantic Stratocumulus Transition Experiment/Marine Aerosol Gas Exchange, *J. Geophys. Res*., *101*, 4413–4423, 1996.

Hynes, A. J., P. H. Wine, and D. H. Semmes, Kinetics and mechanism of OH reactions with organic sulfides, *J. Phys. Chem*., *90*, 4148–4156, 1986.

Johansen, A. M., R. L. Siefert, and M. R. Hoffmann, Chemical characterization of ambient aerosol collected during the southwest monsoon and intermonsoon seasons over the Arabian Sea: Anions and cations, *J. Geophys. Res*., *104*, 26,325–26,347, 1999.

Kawamura, K., and K. Ikushima, Seasonal changes in the distribution of dicarboxylic acids in the urban atmosphere, *Environ. Sci. Technol*., *27*, 2227–2235, 1993.

Keene, W. C., A. A. P. Pszenny, D. J. Jacob, R. A. Duce, J. N. Galloway, J. J. Schultz-Tokos, H. Sievering, and J. F. Boatman, The geochemical cycling of reactive chlorine through the marine troposphere, *Global Biogeochem. Cycles*, *4*(4), 407–430, 1990.

Keene, W. C., D. J. Jacob, and S.-M. Fan, New directions: Reactive chlorine: A potential sink for dimethylsulfide and hydrocarbons in the marine boundary layer, *Atmos. Environ*., *30*(6), i–iii, 1996.

Keene, W. C., R. Sander, A. A. P. Pszenny, R. Vogt, P. J. Crutzen, and J. N. Galloway, Aerosol pH in the marine boundary layer: A review and model evaluation, *J. Aerosol Sci*., *29*(3), 339–356, 1998.

Kerminen, V.-M., M. Aurela, R. E. Hillamo, and A. Virkkula, Formation of particulate MSA: Deductions from size distribution measurements in the Finnish Arctic, *Tellus*, *Ser. B*, *49*, 159–171, 1997.

Kerminen, V.-M., K. Teinilä, R. Hillamo, and T. Pakkanen, Substitution of chloride in sea-salt particles by inorganic and organic anions, *J. Aerosol Sci*., *29*(8), 929–942, 1998.

Kolber, Z. S., R. T. Barber, K. H. Coale, S. E. Fitzwater, R. M. Greene, K. S. Johnson, S. Lindley, and P. G. Falkowski, Iron limitation of phytoplankton photosynthesis in the equatorial Pacific Ocean, *Nature*, *371*, 145–149, 1994.

Kopcewicz, B., and M. Kopcewicz, Mössbauer study of iron-containing atmospheric aerosols, *Struct. Chem*., *2*(95), 303–312, 1991.

Kopcewicz, B., and M. Kopcewicz, Seasonal variations of iron concentration in atmospheric aerosols, *Hyperfine Interact*., *71*, 1457–1460, 1992.

Kopcewicz, B., and M. Kopcewicz, Iron-containing atmospheric aerosols, *Hyperfine Interact*., *11*, 179–187, 1998.

Kotronarou, A., and L. Sigg, SO_2 oxidation in atmospheric water: Role of Fe(II) and effect of ligands, *Environ. Sci. Technol*., *27*, 2725–2735, 1993.

Kraft, J., and R. van Eldik, Kinetics and mechanism of the iron(III)-catalyzed autoxidation of sulfur(IV) oxides in aqueous solution, 2, Decomposition of transient iron(III)-sulfur(IV) complexes, *Inorg. Chem*., *28*, 2306–2312, 1989.

Kuma, K., J. Nichioka, and K. Matsunaga, Controls on iron(III) hydroxide solubility in seawater: The influence of pH and natural organic chelators, *Limnol. Oceanogr*., *41*(3), 396–407, 1996.

Langer, S., B. T. McGovney, B. J. Finlayson-Pitts, and R. M. Moore, The dimethyl sulfide reaction with atomic chlorine and its implications for the budget of methyl chloride, *Geophys. Res. Lett*., *23*, 1661–1664, 1996.

Li, X., H. Maring, D. Savoie, K. Voss, and J. M. Prospero, Dominance of mineral dust in aerosol light-scattering in the North Atlantic trade winds, *Nature*, *380*, 416–418, 1996.

Li-Jones, X., and J. M. Prospero, Variations in the size distribution of non-sea-salt sulfate aerosol in the marine boundary layer at Barbados: Impact of African dust, *J. Geophys. Res*., *103*, 16,073–16,084, 1998.

Losno, R., G. Bergametti, and P. Carlier, Origins of atmospheric particulate matter over the North Sea and the Atlantic Ocean, *J. Atmos. Chem*., *15*, 333–352, 1992.

Martin, J. H., and S. F. Fitzwater, Iron deficiency limits phytoplankton growth in the northeast Pacific subarctic, *Nature*, *331*, 341–342, 1988.

Martin, J. H., R. M. Gordon, and S. E. Fitzwater, The case of iron, *Limnol. Oceanogr*., *36*(8), 1793–1802, 1991.

Martin, J. H., et al., Testing the iron hypothesis in ecosystems of the equatorial Pacific Ocean, *Nature*, *371*, 123–129, 1994.

Martin, R. L., and M. W. Hill, The iron catalyzed oxidation of sulfur: Reconciliation of the literature rates, *Atmos. Environ*., *21*(6), 1487–1490, 1987.

McConnell, J. C., G. S. Henderson, L. Barrie, J. Bottenheim, H. Niki, C. H. Langford, and E. M. J. Templeton, Photochemical bromine production implicated in Arctic boundary-layer ozone depletion, *Nature*, *355*, 150–152, 1992.

McInnes, L. M., D. S. Covert, P. K. Quinn, and M. S. Germani, Measurements of chloride depletion and sulfur enrichment in individual sea-salt particles collected from the remote marine boundary layer, *J. Geophys. Res*., *99*, 8257–8268, 1994.

Miller, L. A., and K. W. Bruland, Determination of copper speciation in marine waters by competitive ligand equilibration/liquid-liquid extraction: An evaluation of the technique, *Anal. Chim. Acta*, *284*, 573–586, 1994.

Millero, F. J., and M. L. Sohn, *Chemical Oceanography*, CRC Press, Boca Raton, Fla., 1992.

Millero, F. J., S. Sotolongo, D. J. Stade, and C. A. Vega, Effect of ionic interactions on the oxidation of Fe(II) with H_2O_2 in aqueous solutions, *J. Solution Chem*., *20*(11), 1079–1092, 1991.

Millero, F. J., W. Yao, and J. Aicher, The speciation of Fe(II) and Fe(III) in natural waters, *Mar. Chem*., *50*, 21–39, 1995.

Moffett, J. W., and R. G. Zika, Reaction kinetics of hydrogen peroxide with copper and iron in seawater, *Environ. Sci. Technol*., *1*, 804–810, 1987.

Muhs, D. R., R. C. Crittenden, J. N. Rosholt, C. A. Bush, and K. C. Stewart, Genesis of marine terrace soils, Barbados, West Indies: Evidence from mineralogy and geochemistry, *Earth Surf. Processes Landforms*, *12*, 605–618, 1987.

Muhs, D. R., C. A. Bush, K. C. Stewart, T. R. Rowland, and R. C. Crittenden, Geochemical evidence of Saharan dust parent material for soils developed on Quaternary limestones of Caribbean and western Atlantic islands, *Quat. Res*., *33*, 157–177, 1990.

National Oceanic and Atmospheric Administration (NOAA), HYSPLIT4 (HYbrid Single-Particle Lagrangian Integrated Trajectory) model, Silver Spring, Md., 1997.

O'Dowd, C., M. H. Smith, I. E. Consterdine, and J. A. Lowe, Marine aerosol, sea-salt, and the marine sulphur cycle: A short review, *Atmos. Environ*., *31*(1), 73–80, 1997.

O'Sullivan, D. W., A. K. Hanson Jr., and D. R. Kester, Stopped flow luminol chemiluminescence determination of Fe(II) and reducible iron in seawater at subnanomolar levels, *Mar. Chem*., *49*, 65–77, 1995.

Paerl, H. W., L. E. Prufert-Bebout, and C. Guo, Iron-stimulated N_2 fixation and growth on natural and cultured populations of the planktonic marine cyanobacteria *Trichodesmium* spp., *Appl. Environ. Microbiol*., *60*(3), 1044–1047, 1994.

Paquet, H., G. Coudé-Gaussen, and P. Rognon, Mineralogical datas about desertic dusts along a Saharan transect from north 19° to 35° lat, *Rev. Geol. Dyn. Géogr. Phys*., *25*(4), 257–265, 1984.

Patterson, C. C., and D. M. Settle, The reduction of orders of magnitude errors in lead analysis of biological materials and natural waters by evaluating and controlling the extent and sources of industrial

lead contamination introduced during sampling, collecting, handling and analysis, *NBS Spec. Publ. U.S.*, *422*, 321–351, 1976.

Pehkonen, S. O., R. Siefert, Y. Erel, S. Webb, and M. Hoffmann, Photoreduction of iron oxyhydroxides in the presence of important atmospheric organic compounds, *Environ. Sci. Technol.*, *27*, 2056–2062, 1993.

Price, N. M., B. A. Ahner, and F. M. M. Morel, The equatorial Pacific Ocean: Grazer-controlled phytoplankton populations in an iron-limited ecosystem, *Limnol. Oceanogr.*, *39*(3), 520–534, 1994.

Prospero, J. M., Atmospheric dust studies on Barbados, *Bull. Am. Meteorol. Soc.*, *49*(6), 645–652, 1968.

Prospero, J. M., and T. N. Carlson, Vertical and areal distribution of Saharan dust over the western equatorial North Atlantic Ocean, *J. Geophys. Res.*, *77*, 5255–5265, 1972.

Prospero, J. M., and R. T. Nees, Dust concentration in the atmosphere of the equatorial North Atlantic: Possible relationship to the Sahelian Drought, *Science*, *196*, 1196–1198, 1977.

Prospero, J. M., and D. L. Savoie, Effect of continental sources on nitrate concentrations over the Pacific Ocean, *Nature*, *339*, 687–689, 1989.

Prospero, J. M., E. Bonatti, C. Schubert, and T. N. Carlson, Dust in the Caribbean atmosphere traced to an African dust storm, *Earth Planet. Sci. Lett.*, *9*, 287–293, 1970.

Prospero, J. M., R. A. Glaccum, and R. T. Nees, Atmospheric transport of soil dust from Africa to South America, *Nature*, *289*, 570–572, 1981.

Prospero, J. M., D. L. Savoie, E. S. Saltzman, and R. Larsen, Impact of oceanic sources of biogenic sulphur on sulphate aerosol concentrations at Mawson, Antarctica, *Nature*, *350*, 221–223, 1991.

Prospero, J. M., K. Barrett, T. Church, F. Dentener, R. A. Duce, J. N. Galloway, H. Levy II, J. Moody, and P. Quinn, Atmospheric deposition of nutrients to the North Atlantic basin, *Biogeochemistry*, *35*, 27–73, 1996.

Pszenny, A. A. P., Particle size distributions of methanesulfonate in the tropical Pacific marine boundary layer, *J. Atmos. Chem.*, *14*, 273–284, 1992.

Pszenny, A. A. P., A. J. Castelle, and J. N. Galloway, A study of the sulfur cycle in the Antarctic marine boundary layer, *J. Geophys. Res.*, *94*, 9818–9839, 1989.

Pszenny, A. A. P., W. C. Keene, D. J. Jacob, S. Fan, J. R. Maben, M. P. Zetwo, M. Springer-Young, and J. N. Galloway, Evidence of inorganic chlorine gases other than hydrogen chloride in marine surface air, *Geophys. Res. Lett.*, *20*, 699–702, 1993.

Putaud, J.-P., S. Belviso, B. C. Nguyen, and N. Mihalopoulos, Dimethylsulfide, aerosols, and condensation nuclei over the tropical northeastern Atlantic Ocean, *J. Geophys. Res.*, *98*, 14,863–14,871, 1993.

Qian, G.-W., and Y. Ishizaka, Electron microscope studies of methane sulfonic acid in individual aerosol particles, *J. Geophys. Res.*, *98*, 8459–8470, 1993.

Quinn, P. K., W. E. Asher, and R. J. Charlson, Equilibria of the marine multiphase ammonia system, *J. Atmos. Chem.*, *14*, 11–30, 1992.

Quinn, P. K., D. S. Covert, T. S. Bates, V. N. Kapustin, D. C. Ramsey-Bell, and L. M. McInnes, Dimethylsulfide/cloud condensation nuclei/climate system: Relevant size-resolved measurements of the chemical and physical properties of atmospheric aerosol particles, *J. Geophys. Res.*, *98*, 10,411–10,427, 1993.

Saltzman, E. S., D. L. Savoie, R. G. Zika, and J. M. Prospero, Methane sulfonic acid in the marine atmosphere, *J. Geophys. Res.*, *88*, 10,897–10,902, 1983.

Saltzman, E. S., D. L. Savoie, J. M. Prospero, and R. G. Zika, Atmospheric methanesulfonic acid and non-sea-salt sulfate at Fanning and American Samoa, *Geophys. Res. Lett.*, *12*, 437–440, 1985.

Sander, R., and P. J. Crutzen, Model study indicating halogen activation and ozone destruction in polluted air masses transported to the sea, *J. Geophys. Res.*, *101*, 9121–9138, 1996.

Savoie, D. L., and J. M. Prospero, Aerosol concentration statistics for the northern tropical Atlantic, *J. Geophys. Res.*, *82*, 5954–5964, 1977.

Savoie, D. L., and J. M. Prospero, Water-soluble potassium, calcium, and magnesium in the aerosols over the tropical North Atlantic, *J. Geophys. Res.*, *85*, 385–392, 1980.

Savoie, D. L., and J. M. Prospero, Particle size distribution of nitrate and sulfate in the marine atmosphere, *Geophys. Res. Lett.*, *9*, 1207–1210, 1982.

Savoie, D. L., and J. M. Prospero, Comparison of oceanic and continental sources of non-sea-salt sulphate over the Pacific Ocean, *Nature*, *339*, 685–687, 1989.

Savoie, D. L., and J. M. Prospero, Non-sea-salt sulfate and methansulfonate at American Samoa, *J. Geophys. Res.*, *99*, 3587–3596, 1994.

Savoie, D. L., J. M. Prospero, and R. T. Nees, Nitrate, non-sea-salt sulfate, and mineral aerosol over the northwestern Indian Ocean, *J. Geophys. Res.*, *92*, 933–942, 1987.

Savoie, D. L., J. M. Prospero, J. T. Merrill, and M. Uematsu, Nitrate in the atmospheric boundary layer of the tropical South Pacific: Implications regarding sources and transport, *J. Atmos. Chem.*, *8*, 391–415, 1989a.

Savoie, D. L., J. M. Prospero, and E. S. Saltzman, Non-sea-salt sulfate and nitrate in trade wind aerosols at Barbados: Evidence for long-range transport, *J. Geophys. Res.*, *94*, 5069–5080, 1989b.

Savoie, D. L., J. M. Prospero, R. J. Larsen, and E. S. Saltzman, Nitrogen and sulfur species in aerosols at Mawson, Antarctica, and their relationship to natural radionuclides, *J. Atmos. Chem.*, *14*, 181–204, 1992.

Schollaert, S. E., and J. T. Merrill, Cooler sea surface west of the Sahara Desert, *Geophys. Res. Lett.*, *25*, 3529–3532, 1998.

Schütz, L., Long range transport of desert dust with special emphasis on the Sahara, *Ann. N. Y. Acad. Sci.*, *338*, 515–532, 1980.

Schütz, L., and M. Sebert, Mineral aerosols and source identification, *J. Aerosol Sci.*, *18*(1), 1–10, 1987.

Schütz, L., R. Jaenicke, and H. Pietrek, Saharan dust transport over the North Atlantic Ocean, *Spec. Pap. Geol. Soc. Am.*, *186*, 87–100, 1981.

Sedlak, D. L., and J. Hoigné, The role of copper and oxalate in the redox cycling of iron in atmospheric waters, *Atmos. Environ.*, *Part A*, *27*(14), 2173–2185, 1993.

Sedlak, D. L., and J. Hoigné, Oxidation of S(IV) in atmospheric water by photooxidants and iron in the presence of copper, *Environ. Sci. Technol.*, *28*, 1898–1906, 1994.

Seinfeld, J. H., and S. N. Pandis, *Atmospheric Chemistry and Physics: From Air Pollution to Climate Change*, John Wiley, New York, 1997.

Siefert, R. L., S. O. Pehkonen, Y. Erel, and M. R. Hoffmann, Iron photochemistry of aqueous suspensions of ambient aerosol with added organic acids, *Geochim. Cosmochim. Acta*, *58*, 3271–3279, 1994.

Siefert, R. L., S. M. Webb, and M. R. Hoffmann, Determination of photochemically available iron in ambient aerosols, *J. Geophys. Res.*, *101*, 14,441–14,449, 1996.

Siefert, R. L., A. M. Johansen, and M. R. Hoffmann, Measurements of trace metal (Fe, Cu, Mn, Cr) oxidation states in fog and stratus clouds, *J. Air Waste Manage. Assoc.*, *48*, 128–143, 1998.

Siefert, R. L., A. M. Johansen, and M. R. Hoffmann, Chemical characterization of ambient aerosol collected during the southwest monsoon and intermonsoon seasons over the Arabian Sea: Labile-Fe(II) and other trace metals, *J. Geophys. Res.*, *104*, 3511–3526, 1999.

Sievering, H., G. Ennis, E. Gorman, and C. Nagamoto, Size distribution and statistical analysis of nitrate, excess sulfate, and chloride deficit in the marine boundary layer during GCE/CASE/WATOX, *Global Biogeochem. Cycles*, *4*(4), 395–405, 1990.

Sievering, H., J. Boatman, E. Gorman, Y. Kim, L. Anderson, G. Ennis, M. Luria, and S. Pandis, Removal of sulphur from the marine boundary layer by ozone oxidation in sea-salt aerosols, *Nature*, *360*, 571–573, 1992.

Sisterson, D. L., A method for evaluation of acidic sulfate and nitrate in precipitation, *Water Air Soil Pollut.*, *43*, 61–72, 1989.

Spokes, L. J., and P. S. Liss, Photochemically induced redox reactions in seawater, I, Cations, *Mar. Chem.*, *49*, 201–213, 1995.

SPSS, Inc., *SPSS for Windows*, Chicago, Ill., 1997.

Stickel, R. E., J. M. Nicovich, Z. Zhao, and P. H. Wine, Kinetic and mechanistic study of the reaction of atomic chlorine with dimethyl sulfide, *J. Phys. Chem.*, *96*, 9875–9883, 1992.

Sturges, W. T., and L. A. Barrie, Chlorine, bromine and iodine in Arctic aerosols, *Atmos. Environ.*, *22*(6), 1179–1194, 1988.

Sturges, W. T., and G. E. Shaw, Halogens in aerosol in central Alaska, *Atmos. Environ.*, *Part A*, *27*(17/18), 2969–2977, 1993.

Swap, R., M. Garstang, S. Greco, R. Talbot, and P. Kålleberg, Saharan dust in the Amazon Basin, *Tellus*, *Ser. B*, *44*, 133–149, 1992.

Swap, R., S. Ulanski, M. Cobbett, and M. Garstang, Temporal and spatial characteristics of Saharan dust outbreaks, *J. Geophys. Res.*, *101*, 4205–4220, 1996.

Talbot, R. W., M. O. Andreae, H. Berresheim, P. Artaxo, M. Garstang, R. C. Harriss, K. M. Beecher, and S. M. Li, Aerosol chemistry during

the wet season in central Amazonia: The influence of long-range transport, *J. Geophys. Res*., *95*, 16,955–16,969, 1990.
Taylor, S. R., and S. M. McLennan, *The Continental Crust: Its Composition and Evolution*, Blackwell Sci., Malden, Mass., 1985.
Tegen, I., and I. Fung, Contribution to the atmospheric mineral load from land surface modification, *J. Geophys. Res*., *100*, 18,707–18,726, 1995.
Tegen, I., A. A. Lacis, and I. Fung, The influence on climate forcing of mineral aerosols from disturbed soils, *Nature*, *380*, 419–422, 1996.
Turekian, K. K., and K. H. Wedepohl, Distribution of the elements in some major units of the Earth's crust, *Geol. Soc. Am. Bull*., *72*, 175–192, 1961.
Turner, S. M., P. D. Nightingale, L. J. Spokes, M. I. Liddicoat, and P. S. Liss, Increased dimethyl sulphide concentrations in sea water from in situ iron enrichment, *Nature*, *383*, 513–517, 1996.
Voelker, B. M., and D. L. Sedlak, Iron reduction by photoproduced superoxide in seawater, *Mar. Chem*., *50*, 93–102, 1995.
Vogt, R., P. J. Crutzen, and R. Sander, A mechanism for halogen release in the remote marine boundary layer, *Nature*, *383*, 327–330, 1996.
Waite, D. T., and F. M. M. Morel, Coulometric study of the redox dynamics of iron in seawater, *Anal. Chem*., *56*, 787–792, 1984.
Wells, M. L., N. M. Price, and K. W. Bruland, Iron chemistry in seawater and its relationship to phytoplankton: A workshop report, *Mar. Chem*., *48*, 157–182, 1995.
Yin, F., D. Grosjean, and J. H. Seinfeld, Analysis of atmospheric photooxidation mechanisms for organosulfur compounds, *J. Geophys. Res*., *91*, 14,417–14,438, 1986.
Zar, J. H., *Biostatistical Analysis*, Prentice-Hall, Englewood Cliffs, N. J., 1996.
Zhang, L.-P., and K. Terada, Spectrophotometric determination of iron(II) in sea water after preconcentration by sorption of its 3-(2-pyridyl)-5,6-bis(4-phenylsulphonic acid)-1,2,4-triazine complex with poly(chlorotrifluoroethylene) resin, *Anal. Chim. Acta*, *293*, 311–318, 1994.
Zhu, X., J. M. Prospero, F. J. Millero, D. L. Savoie, and G. Brass, The solubility of ferric ion in marine mineral aerosol solutions at ambient relative humidities, *Mar. Chem*., *38*, 91–107, 1992.
Zhu, X., J. M. Prospero, D. L. Svoie, F. J. Millero, R. G. Zika, and E. S. Saltzman, Photoreduction of iron(III) in marine mineral aerosol solutions, *J. Geophys. Res*., *98*, 9039–9046, 1993.
Zhu, X. R., J. M. Prospero, and F. J. Millero, Diel variability of soluble Fe(II) and soluble total Fe in North African dust in the trade winds at Barbados, *J. Geophys. Res*., *102*, 21,297–21,305, 1997.
Zhuang, G., R. A. Duce, and D. R. Kester, The dissolution of atmospheric iron in surface seawater of the open ocean, *J. Geophys. Res*., *95*, 16,207–16,216, 1990.
Zhuang, G., Z. Yi, and R. A. Duce, Chemistry of iron in marine aerosols, *Global Biogeochem. Cycles*, *6*(2), 161–173, 1992a.
Zhuang, G., Z. Yi, R. A. Duce, and P. R. Brown, Link between iron and sulphur cycles suggested by detection of Fe(II) in remote marine aerosols, *Nature*, *355*, 537–539, 1992b.
Zuo, Y., Kinetics of photochemical/chemical cycling of iron coupled with organic substances in cloud and fog droplets, *Geochim. Cosmochim. Acta*, *59*, 3123–3130, 1995.
Zuo, Y., and J. Hoigné, Formation of hydrogen peroxide and depletion of oxalic acid in atmospheric water by photolysis of iron(III)-oxalato complexes, *Environ. Sci. Technol*., *26*, 1014–1022, 1992.
Zuo, Y., and J. Hoigné, Photochemical decomposition of oxalic, glyoxalic and pyruvic acid catalysed by iron in atmospheric waters, *Atmos. Environ*., *28*(7), 1231–1239, 1994.

M. R. Hoffmann and A. M. Johansen, Environmental Engineering Science, W. M. Keck Laboratories, California Institute of Technology, Mail Code 138-78, Pasadena, CA 91125. (mrh@cco.caltech.edu)

R. L. Siefert, Chesapeake Biological Laboratory, University of Maryland Center for Environmental Science, P.O. Box 38, One Williams Street, Solomons, MD 20688.

(Received August 19, 1999; revised November 16, 1999;
accepted January 10, 2000.)